TRABAJO ESPECIAL DE GRADO

ANÁLISIS DE LAS ONDAS DE SUPERFICIE PARA CONSTRUIR MODELOS DE VELOCIDADES SOMEROS: EL ROL DE LOS MODOS SUPERIORES

(SURFACE WAVE ANALYSIS FOR BUILDING NEAR SURFACE VELOCITY MODELS: THE ROLE OF HIGHER MODES)

Presentado ante la Ilustre
Universidad Central de Venezuela
Por el Br. Barreto C., Yozet R.
Para optar al Título
de Ingeniero en Petróleo

Caracas, 2013

TRABAJO ESPECIAL DE GRADO

ANÁLISIS DE LAS ONDAS DE SUPERFICIE PARA CONSTRUIR MODELOS DE VELOCIDADES SOMEROS: EL ROL DE LOS MODOS SUPERIORES

(SURFACE WAVE ANALYSIS FOR BUILDING NEAR SURFACE VELOCITY MODELS: THE ROLE OF HIGHER MODES)

TUTORES ACADÉMICOS: Prof. Laura Socco
Dr. Paolo Bergamo

Presentado ante la Ilustre
Universidad Central de Venezuela
Por el Br. Barreto C., Yozet R.
Para optar al Título
de Ingeniero en Petróleo

Caracas, 2013

AGRADECIMIENTOS

A la Universidad Central de Venezuela, la Facultad de Ingeniería y la Escuela de Ingeniería de Petróleo y adicionalmente al Politecnico di Torino, por haberme formado como ingeniero.

A mis tutores Prof. Laura Socco, muchas gracias por su comprensión, paciencia y guía durante este trabajo de tesis y Dr. Paolo Bergamo por su ayuda, sugerencias y asistencia específicamente con el código dentro del lenguaje de Matlab.

A los Profesores Evelyn Azuaje y Sandro Gasbarri, por su múltiple colaboración en mi carrera dentro de la UCV.

A mi tía e ingeniero de petróleo Jehovah Sorondo y al ingeniero Julio Cesar Oliveros por siempre haberme prestado de su ayuda tanto técnica y de ánimo a superarme.

Agradezco a mis amigos Rosa Espinoza, Jeshua Guzmán, Ruben Mejías, Liza Nabila, Olga Gonzaléz y Assel Baiganova por brindarme gratos momentos y por su soporte. Adicionalmente personas que hicieron más agradable estos últimos meses y que conocí en el departamento de geofísica aplicada del Politecnico di Torino, la Ing. Flora Garofalo y el Dr. Alessandro Arato.

Finalmente le doy gracias a todos los miembros de mi familia, a mi madre Heibory Castillo y a mi padre Raúl Barreto por su dedicación y ayuda en momentos difíciles en mi vida. También a mi abuela Mery Guevara por inculcarme sus principios y apoyarme en todo momento y mi hermana Heimary Barreto por su ayuda y cariño. Gracias a ustedes, por permitirme terminar esta fase de estudios y esta etapa de mi carrera.

Yozet Rafael Barreto Castillo

Barreto C., Yozet R

ANÁLISIS DE LAS ONDAS DE SUPERFICIE PARA CONSTRUIR MODELOS DE VELOCIDADES SOMEROS: EL ROL DE LOS MODOS SUPERIORES

Tutores Académicos: Prof. Laura Socco y Dr. Paolo Bergamo. Tesis. Caracas, U.C.V.

Facultad de Ingeniería. Escuela de Ingeniería de Petróleo. Año 2013, 106 p.

Palabras Claves: Curvas de dispersión, Velocidades de onda S estratos superficiales, Velocidades de onda P estratos superficiales, Procesamiento e Inversión ondas de Rayleigh, Ruido coherente.

Resumen. La razón para estudiar las ondas de superficie en el campo de la ingeniería de petróleo, es principalmente para proveer un modelo de velocidades de los estratos someros, ya que sirven para aplicar correcciones estáticas dentro de la sísmica. Adicionalmente, la información derivada de las ondas de superficie, puede ser beneficiosa para aplicar mejores algoritmos durante la migración, previa al pre-apilamiento en profundidad de la sísmica que es adquirida en tiempo y provee datos que sirven para la aplicación de técnicas robustas, para atenuar el efecto del ruido coherente en los registros sísmicos. El análisis de las ondas superficiales o de tierra, permiten explotar la presencia de las ondas de Rayleigh en la sísmica de reflexión, para determinar la geología de los estratos someros y finalmente mejorar la resolución de la imagen de los estratos profundos. Las ondas de superficie suelen ser aplicadas para obtener las velocidades de onda S (Vs), pero para la sísmica de exploración un modelo de velocidades de onda P (Vp) es más importante. Por ello se estudia el uso de los modos superiores, para determinar consistentemente Vp por medio de la inversión de las ondas superficiales.

ANÁLISIS DE LAS ONDAS DE SUPERFICIE PARA CONSTRUIR MODELOS DE VELOCIDADES SOMEROS: EL ROL DE LOS MODOS SUPERIORES.

Yozet R. Barreto C.[1]

[1] *Dirección de afiliación: Urb. Santa Mónica, Edif. Centauro. Torre A, Apartamento 9B. Caracas, Venezuela. Correo electrónico: yozetbarreto@gmail.com*

INTRODUCCIÓN

La principal técnica de exploración para la detección y caracterización de los yacimientos de petróleo, es la sísmica de reflexión. Esta es usada para identificar y construir mapas de las zonas de hidrocarburos y es basada en la generación, registro y procesamiento de las ondas sísmicas, que se propagan dentro del subsuelo. A través de la interpretación de volúmenes de data sísmica, información estructural y petrofísica es obtenida. Las ondas sísmicas que viajan por el subsuelo y que son usadas para construir una imagen de la estructura de los estratos más profundos, también pasan por estratos superficiales que son de baja velocidad y altamente heterogéneos. Estos estratos, también referidos como estratos meteorizados, producen fuertes efectos en los datos sísmicos, los cuales de no ser corregidos pueden generar efectos negativos en la calidad de las imágenes a mayor profundidad y pobres resultados. Por ello es importante obtener un modelo de velocidades de los estratos superficiales, para la corrección de la data de reflexión a mayores profundidades, en consecuencia distintas técnicas han sido desarrolladas para este propósito.

Cuando una fuente sísmica es disparada en la superficie, conjuntamente con las ondas de volumen, que son usadas para la exploración de hidrocarburos, también ondas superficiales son generadas. Estas ondas representan eventos altamente energéticos, que se propagan cerca de la superficie a una profundidad que es aproximadamente igual a la longitud de onda. En un medio estratificado estas ondas se vuelven dispersivas y multimodales, permitiendo extraer información de velocidades de los estratos someros. En la sísmica de reflexión convencional las ondas superficiales eran consideradas solo ruido coherente, que debía ser atenuado lo más pronto posible durante el procesamiento o filtradas modificando los parámetros de la adquisición. Sin embargo, esta tendencia está cambiando porque las ondas de superficie, son ahora reconocidas como una posible herramienta para construir modelos de velocidades a bajas profundidades. Adicionalmente, el análisis de las ondas de superficie está enfocándose como parte del flujo de trabajo dentro del procesamiento de los datos y considerándose como una señal y no más como ruido. Actualmente existe un aumento en la tendencia para ampliar la adquisición y registrar también la banda de frecuencia baja, perteneciente a las ondas de superficie. Ya que éstas pueden ser aisladas dentro del registro sísmico, luego procesadas y finalmente invertidas, para proveer los modelos requeridos de velocidades.

El interés en obtener confiables modelos de velocidades someros, no está limitado a la implementación de correcciones estáticas consistentes, sino también a la posibilidad de tener un modelo inicial para conseguir filtros optimizados en la atenuación del ruido, que a su vez sirve como dato, para aplicar algoritmos de migración previos al apilamiento. La adquisición de las ondas de superficie es importante en el ámbito de la ingeniería de petróleo, especialmente en la etapa de exploración para los geólogos, geofísicos y los ingenieros de yacimientos. Su análisis ayuda a establecer correcciones estáticas, que consisten en el ámbito de la data sísmica en

compensaciones por los efectos de variaciones en la elevación, espesor meteorizado, velocidades o referencia a un *datum*. El objetivo es determinar los tiempos de llegada de las reflexiones que habrían sido observadas, si todas las medidas hubiesen sido hechas sobre un plano, sin presencia de estratos meteorizados o materiales de bajas velocidades (Sheriff, 1989; Sheriff, 1991).

Los beneficios del análisis de las ondas de superficie, como mencionado previamente ayuda al procesamiento de los datos a través de las correcciones estáticas, además de proveer técnicas robustas para la atenuación del ruido debido a las ondas de Rayleigh y una mejor resolución. Finalmente, existe una nueva tendencia en la etapa de exploración, que se está dirigiendo hacia un mejoramiento de los modelos de velocidades de los estratos someros, antes del pre-apilamiento durante la migración a profundidad de los datos de la sísmica de reflexión (Strobbia et al., 2010).

Previos estudios del análisis de las ondas de superficie, fueron usados para detectar la presencia de hidratos de gas (Wright et al., 1991). En otro caso, la inversión de las ondas de Rayleigh ayudó a caracterizar campos someros de petróleo pesado, e.g., los yacimientos de petróleo del campo Lower Fars ubicados en Kuwait (Strobbia et al., 2010). Distintas aproximaciones han sido desarrolladas para analizar las ondas de superficie, en distintos campos de aplicación. En la escala de la exploración de hidrocarburos, técnicas de adquisición con múltiples canales presentan ciertas ventajas; no solo por su superior robustez y precisión, sino también por su habilidad para analizar distintos modos de propagación que son esenciales.

El modelaje de los estratos someros a través de la inversión de las ondas superficiales, da información geométrica de los estratos superficiales, geología, velocidad y distribución de atenuación bajando hasta la profundidad de investigación. Con fuentes de baja frecuencia y receptores, la profundidad de investigación puede alcanzar cientos de metros (Strobbia et al., 2009). Las ondas de Rayleigh usualmente son empleadas para el análisis de las ondas superficiales durante la adquisición y se sabe de acuerdo a la literatura existente en la rama de geofísica (Xia et al., 1999; Everett, 2013), que ellas tienen mayor sensibilidad a la velocidad de las ondas de corte (Vs), comparadas con la velocidad de las ondas P (Vp), no obstante para el modelado de velocidades y correcciones estáticas, calcular Vp es en general más importante y requerida para la etapa de exploración de la sísmica de reflexión. La conversión de Vs a Vp, algunas veces puede ser realizada por medio de correlaciones, basadas en información litológica e hidrogeológica, extraída de las capas someras. A pesar de ello, otra manera para obtener Vp puede ser valiosa, cuando información previa no está disponible sobre el sitio o para justificar resultados locales en los cálculos de éste parámetro.

METODOLOGÍA

El objetivo de esta tesis se enfoca en resolver adecuadamente la velocidad de las ondas P (Vp). El método estará basado en el estudio de las curvas de dispersión (ver Figura 1), que pueden ser usadas para estimar las propiedades de los estratos someros en caso de un medio estratificado (ver Figura 2). No obstante, el modo fundamental de las ondas de Rayleigh, no posee tanta sensibilidad a Vp y tiene limitada profundidad de investigación (Ernst, 2008). Por ello, para determinar Vp a través del análisis de las ondas superficiales, se propuso el estudio de los modos superiores que serán añadidos durante el proceso de inversión (ver Figura 3).

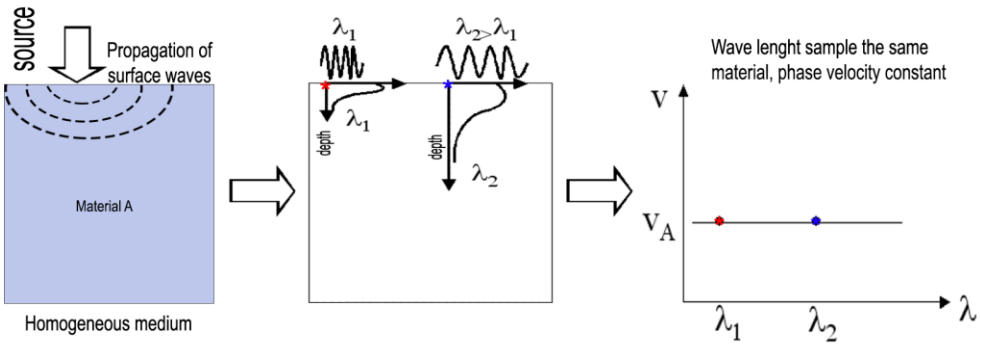

Figura 1. Dispersión geométrica de las ondas Rayleigh en un medio homogéneo, elástico e isotrópico.

La Figura N^{o} 1 muestra que cada longitud de onda, registra el mismo material a varias profundidades, generando un modelo donde la velocidad de fase es constante para distintas longitudes de onda.

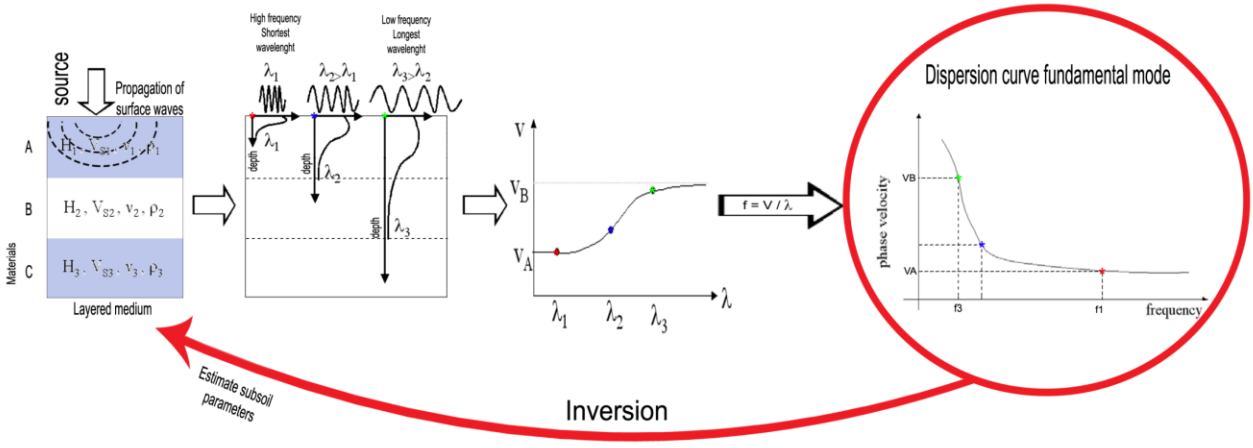

Figura 2. Modelo de dispersión geométrica de las ondas Rayleigh en un medio estratificado (heterogéneo), compuesto por estratos elásticos e isotrópicos.

La Figura N^{o} 2 permite observar el fenómeno del efecto de la dispersión geométrica de las ondas de Rayleigh, en un medio estratificado (que depende de las propiedades físicas del medio), para este caso cada longitud de onda registra diferentes materiales, provocando un modelo de velocidades de fases que no es uniforme y que depende de las distintas longitudes de onda. Ya que la velocidad de fase (V) y la longitud de onda (λ) están relacionadas con la frecuencia (*f*). Se puede obtener la gráfica de velocidad de fase en función de la frecuencia, mejor conocida como curva de dispersión (Para la Figura N° 2 solo el modo fundamental se muestra). La curva de dispersión es muy importante, ya que esta puede ser obtenida experimentalmente. En consecuencia, mediante un proceso de inversión son calculados los parámetros físicos del subsuelo: hablamos de las velocidades de corte (Vs), los espesores (H), las densidades (ρ) y los módulos de Poisson (ν) o velocidades de onda P (Vp) de cada estrato.

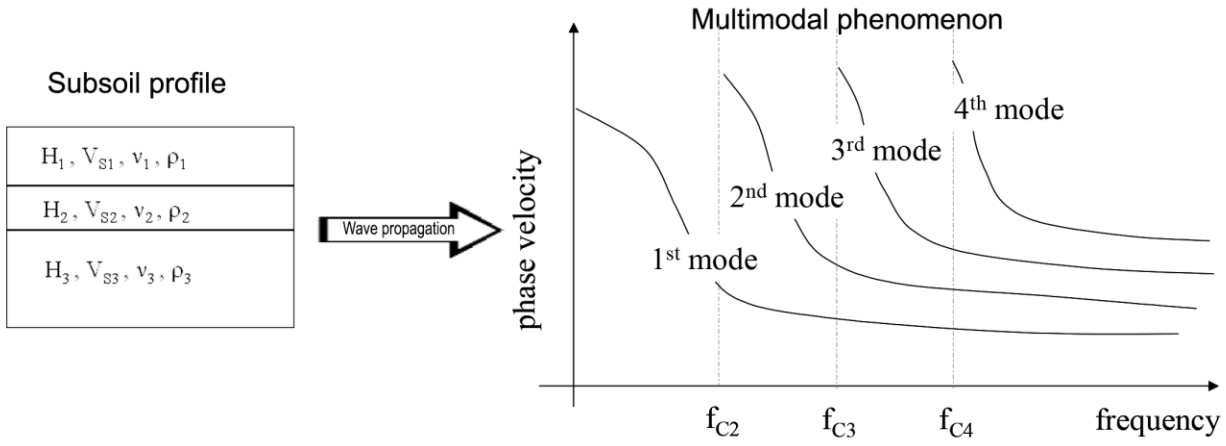

Figura 3. Modos superiores de las ondas de Rayleigh. (Strobbia, 2003, modificado)

La Figura N° 3, muestra que para un determinado modelo estratificado, la propagación de las ondas superficiales es un fenómeno multimodal.

Los pasos a seguir dentro de la tesis de investigación se enfocarán en:

- Un modelo sintético de referencia que será simulado por medio de un operador directo, para determinar el modo de propagación fundamental y los modos superiores, luego se aplicará un modelo de sensibilidades realizando una perturbación al modelo inicial de acuerdo al cambio del módulo de Poisson o relación de velocidades (Vp/Vs), obteniendo las curvas de dispersión y expresando los resultados en otros dominios de interés.
- Posteriormente, la sensibilidad de las curvas de dispersión al módulo de Poisson, será evaluada aplicando el proceso de inversión de los datos, teniendo como modelo experimental el modelo sintético de referencia inicial.
- Para ello se elegirá una estrategia multimodal para la inversión, aplicando una aproximación por el método de Monte Carlo, donde un universo de 2 millones de modelos aleatorios y uniformemente distribuidos en base a Vs, ν y H serán escogidos, adaptando ciertos límites dentro de la simulación. La densidad en todo el estudio será establecida *a priori.*
- La data sintética será invertida para precisar la sensibilidad hacia Vp o módulo de Poisson, primero analizando el uso del modo fundamental y luego con modos superiores.
- Un análisis estadístico ayudará a cuantificar y comparar el uso de los modos superiores respecto al modo fundamental en los estimados de las velocidades de onda P (Vp) y determinar si existe una mejoría en los resultados aplicando la inversión multimodal.
- Finalmente, los procedimientos aplicados al modelo de inversión de la data sintética, serán usados para analizar los datos de una adquisición en superficie de un registro sísmico de exploración para hidrocarburos. El objetivo consistirá en estimar las velocidades de onda P (Vp) o los módulos de Poisson de los estratos someros.

El código numérico para el análisis de las ondas de superficie en esta tesis está basado en el lenguaje de programación de Matlab para la inversión de las ondas de Rayleigh. El código está compuesto de dos partes: El modelo directo y el modelo de inversión. El primero fue desarrollado en el *Politecnico di Torino* por: Foti, (2000) y Strobbia, (2003) y adicionalmente mejorado por

Maraschini, (2007) quien implementó la matriz de Haskell y Thomson con la modificación sugerida por Dunkin, (1965). El modelo de inversión será aplicado por medio de una aproximación de Monte Carlo, que consistirá en estudiar el universo de valores de una muestra aleatoria y uniforme de un cierto rango y reconstruir la solución de acuerdo a modelos aceptables.

La Figura N° 4 explica el procedimiento lógico que será seguido para realizar el estudio de sensibilidad dentro del modelo sintético. Inicialmente se poseerá un modelo de referencia, que será nuestro medio estratificado, luego se aplicará el operador directo basado en el determinante de la matriz de Haskell y Thomson, que permitirá estimar la primera curva de dispersión. Después se realizará una perturbación en el modelo inicial estratificado, variando el módulo de Poisson de los estratos que a su vez modificará las velocidades de onda P y las respectivas curvas de dispersión. Finalmente, se compararán las curvas modales respecto al rango de valores del módulo de Poisson o relación de velocidades (Vp/Vs) asumidos, aplicando adicionalmente transformaciones en diferentes dominios.

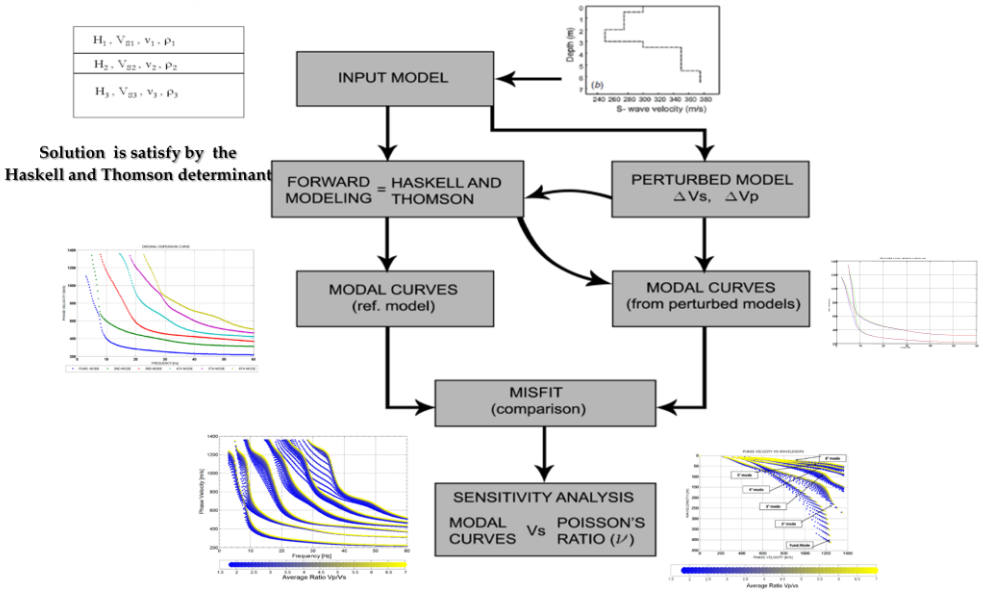

Figura 4. Esquema Lógico para el desarrollo del modelo de sensibilidad del modelo sintético.

RESULTADOS Y DISCUSIÓN

La Figura N° 5 muestra los resultados para la curva de dispersión (lado derecho) del modelo estratificado inicial de nuestro modelo sintético (lado izquierdo), con distintos parámetros para Vs, H, ρ y ν en cada estrato y considerando seis modos en el estudio.

Dentro de la Figura N° 6, el 1er gráfico (esquina superior izquierda) representa la sensibilidad de la curva de dispersión para los seis modos, variando las relaciones de velocidades Vp/Vs, el 2do gráfico (esquina superior derecha) representa la sensibilidad en el dominio de velocidad de fase vs longitud de onda, el 3er gráfico (esquina inferior izquierda) representa la sensibilidad en el dominio de frecuencia vs número de onda y el 4to gráfico (esquina inferior derecha) representa la sensibilidad en el dominio de diferencias en velocidad de fase para modos sucesivos vs frecuencia.

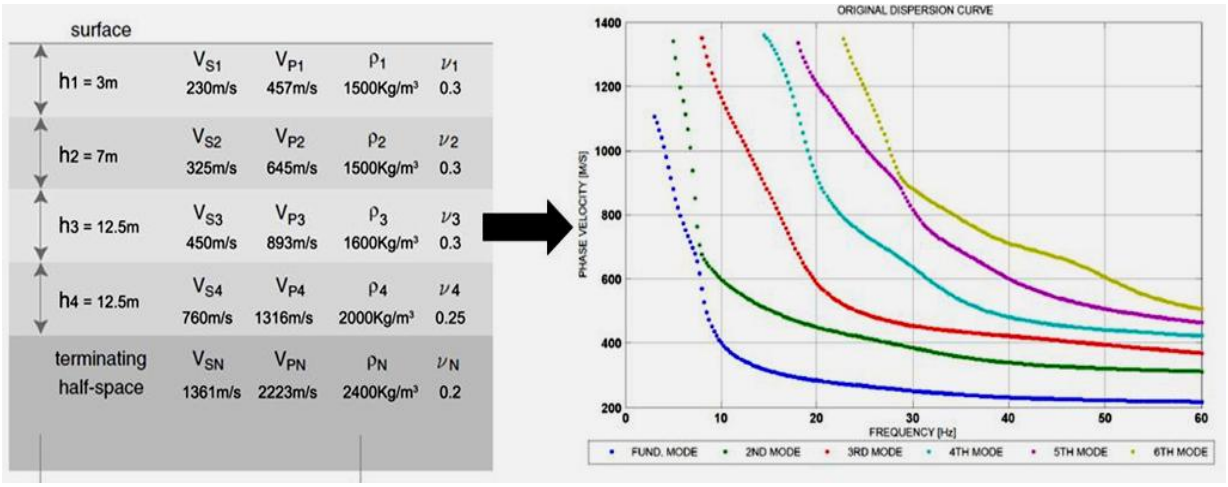

Figura 5. Parámetros iniciales del modelo sintético (lado izquierdo) y la respectiva curva de dispersión (lado derecho).

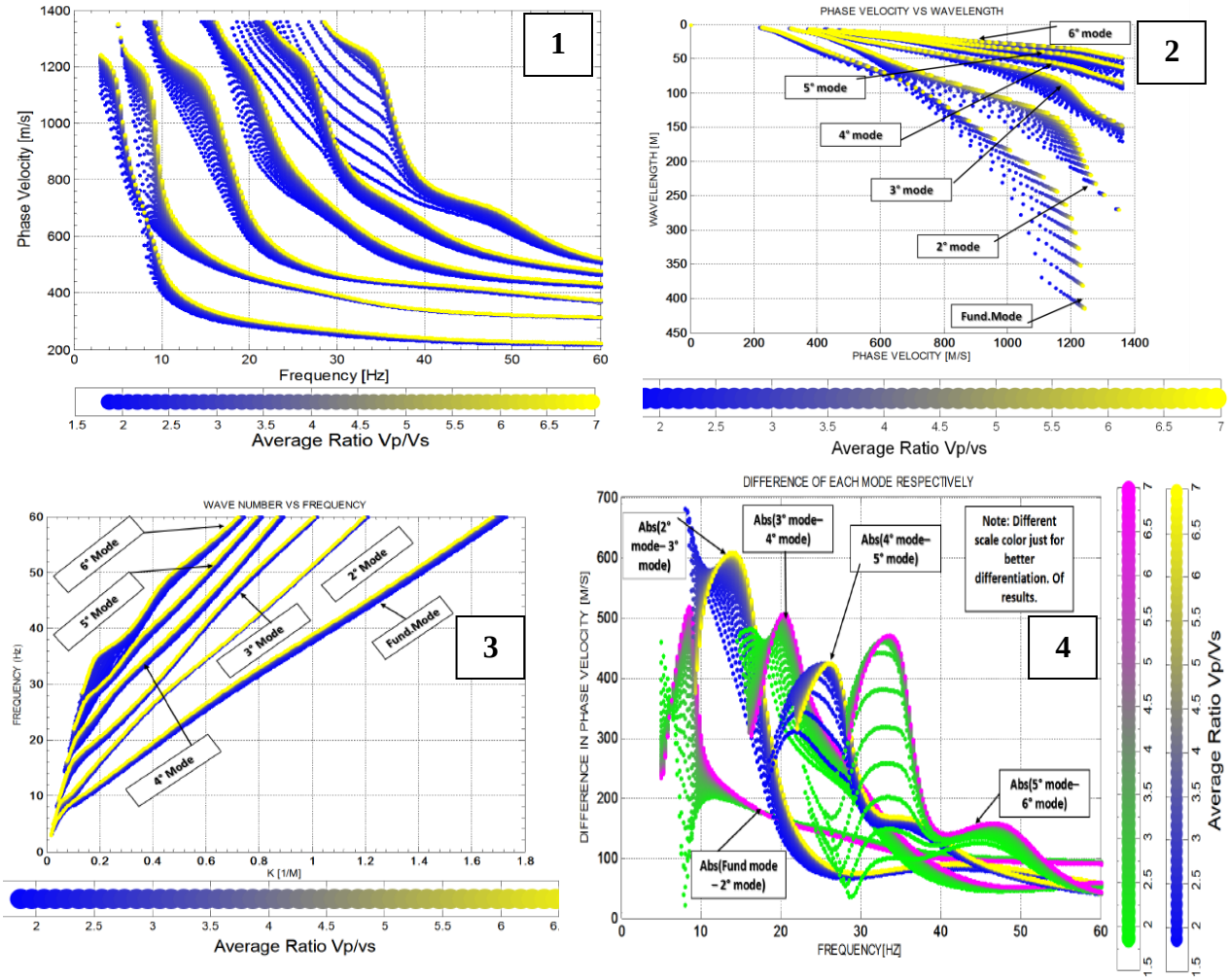

Figura 6. Análisis de sensibilidad sobre el modelo sintético para distintas relaciones de velocidades Vp/Vs, adicionalmente con el uso de distintos dominios.

Los resultados de la Figura N° 6 muestran, que en el dominio de velocidad de fase vs frecuencia existe una mayor sensibilidad por debajo de los 25 Hz para los primeros tres modos y para los últimos tres modos, a partir de 50Hz. Para el dominio de longitud de onda en función de la velocidad de fase, ya que la longitud de onda está relacionada con la profundidad de investigación, se detalla que existe una sensibilidad a Vp/Vs para diferentes profundidades, i.e., para cortas longitudes de onda (banda de frecuencia alta) existe una variación menor a Vp/Vs, mientras que a mayores longitudes de onda (banda de frecuencia baja), alrededor de 75 metros existe un mayor cambio de la velocidad de fase para un cambio en la relación Vp/Vs. En el dominio frecuencia – número de onda (*f-k)*, se muestra la pobre sensibilidad que existe; esto es importante ya que la extracción de las curvas de dispersión experimentales, se realizan en este dominio y un ligero error durante la extracción, podría conllevar a resultados errados de Vp. Adicionalmente, en el dominio de diferencias en velocidad de fase para modos sucesivos vs frecuencia, se detalla que la sensibilidad cambia drásticamente en este dominio, de un modo a otro y en diferentes rangos de frecuencia.

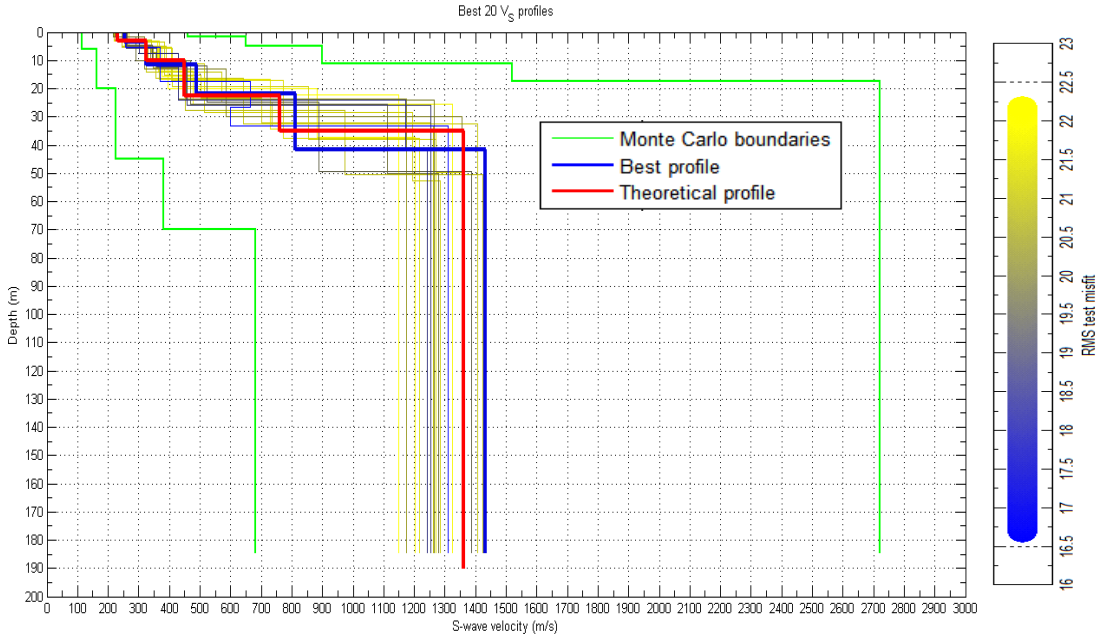

Figura 7. Mejores 20 perfiles de acuerdo al error RMS obtenidos para las velocidades de onda de corte (Vs) de cada estrato con sus respectivos espesores. Modelo de inversión considerando el modo fundamental y dos modos superiores para el ajuste.

La Figura N° 7 muestra la velocidad de corte (unidades de m/s) para los mejores 20 perfiles obtenidos por medio de la simulación de Monte Carlo de un universo de 2 millones de modelos, escogidos aleatoriamente y distribuidos uniformemente para Vs, H y ν. Mientras que la Figura N° 8 muestra las velocidades de onda P (m/s) respectivamente, pero fijando previamente Vs y H.

Los resultados (ver Figuras 7 y 8) muestran que la mejor manera para calcular los módulos de Poisson (ν) o perfil de Vp del medio estratificado, consiste en una inversión etapa por etapa. Inicialmente, se deben obtener las velocidades de onda de corte (Vs) y los espesores del medio estratificado dentro de la primera inversión. Luego, con el mejor perfil de Vs y de espesores, se

procede a un segundo modelo de inversión más focalizado, donde se corre una simulación de Monte Carlo pero fijando estos dos parámetros (Vs y H) y se obtiene el modelo final con el perfil de Vp (ver Figura 8). Se observó que un buen ajuste de la Vp era obtenido y fue respaldado al ser contrastado con el perfil de Vp sintético de referencia, especialmente para un ajuste multimodal teniendo en cuenta tres modos de ajuste (ver Figura 8).

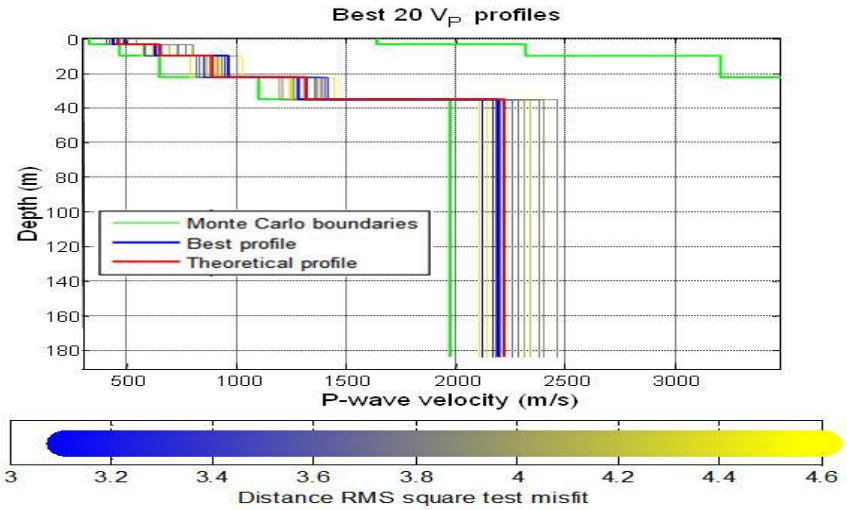

Figura 8. Mejores 20 perfiles de acuerdo al error RMS obtenidos para las velocidades de onda de compresión (Vp) de cada estrato. Modelo de inversión considerando tres modos para el ajuste y considerando el mejor perfil de Vs de la Figura N° 7.

Considerando los resultados de la inversión del modelo de referencia al caso sintético, se procedió a calcular las velocidades de onda P de una data real correspondiente a un registro sísmico, de una exploración de hidrocarburos (ver Figura 9). Para ello se aisló la data superficial y se aplicó un proceso de extracción de las curvas de dispersión en el espectro (ver Figura 10), éstas luego fueron invertidas por medio de un ajuste multimodal mediante una aproximación de Monte Carlo, aplicando recurrentemente el operador directo basado en el determinante de la matriz de Haskell y Thomson desarrollado en el código de Matlab.

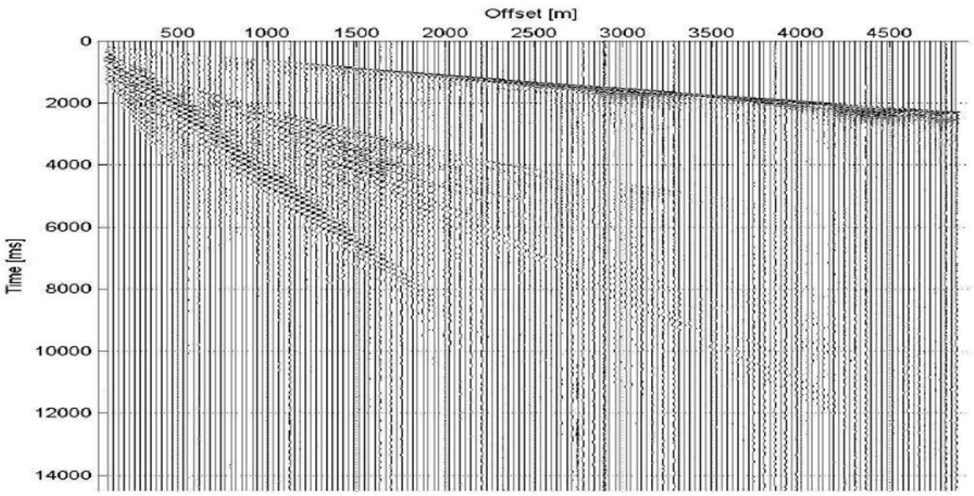

Figura 9. Data de la sísmica de exploración.

Los resultados de los 20 mejores ajustes, indicó que hay una buena concordancia de los dos modos experimentales con aquellos de la inversión (ver Figura 11; lado izquierdo), mientras que los 20 mejores perfiles de Vs son consistentes (ver Figura 11; lado derecho). Ellos sirvieron de base, para obtener el modelo final de Vp (ver Figura 12).

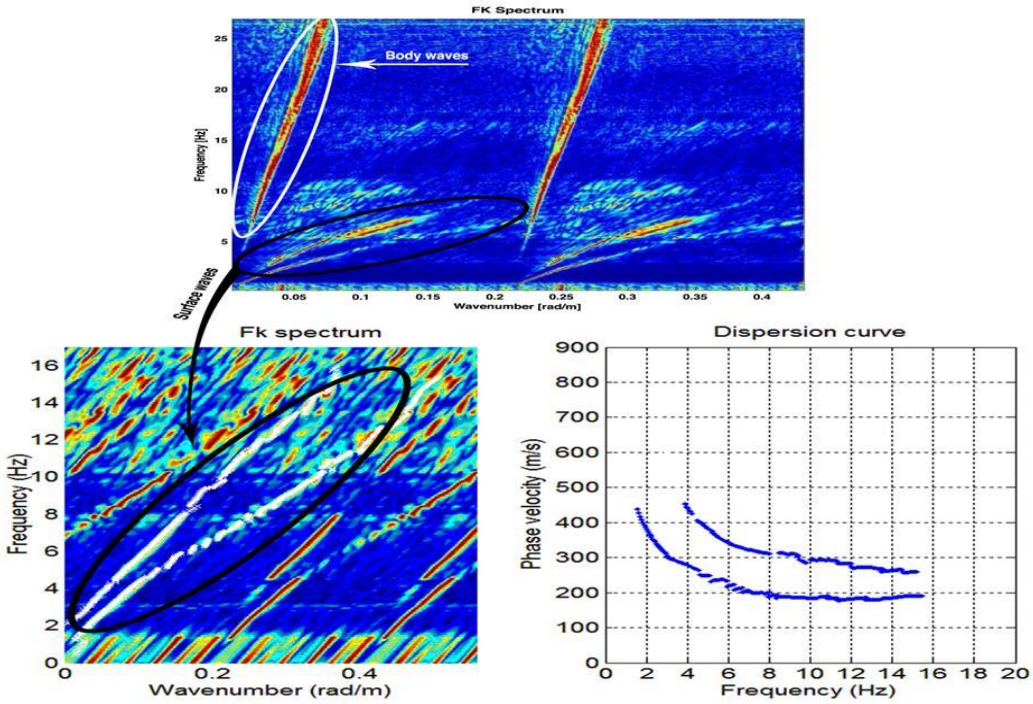

Figura 10. Análisis del espectro en el dominio *f-k* durante el procesamiento de los datos sísmicos. Adicionalmente, extracción final de las curvas de dispersión.

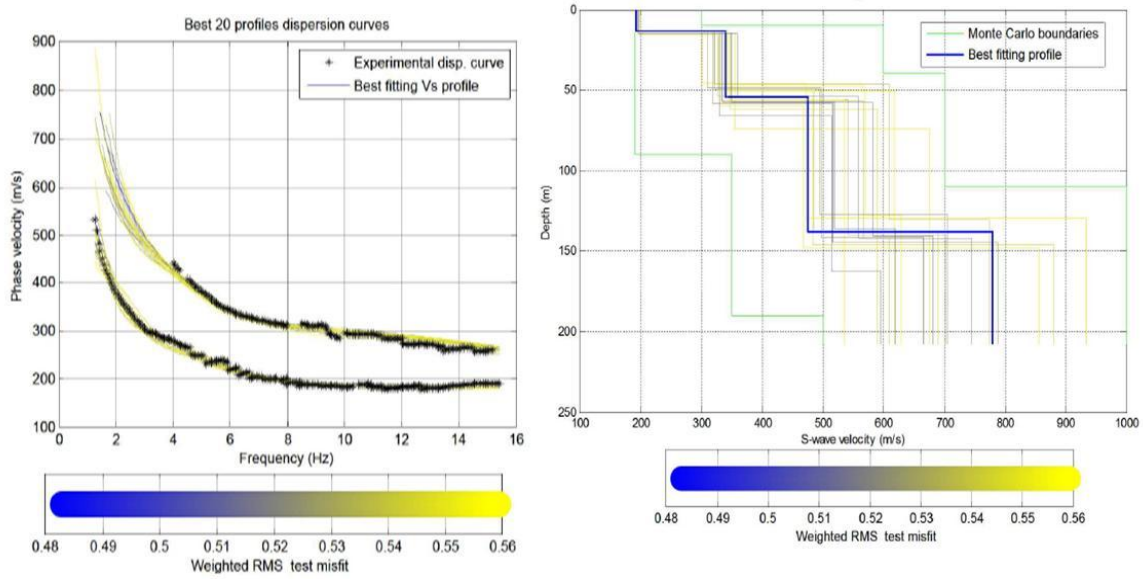

Figura 11. Mejores 20 ajustes del modo superior y del fundamental (lado izquierdo) y mejores 20 perfiles de Vs (lado derecho). Aplicando un modelo multimodal de inversión con el método de Monte Carlo. Datos experimentales del registro sísmico de exploración.

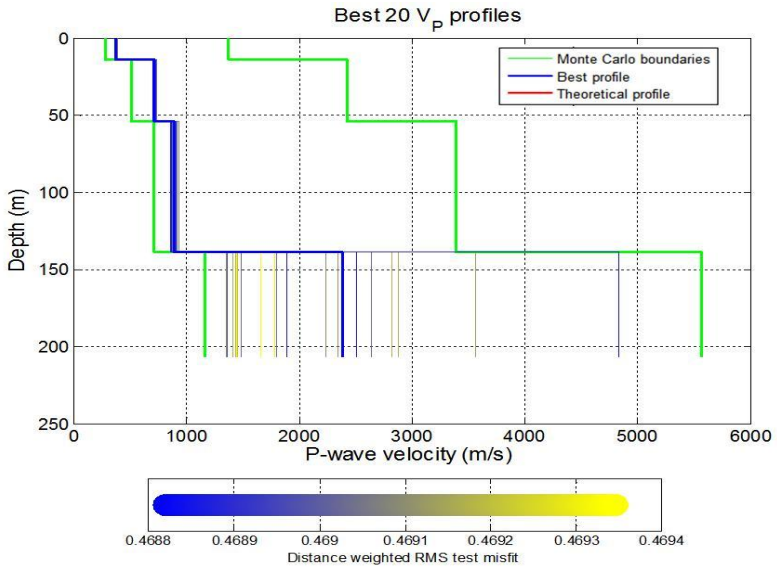

Figura 12. Mejores 20 perfiles de Vp. Inversión multimodal de la data superficial del registro.

CONCLUSIONES

La razón de estudiar las ondas superficiales, es para proveer un modelo de velocidades de los estratos someros consistentes, ya que puede ser usado dentro de la misma sísmica de reflexión, para su respectiva corrección durante el procesamiento. En particular, después de analizar los aspectos importantes dentro de la propagación de las ondas de superficie y el procesamiento necesario para el análisis de ellas para obtener las velocidades de corte (Vs), este trabajo se enfocó en extraer adicionalmente las velocidades de onda P (Vp), agregando al modelo de inversión los modos superiores dentro del flujo de trabajo. La idea viene de un estudio previo, realizado y divulgado por Bergamo y Socco, (2013) respecto al análisis de las ondas de superficie para proveer un significativo modelo de Vp, para un material granular homogéneo y aquí es extendido el análisis a un modelo estratificado.

El análisis de sensibilidad de las curvas modales de las ondas de Rayleigh dentro del modelo sintético, muestra que existe una mayor sensibilidad de las curvas de dispersión particularmente en el rango de baja frecuencia (de un total de 371 simulaciones). Adicionalmente la inclusión de los modos superiores, mostró que puede incrementar la sensibilidad a Vp durante la inversión de las ondas superficiales. A través de un análisis estadístico para el modelo sintético, se determinó que el módulo de Poisson presentaba menor desviación estándar y menor error relativo en el caso de la inversión ajustando tres modos (desviación estándar de 6.2 y error relativo de 6%), con respecto al modo fundamental (desviación estándar de 7.8 y error relativo de 8%). Finalmente, gracias al efecto combinado de los modos superiores dentro del caso de estudio, se estimó que el error porcentual de usar sólo el modo fundamental, genera en los estimados de Vp un error del 16 % para el primer estrato, un 25% para el segundo estrato, un 9% para el tercer estrato y un 10% para el semi-espacio (aunque para el semi-espacio la sensibilidad fue baja en el caso de estudio).

Los resultados alcanzados son promisorios pero merecen mayor investigación. En particular, las distintas formas de definir los modelos de velocidades y la inclusión de algunas restricciones que vengan de las ondas de volumen.

POLITECNICO DI TORINO

Department of Environment, Land and Infrastructure Engineering

Master of Science in Petroleum Engineering

Surface wave analysis for building near surface velocity models: The role of higher modes

Supervisor(s):
Prof. Laura Socco
Dr. Paolo Bergamo

Yozet R. BARRETO C.

OCTOBER 2013

Thesis submitted in compliance with the requirements for the Master of Science degree.

Summary

Geophysical methods present unique advantages, including a strong theoretical basis, the ability to perform the same basic measurement in the laboratory and field, and the non-invasive nature of the tests. The reason for studying surface wave in the field of petroleum engineering is mainly to provide a near surface velocity model to be used for correcting seismic. Nonetheless, information regarding the surface waves could be also important in land hydrocarbon exploration for prestack depth migration and to provide robust techniques for the attenuation of surface wave noise . Among different techniques that are used for near surface velocity models estimation, recent use of surface wave analysis exploit the ground roll present in seismic reflection records to get the near surface geology and ultimately, a better image of the reservoir.

Surface waves are widely applied to retrieve the shear wave velocity (V_S) model, but certainly for seismic exploration the compressional wave velocity (V_P) is more relevant, so, it is important to assess the possibility to get both V_S and V_P from the inversion method. Surfaces waves are considered poorly sensitive to V_P , but in this work there is an interest to show that by including higher modes this sensitivity could be improved.

Acknowledgements

My deepest gratitude to my academic advisor Prof. Laura Valentina Socco, whose expertise, understanding, and patience, added considerably to my graduate experience. I appreciate her vast knowledge in Surface wave methods and skill in many areas, and her assistance in writing reports (i.e., like this thesis). It is with immense gratitude that I acknowledge the support and help of my co- advisor, the Dr. Paolo Bergamo, for his suggestions and for provision of all the assistance in the programming environment in Matlab language and additionally, some ideas to proceed with the aim of the master thesis.

For the two universities that were fundamental in my education the "Politecnico di Torino" and the "Universidad Central de Venezuela" ("La Casa que vence las sombras"). Thank you to the Profs. Evelyn Azuaje and Sandro Gasbarri, for their patience and guidance during my career in Venezuela. I want to thank my friends Assel Baiganova, Rosa Espinoza, Jeshua Guzmán, Rubén Mejías, Liza Nabila and Olga González for their support. Also, my aunt Eng. Jehovah Sorondo and Eng. Julio Cesar Oliveros for their help in my studies. I would like to mention some people , I met during this time at the DITAG department , Eng. Flora Garofalo and Dr. Alessandro Arato.

Last but not the least important , I owe more than thanks to my family members, which includes my parents (Heibory Castillo and Raúl Barreto), my grandmother (Mery Guevara) and my sister (Heimary Barreto), for their encouragement throughout my life. Without their support, it is impossible for me to finish my graduate education.

List of Symbols

V_S	Shear wave velocity or S-wave velocity (β)
V_P	Compression wave velocity or P-wave velocity (α)
V_R	Rayleigh wave velocity (c)
ρ	Density
λ	Wavelength
f	Frequency
G	Shear Modulus
ϵ	Strain Tensor
σ	Stress Tensor
k	Wavenumber
$\omega = 2\pi f$	Pulsatance
ν	Poisson's ratio
K	Bulk modulus
$\mathbf{d_i}$	Thickness of ith layer
v	Velocity
V_{smin}	Minimum shear wave velocity
V_{smax}	Maximum shear wave velocity
H_{max}	Maximum thickness of the layer
H_{min}	Minimum thickness of the layer
ν_{min}	Minimum Poisson's ratio
ν_{max}	Maximum Poisson's ratio

Glossary

Active test : Measurement performed recording the motion caused by a seismic source activated on purpose at the site. Also known as **active source test** . Reference: (Socco et al., 2010)

Apparent Velocity : The phase velocity of surface waves as determined from the analysis of field measurements in which it is impossible to isolate the contribution of the different modes of propagation because of the limited resolution of finite recording arrays. Also referred to as **effective velocity**.

Body waves : Waves that travel within a medium in the form of compressional (primary) P-waves or shear (secondary) S-waves.

Dispersion : Variation of velocity with frequency. Associated with the term: geometric dispersion, inverse dispersion, material dispersion, normal dispersion.

Fundamental mode : The mode that shows lowest phase velocity.

Full-waveform inversion : Inversion based on the synthesis of the complete wavefield, comprised of body waves and surface waves with their modes of propagation.

Geometric dispersion : Dispersion caused by heterogeneity of a medium.

Higher modes : Modes propagating with higher phase velocity, than that associated with the fundamental mode.

Ground roll : Term adopted in geophysical exploration to indicate surface-wave energy that travels near the surface of the ground and that can mask the reflection signals in seismic surveys. For this reason, the term has a negative connotation. Several techniques have been developed to suppress it during processing. In a certain sense, the term can be considered a synonym of Rayleigh waves because, in most cases, ground roll is caused by their propagation.

Trace : A trace is a seismic time measurement corresponding to one source - receiver pair. Also, defined like the seismic data recorded for one channel, that represents the response of the elastic wavefield to velocity and density contrast across interfaces of sediments.

Offset : Distance between source and receiver for a given trace.

The common depth point CDP : Halfway point of the path only where the Earth is horizontally layered ; it is situated vertically below the common midpoint (CMP).

Gather : Family of traces (e.g shot-point gather is the family of all traces corresponding to the same source firing) .

CMP-gather : Sorting of traces by collecting traces that have the same midpoint

Fold : Corresponds to the number of traces summed or stacked. (E.g, in 24-fold data, every stacked trace represents the average of 24 traces) . Typical values of fold for modern seismic data range from 60 to 240 for 2D seismic data.

Wavelength : Distance between two similar points (peak , trough or zero crossing are most often used) of any consecutive waves and is symbolized by the Greek letter λ .

Amplitude : Maximum value of displacement of the particle from its position of equilibrium or half of the peak to peak distance on the ordinate axis: the symbol is usually A.

Frequency : Inverse of the period that is the peak to peak distance on the x-axis (time). $f = 1/T$ (Hz)

Phase lag (ϕ) : Time delay expressed as an angle.

Wave Number : Scalar of the wave vector $Acos(\phi + \omega t)$. Defined in a circular wave number as: $\kappa = 2\pi/\lambda$.

Contents

List of Tables

List of Figures

Chapter 1

Introduction

The main exploration technique for hydrocarbon reservoir detection and characterization is seismic reflection. It is used to identify and map hydrocarbon bearing zones and it is based on the generation, recording and processing of seismic waves propagating in the subsurface. Through the geological interpretation of seismic data volumes, structural and petrophysical information can be retrieved. The seismic waves that travel through the subsurface and are used to image the structure of the earth also passes through the shallow layers which are low velocity layers and strongly heterogeneous. These layers, also referred as weathering layers or, generally as near surface, produce strong effects in the data which, if not properly addressed and corrected can significantly affect the quality of deep images creating artifacts and poor quality results. It is hence very important to retrieve a near surface velocity model to be used for deep data corrections and several techniques have been developed for this purpose.

When a seismic source is shot on the ground surface, together with the body waves which are used to image the deep subsurface, also surface waves are generated. These waves are high energy events that propagate close to the surface at a depth that is roughly equal to the wavelength. In layered media these waves become dispersive and multimodal and can be used to extract information about the velocity in shallow layers. In engineering and geo-hazard studies, the methods based on surface wave analysis to retrieve near surface velocity are popular and

well established, but in conventional land seismic reflection, surface waves were just considered coherent noise to be attenuated as early as possible in the processing or filtered out by the acquisition parameters. Nonetheless, the perspective of coherent noise in the context of reflection seismic is changing because surface waves are now recognized a possible tool for building near surface velocity models; whereby, surface wave analysis is leading as part of the data processing work-flow and surface waves are considered as signal and not noise. Nowadays, there is an increasingly trend to broadening the acquisition and record also the low frequency band corresponding to the surface waves. Surface waves can be then isolated from the seismic record, processed and inverted to provide the required velocity models.

The interest in getting reliable near surface velocity models is not limited to the implementation of consistent static correction but also to the possibility of having an input modeling, optimized filters for a better noise attenuation, input for pre-stack migration algorithms. Surface wave acquisition allows to design filters to remove the noise in reflection data due to mud and ground roll (Maraschini, 2007). So, in consequence surface waves are important in the field of petroleum engineering, especially in the exploration stage for geologists , geophysicist and reservoir engineers. Surface wave analysis is useful for making static corrections. Applied to seismic data to compensate for the effects of variations in elevation, weathering thickness, velocity, or reference to a datum. The objective is to determine the reflection arrival times which would have been observed if all measurements had been made on a (usually) at plane with no weathering or low-velocity material present (Sheriff, 1989 ; Sheriff, 1991). Traditionally, the surface waves in land seismic data have been regarded as coherent noise to be removed. But, in some cases, with a complex near surface or spatial aliasing , their attenuation can be challenging. As part of near surface characterization. Among different techniques, the developed of surface wave analysis, modeling and inversion processing, enables to extract information from the surface waves before removing them from the seismic data.

The benefits of the Surface wave analysis, as mentioned before could improve the data processing trough static corrections, provide robust techniques for the attenuation of surface wave noise and provide higher resolution and last but not less, the recent trend in the hydrocarbon exploration is heading toward the improvement

in near surface velocity models for prestacking depth migration (Strobbia et al., 2010).

Moreover, there have been studies in surface wave in previous years, that used to detect the presence of gas hydrates, which can result in stiffness profiles, consisting of stiffer materials (hydrates) overlying between softer soil sediments. (Wright et al., 1991). Additionally, Rayleigh wave inversion has been used for the near surface characterization of shallow targets in heavy oil fields. e.g., the Lower Fars field oil reservoir in Kuwait. (Strobbia et al., 2010)

Finally, it could be mentioned that the knowledge of the near surface velocity model is valuable information for geo-technical characterization, geo-hazard studies, vibration propagation modeling and seismic site response studies, in the field of engineering. (Maraschini and Foti, 2010).

Several approaches have been developed for analyzing surface waves in different fields of application. At the hydrocarbon exploration scale, multichannel techniques have several advantages: not only their superior robustness and accuracy, but also the ability to analyze several modes of propagation that are essential.

The near surface model obtained through surface wave inversion gives geometric information about the near surface layers, geology, velocity and attenuation distribution down to the investigation depth. With low- frequency sources and receivers, the investigated depth can reach hundreds of meters. (Strobbia et al., 2009) The Rayleigh waves are usually employed for the analysis of surface waves during the acquisition, and it is known according to the literature available in geophysics, (Xia et al., 1999 ; Everett, 2013) that they are more sensitive to shear wave velocity (V_S) compare to compressional wave velocity (V_P) , whereas for velocity modeling and static computation, a V_P model is in general more important and required for seismic reflection exploration. The conversion from V_S to V_P sometimes can be done with correlations based in lithological and hydrogeophysical information extracted from the near surface. Nevertheless, another way to retrieve the V_P could be valuable when detail information is not available in the site or to justify local results on the calculation of this parameter.

1.1 Purpose of the thesis

The objective of this master thesis focuses on resolve adequately the shallow subsurface P-waves velocities (V_P) which are useful in hydrocarbon exploration for static corrections and to characterize the near surface model which is often a major source of wavefield distortion and consequently reduces the quality of the seismic images at the exploration target level (Strobbia et al., 2010). The method will rely on the study of the dispersion curves that can be used to estimate near-surface properties.

However, the fundamental mode of the Rayleigh wave is not so sensitive to V_P and has only limited penetration depth (Ernst, 2008) . To assess the possibility to retrieve V_P from surface waves , analysis by adding higher modes to inversion was used, where a sensitivity study have been performed:

1. A synthetic model has been used to simulate by a forward modeling the fundamental and higher mode of propagation; where, the sensitivity to Poisson's and velocity ratios were depicted in the dispersion curves and different domains.

2. Then, the sensitivity to Poisson's ratio has been evaluated by inverting the data.

3. A strategy for multi-modal inversion has been implemented using a Monte Carlo approach.

4. A synthetic data has been inverted to see the sensitivity to V_S , V_P or Poisson's ratio, initially with fundamental mode and then, using higher modes.

5. A statistical analysis has been proposed to compare the possibility of improvement on V_P with higher modes respect to fundamental modes. In case to be presented during the analysis.

6. Finally, the approach has been applied to a real data from an hydrocarbon exploration acquisition on land, where the target was to depict the Poisson's ratio (or V_P).

Some important features that will be addressed during this master thesis will take into account:

A qualitative and quantitative analysis to compare the improvements toward handling with higher modes respect to fundamental mode to retrieve V_P or Poisson's ratio.

The experimental dispersion curves are going to be obtained by the processing of the seismic data and from here, the thicknesses and V_S are going to be retrieved by the inversion model that will be useful to get the final V_P model. The solution of this inversion problem will be deal previously on the based of Monte Carlo multi-modal approach as mentioned in step 3.

The final fitting of the modal curves will be calculated on the base of a root mean square error (RMS). So, this will allow to select the best fitting models derived from the Monte Carlo multimodal inversion, that will be obtained, from the determinant misfit based on the Haskell Thomson matrix (Haskell, 1953) modified by Maraschini, (2007). It has to be mentioned, that when the inversion is performed with fundamental mode only, the higher modes are not expected to be matched.

Several assumptions could be proposed during this work in order to find some representative results. In consequence, some input parameters of the Monte Carlo multimodal inversion could be changed or fixed , in order to see any sensitivity to V_P or Poisson's ratio.

1.2 Numerical code for Surface Wave Analysis

For this thesis a previously code developed in Matlab environment (Maraschini, 2007) for the inversion of Rayleigh waves is going to be used. This code is composed by two parts: The forward model and the inversion model. The code used for forward modeling was developed at Politecnico di Torino (See references: Foti, (2000) and Strobbia, (2003)) and further, improved by Maraschini, (2007) who implemented the Haskell and Thomson matrix with the modification suggested by Dunkin, (1965). Also, the Inversion algorithm was developed implementing a Monte Carlo approach where there is randomly sample the model space and the solution is reconstructed according to acceptable models . Moreover, two choices for the misfit distance were considered. (Tarantola, 2005).

Chapter 2

Theoretical Background

2.1 Introduction

This chapter aims at providing the theoretical basis to understand this thesis work. –Seismic wave propagation is schematically outlined with particular focus on surface waves.

2.2 Body Waves

Seismic wave : A periodic vibrational disturbance in which energy is propagated through or on the surface of a medium without translation of the material. Waves can be differentiated by their frequency, amplitude, wavelength and speed of propagation. Seismic waves are waves of elastic energy, such as that transmitted by P-waves and S-waves, in the frequency range of approximately 1 to 100 Hz (Oilfield Glossary Schlumberger , 2013).

Compression or P-waves : The particle motion is parallel to the direction of propagation as shown in fig. 2.1(a). They propagate equally well in solids and fluids. P-waves are the waves studied in conventional seismic data.

Shear or S-waves : The particle motion is perpendicular to the direction of propagation as shown in fig. 2.1(b). Travel more slowly than P -waves and cannot

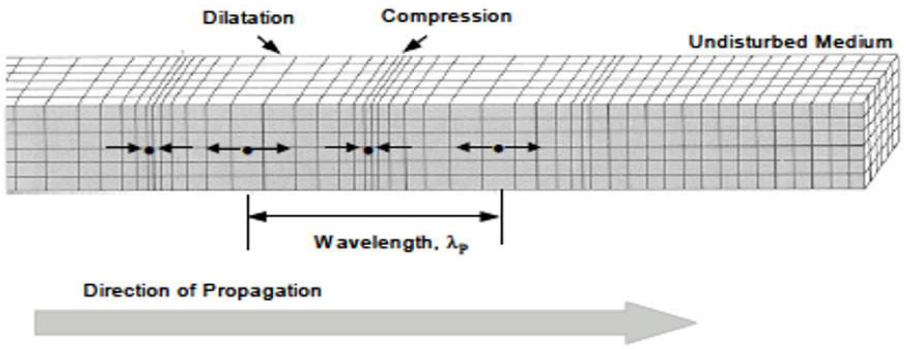

(a) Compressional waves

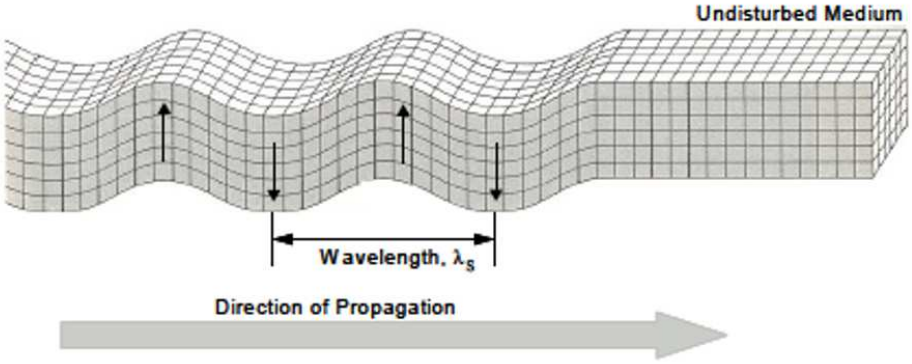

(b) Shear waves

Figure 2.1. Body waves within an uniform and infinite medium. (After Stokoe and Santamarina, 2000)

travel through fluids because fluids do not support shear. Interpretation of S-waves can allow determination of rock properties such as fracture density and orientation, Poisson's ratio and rock type by cross-plotting P-wave and S-wave velocities.

The velocity is defined as the rate at which a wave travels through a medium or the rate at which a body is displaced in a given direction. It is a property of the medium.

The P and S- velocity (V_P and V_S) are defined as:

$$V_P = \sqrt{\frac{K + \frac{4G}{3}}{\rho}} = \sqrt{\frac{E(1-\nu)}{\rho(1+\nu)(1-2\nu)}} \tag{2.1}$$

$$V_S = \sqrt{\frac{G}{\rho}} \tag{2.2}$$

Where: ρ is the mass density , G is the shear modulus, ν is the Poisson's ratio and K is the bulk modulus.

In consequence, that the velocity of wave propagation is related to density and elastic modules. The link, between the V_P and V_S can be expressed by the Poisson's ratio (ν), an important elastic constant, that will be used during the whole thesis. See equation: 2.3

$$\nu = \frac{[\frac{1}{2}(V_P/V_S)^2 - 1]}{[(V_P/V_S)^2 - 1]} \tag{2.3}$$

Where, V_P is the p-wave velocity , V_S is the shear wave velocity and ν is the Poisson's ratio.

Also, a convenient way to express the same equations could be according to the ratio of V_P to V_S , which could be derived from equation (2.3).

$$\frac{V_P}{V_S} = \sqrt{\frac{1-\nu}{0.5-\nu}} \tag{2.4}$$

Where, V_P is the p-wave velocity , V_S is the shear wave velocity and ν is the Poisson's ratio.

Figure 2.2, shows the variation of V_P/V_S according to equation: (2.4). It can be seen that the relationship between these two parameters is non linear.

A Poisson's ratio equal to 0.5, theoretically represents an incompressible material (note that condition of ground motion are undrained, and consequently saturated soil is suppose to have $\nu \to 0.5$) ; hence, $V_P = \infty$, so the ratio $V_P\ /V_S = \infty$.

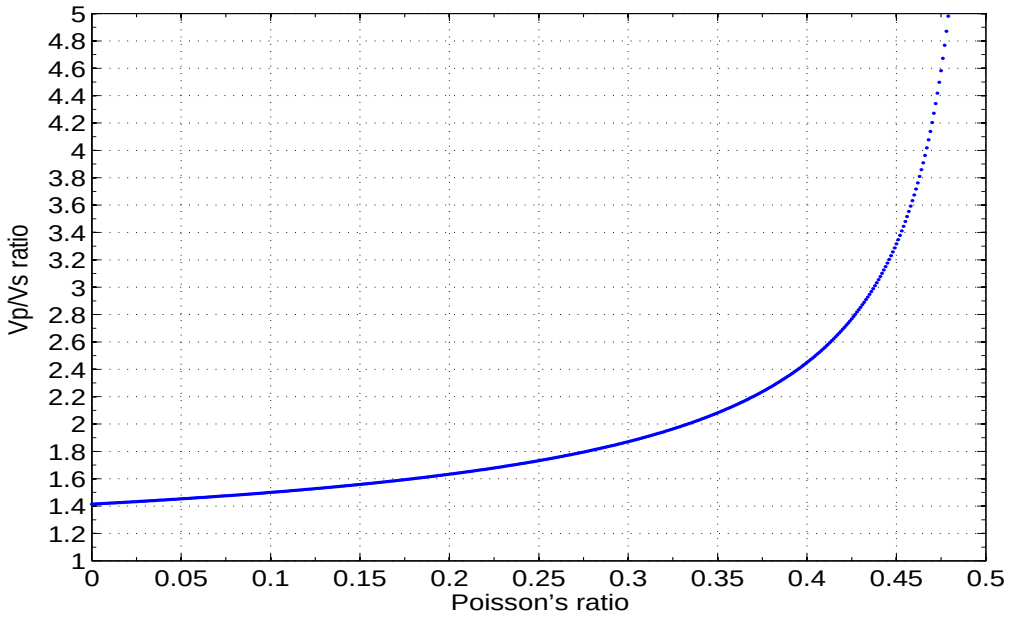

Figure 2.2. Velocity ratio V_P/V_S vs Poisson's ratio

2.3 Basic Principles of Surface Waves

In the context of seismic explorations the near surface is often considered as the shallow part of the sub-surface whose properties, can distort or degrade the observed response of deeper layers.

Surface waves can be defined as those waves which propagate at the interface between two media ; in particular one could say that they can only exist where there is a free surface, for instance, at the boundary between the Earth and air, or the Earth and water. In this view, near surface can be described as a layered waveguide in which the upper boundary is the free surface and the lower boundary is the bottom of the weathering layer.

Several types of surface waves can be generated: Rayleigh waves, Scholte waves (in shallow water environments) , Love waves (on horizontal components when properly excited) , Lamb waves, Stoneley waves (that typically propagate along a solid- fluid interface, and more rarely a solid-solid interface) and guided P and S-waves (Boiero et al., 2013). In this thesis we will focus on Rayleigh waves, that

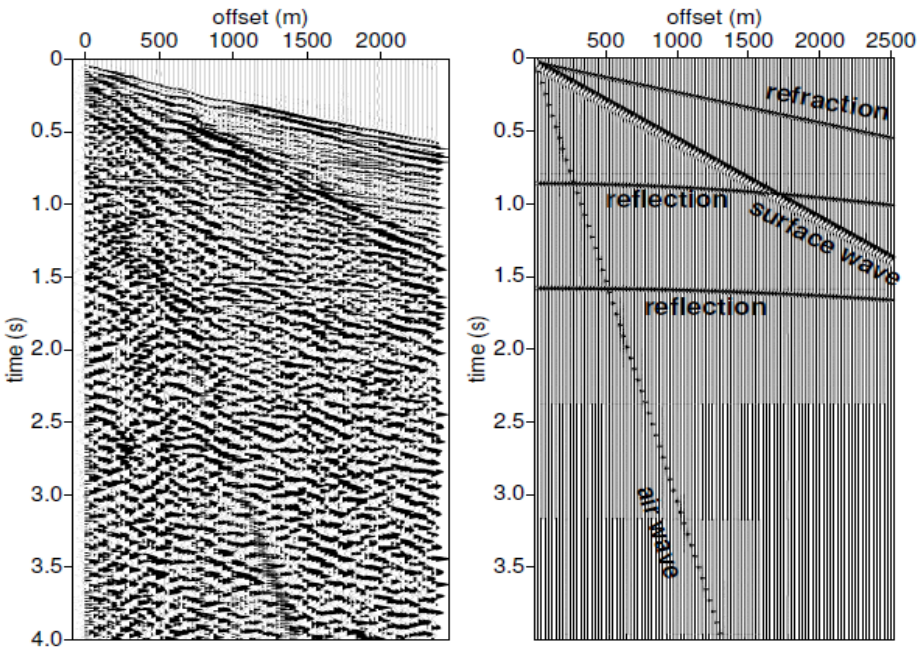

Figure 2.3. Field seismic shot record from land survey (left) and synthetic seismogram (right) with the main events (after Drijkoningen, 2011)

can be analyzed to provide near surface velocity models, because they are easily generated and detected.

Usually, surface waves are generally referred as *ground roll* in exploration seismic records. An example of a land record for seismic exploration is in fig. 2.3, where reflection, refraction , air waves and surface waves are illustrated.

2.4 Rayleigh Waves

When a mechanical disturbance is generated in any kind of solid medium, a stress wave field is produced, and energy propagates away from the disturbance. The simplest solid medium is a single-phase, linear, elastic homogeneous, isotropic, continuum material. This medium is often used as a first approximation to characterize an uniform soil or rock deposit or uniform layers within a soil or rock (Stokoe and Santamarina, 2000).

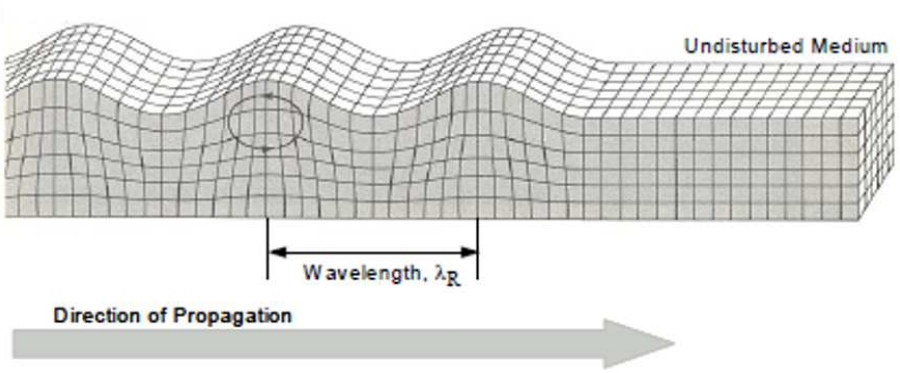

Figure 2.4. Rayleigh waves along the surface of a uniform half-space

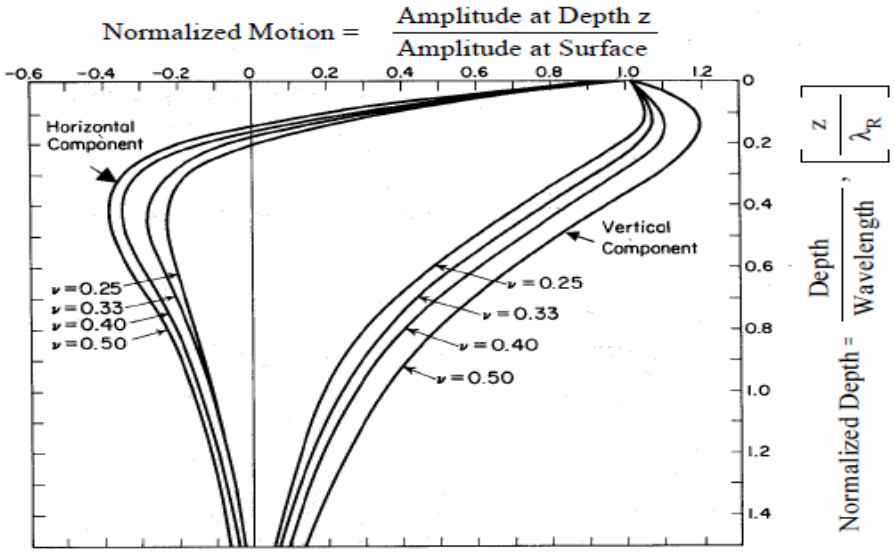

Figure 2.5. Variation in Normalized Particle Motions with Normalized Depth for Rayleigh Waves Propagating Along a Uniform Half Space (After Richart et al., 1970)

Rayleigh wave is a type of surface wave in which particles move in an retrograde elliptical path within the vertical plane containing the direction of wave propagation, as is shown in fig. 2.4. The decay with depth of the vertical and horizontal components of Rayleigh wave particle displacements is depicted in fig. 2.5, where the depth axis is normalized by the Rayleigh wavelength.

The wavefront of body and Rayleigh waves are shown in fig. 2.6 , in this case,

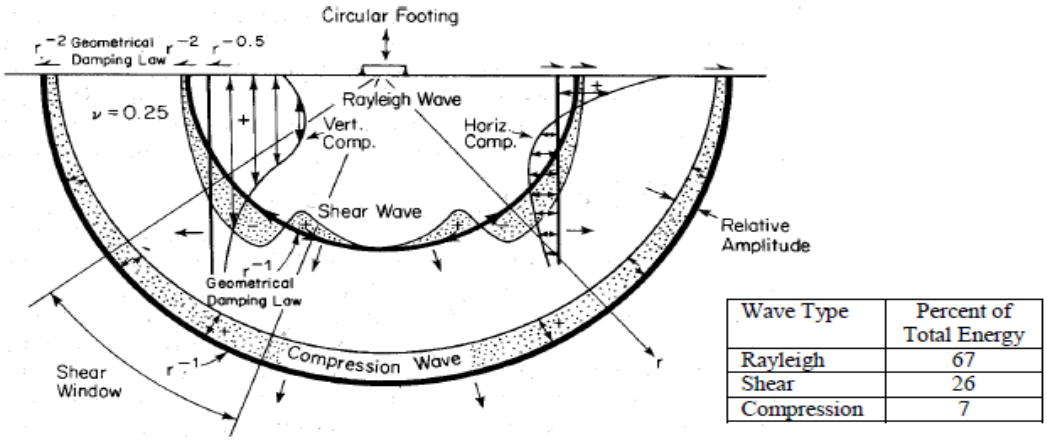

Wave Type	Percent of Total Energy
Rayleigh	67
Shear	26
Compression	7

Figure 2.6. Distribution of Stress Wave Motions from a Vibrating Circular Footing on a Homogeneous, Isotropic, Elastic Half Space (After Woods, R.D. 1968).

body waves propagate away from the source on hemispherical wavefronts while the Rayleigh waves propagates on a cylindrical wavefront, i.e. their amplitude decreases with distance as $\frac{1}{\sqrt{r}}$. Rayleigh waves are also more energetic propagating approximately 67 % of the energy coming from a source located at the free surface (reason why surface waves are dominant events in seismic records and are easy to acquire) and at far offset with respect to body waves, as these are subject to spherical spreading and therefore their amplitude decreases as $\frac{1}{r}$.

2.4.1 Geometrical dispersion of Rayleigh waves

Rayleigh waves are non dispersive in an uniform elastic medium. The term non-dispersive indicates that the propagation velocity is independent of frequency. However, a model with layered medium (stratigraphy) and other heterogeneities cause frequency (f)- dependent velocity (v).

The fundamental premise on which surface-wave characterization method is based , rely in that Rayleigh waves propagation depends on their wavelengths. This fact is responsible for the geometric dispersion, i.e., different frequencies propagate with different phase velocities. (Socco et al., 2010)

The phase velocity of Rayleigh wave (V_R) , depends primarily on the material

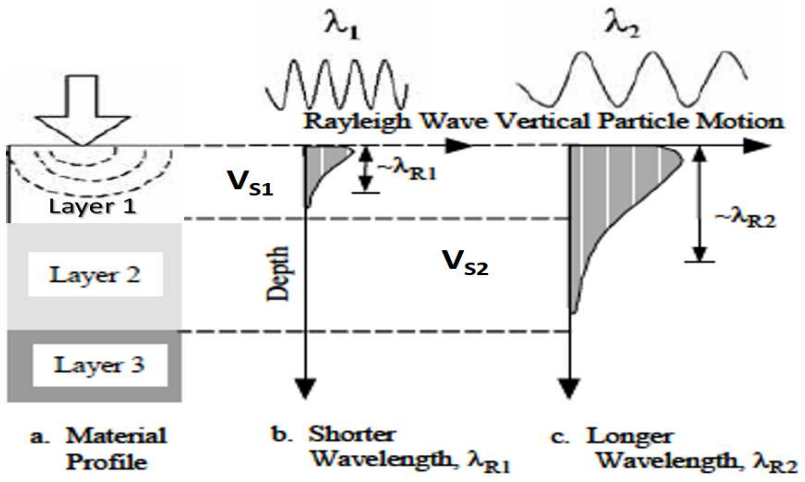

Figure 2.7. Schematic representation of dispersion of Rayleigh waves (Adapted from: Socco and Strobbia, 2004)

properties as V_S , mass density (ρ) and Poisson's ratio (ν) over a depth of approximately one wavelength. In fig. 2.7, the dispersion of Rayleigh waves are shown according to the vertical displacement associated with a short and long wavelength.

Surface wave propagation is a multi-modal phenomenon. For a given sub soil model, each frequency can travel with several velocity values. The curves in the frequency–velocity space representing the propagation modes of the model are called modal dispersion curves and they depend only on model parameters (Maraschini and Foti, 2010). They can be estimated using several spectral analysis aiming at retrieving the fundamental and higher modes of surface wave propagation in a wide frequency band. Often the fundamental mode (the slowest one) is the most energetic (Maraschini and Foti, 2010). So, the information in the dispersion curves of the fundamental mode can sometimes have most of the required information and simplify and reduce the computational time associated with the inversion. An example of a fundamental mode is shown in fig. 2.8 generated through the forward modeling of a set of model parameters.

Just to clarify, the forward problem is used to compute the dispersion curves when the model parameters are known (V_S , ρ , density and ν). While the inverse problem is used to estimate the model parameters if the data (dispersion curves: Rayleigh-wave phase velocities for different frequencies) were measured. This will

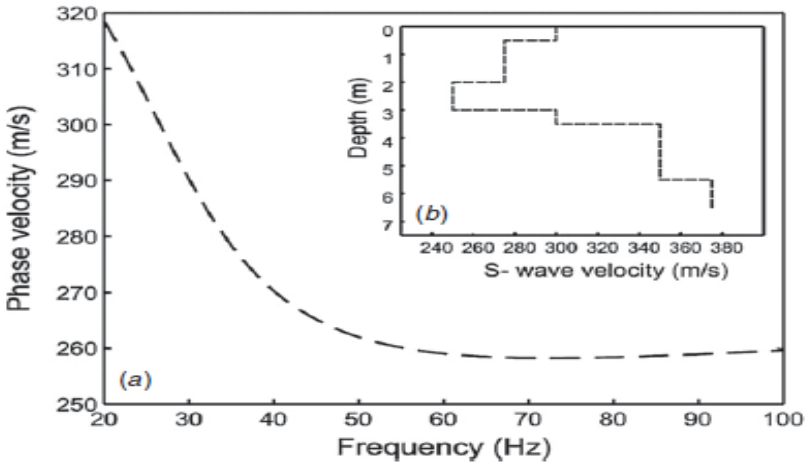

Figure 2.8. Dispersion curve. a) Fundamental mode generated forwardly b) V_S velocity model profile (After Caylak, C, et al., 2012) .

be explained in more general detail in chapter 3.

The following subsection will focus on higher modes, since their contribution are important in surface wave inversion, because they allow more information to be exploited, increase investigation depth and improve model resolution (Maraschini et al., 2010).

2.4.2 Higher modes of Rayleigh wave propagation

An interesting and problematic aspect of propagation of Rayleigh waves in vertically heterogeneous media is that propagation can occur at different modes; in fact, several modes with different propagation velocities for the same frequency can occur at the same time, making it difficult to interpret the dispersive properties of the investigated medium.

Figure 2.9 shows the multi-modal phenomenon of Rayleigh waves, here, it is possible to observe at the right side, the normalized vertical displacement for the fundamental mode and the first and second higher modes. In contrast, at the left side, there is the phase velocity vs frequency, at different modes of propagation.

The modal curves are only related to the kinematics of wave propagation. They are a characteristic of the layered medium and theoretically can be simulated

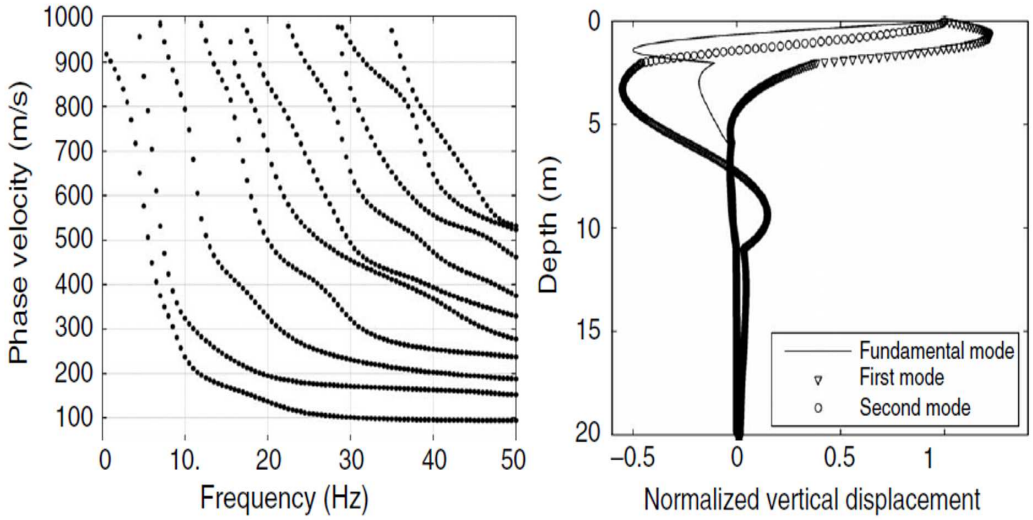

Figure 2.9. Example modal curves (left figure) and modal displacements for 20 Hz (After Socco et al., 2010)

considering only the mechanical and geometric properties of the model. (Socco et al., 2010)

From a mathematical point of view, Rayleigh waves can be modeled in terms of eigenvalues and eigenfunctions. Assuming a laterally homogeneous medium, plane strain field, imposing the boundary conditions of the waves in a half-space with a free surface.– No stress (σ) at the free surface and no σ and strain (ϵ) at infinity. And imposing the continuity of ϵ and σ at the interfaces (Aki & Richards,1980). Equation of motion can be formulated as:

$$\frac{d\mathbf{f}(z)}{dz} = \mathbf{A}(z)\mathbf{f}(z), \tag{2.5}$$

Where the vector $\mathbf{f}$ is made up of two displacement eigenfunctions and two stress eigenfunctions, $\mathbf{A}$ is a matrix of 4×4 which depends on the vertical distribution of the soil properties and z is the vertical axis. (Socco et al., 2010).

The solution to this equation is non-trivial only for specific values of the wavenumber. The resulting equation is known as the Rayleigh secular equation.

That can be written in implicit form as:

$$F_R[\lambda(z), G(z), \rho(z), k_j, f] = 0, \tag{2.6}$$

Where k_j is the wavenumber of the jth mode of propagation, f is the frequency, λ is the Lamé parameter, as defined in Hooke's law, G is the shear modulus and ρ is the mass density. The eq. 2.6 can not be solved analytically; i.e., a numerical solver is needed. In a vertically heterogeneous media, the k is a multivalued function of frequency that gives a reasonable mathematical expression for the so- called modal curves.

The transfer -matrix method , originally proposed by Thomson (1950) and modified by Haskell (1953) is the oldest and probably most famous approach to resolve the eigenvalue problem for the stratified medium with homogeneous linear elastic layers.

Chapter 3

Surface wave method

3.1 Introduction

After schematically described the main features of surface wave propagation we here outline the analysis method that exploit surface waves for retrieving subsurface velocity models. – The basic analysis is made of three main steps: acquisition, processing and inversion. Here we describe them and we focus on the multimodal inversion approach later used in this thesis.

3.2 Principle of the surface wave method

Traditionally, the surface waves in land seismic data has been regarded as coherent noise to be removed. But in some cases, with a complex near surface or spatial aliasing, their attenuation can be difficult to achieve.

Regardless of the type of surface wave used, the standard procedure for surface wave analysis can be divided into three main steps (Socco et al., 2010): a).- Acquisition, b).- Processing and c).- Inversion.

Figure 3.1, shows the work-flow of surface wave analysis. The first step is acquisition of the experimental data (seismogram: time vs offset) , then, the signals

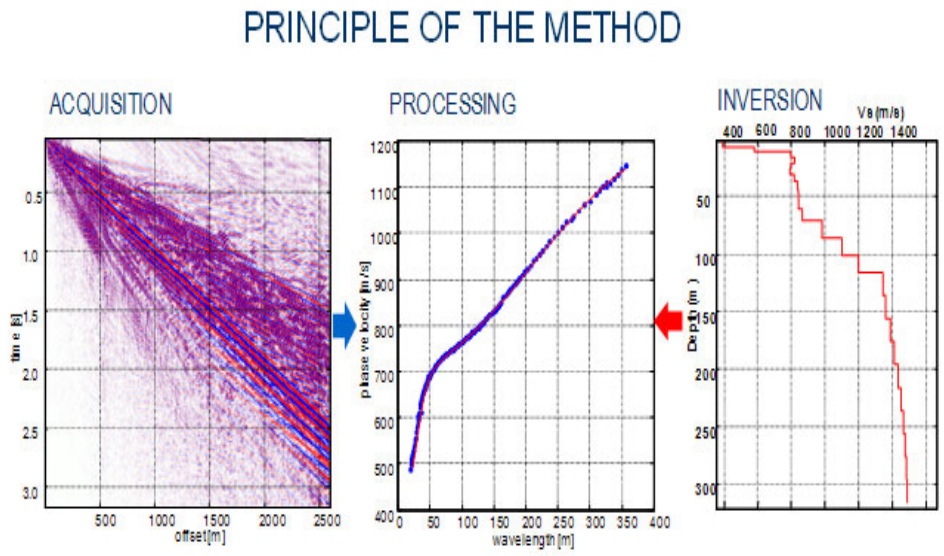

Figure 3.1. Principle of the surface wave method . (From : Schlumberger, WesternGeco, 2013)

are processed to obtain the experimental dispersion curves and finally, the inverse problem is solved to estimate the model parameters.

Each step can be performed using different approaches, according to the scale of the problem, the target, the complexity of the subsoil property distribution, and the available equipment and budgets.

3.2.1 Acquisition

The main aspects to be considered during the acquisition in the $t - x$ domain are related to:

Space sampling

Array length: The array length affects the wavenumber resolution δk and therefore the possibility of mode separation. Long arrays are preferred because they improve the modal separation and they reduce the data uncertainties. In contrast, short arrays are less sensitive to lateral variations, produce a better S/N ratio and are less affected by high frequency attenuation. (Socco & Strobbia, 2004)

Receiver spacing : According to the Nyquist sampling theorem, the maximum wavenumber that can be identified depends on following relationship:

$$k_{Nyq} = \frac{1}{2}\frac{2\pi}{\Delta X} = \frac{\pi}{\Delta X} \tag{3.1}$$

Where ΔX is the receiver spacing and k_{Nyq} is the Nyquist wavenumber. The the energy associated with a wavenumber higher than the k_{Nyq} will be aliased, but possible to recover if possible recognized.

Receiver number: Affects the propagation of the uncertainties over the data, i.e., For a given array length, increasing the number of receivers reduces the uncertainty.

Source offset: A source-offset equal to the desired investigation depth has been suggested by Park et al. (1999).

Time sampling:

Time sampling has a minor effect compared to spatial sampling. Just, the time window has to be long enough to record the whole surface wave on all traces, e.g., with long arrays at low velocity sites, several seconds would be needed. (Socco & Strobbia, 2004)

The main task of the acquisition is to measure surface waves and thus produce information about the dispersion and attenuation characteristics. The data to be processed and inverted should have a high signal to noise (S/N) ratio over a wide frequency band, and should allow for modal separation and recognition . Further, the data acquired should allow for separating and filtering out coherent noise and estimation of uncertainties.

At the exploration scale, most near-surface applications are based on multi-station approaches. They are often identified by the phrase multi-station analysis of surface waves (MASW), introduced by researchers at the Kansas Geological Survey (Park et al., 1999; Xia et al., 1999). This method is the one, on which this thesis will main focus on. (Note: The spectral analysis of surface waves (SASW), which is a two station acquisition method is out of the scope of this master thesis).

The use of multiple receivers enhances the production rate in the field , makes

data processing much faster and less sensitive to operator choices, supplies more robust and accurate dispersion curves which improves the possibility of mode separation and identification, and allows for the recognition and the interpretation of other seismic events present in the data (such as refracted and reflected body waves) (Socco et al., 2010). The most usual array is a linear, evenly spaced array of vertical low-frequency geophones (4.5 Hz) with an in-line-end-off configuration.

Surface wave dispersion can be extracted from active data, where, the acquisition is performed on purpose to get the surface wave information and approaches based on processing the data gathered for other seismic methods, such as reflection surveys. The advantage of on purpose data concerns the choice of optimal equipment and testing setup. The acquisition of deep exploration seismic data focus on body wave analysis, even though, significant presence of surface waves can be encountered. Additionally, the seismic reflection for hydrocarbon exploration, is often performed with larger budgets and more sophisticated equipment, which leads to have more information on surface waves.

To analyze surface waves in exploration data sets, one should perform a preliminary evaluation of the data to assess the presence and quality of the surface waves in the seismic records because of the high- frequency sensors, sensor groups , and low cut filters that could affect significantly the surface-wave signals. (Socco et al., 2009).

As the depth of penetration of surface waves is proportionally to their wavelength, the optimum results are achieved by using sources and detectors that have the maximum bandwidth, especially at low frequency, typical down to approximately 3Hz. (Schlumberger, WesternGeco, 2013).

3.2.2 Processing

The processing has the task of estimating the dispersion curve from the seismic records. Several wave-field transform are widely used to perform the analysis, especially in domains where surface waves are easily identified, e.g., frequency - wavenumber ($f - k$) transform, or f-v transform. Some processing includes muting

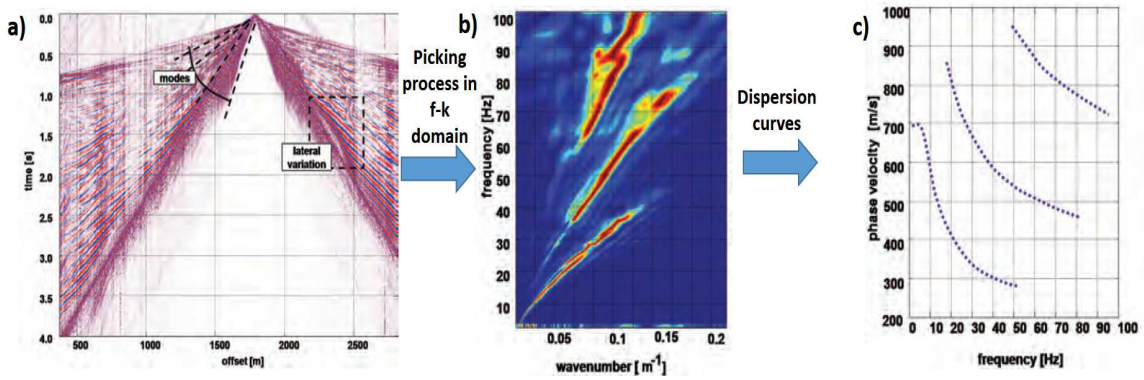

Figure 3.2. Flow diagram of the processing step. a) Shot gather, b) f-k transform and c) Dispersion curve. (After: Strobbia, et al.,2010, modified)

of body waves , filtering of noise etc.(In the case of MASW a normalization of the traces is applied in the frequency domain prior to the transforms).

The frequency- wavenumber $(f-k)$ transform is the first step of processing. Surface waves, can be identified as the dominant events or energy density maxima in a wide frequency band. Some pre-processing like muting, filtering in the frequency-offset domain, etc. is performed to remove eventual low quality portions of the data.

When a good image of the energy density of the propagation is obtained, the analysis of the energy maxima, has to be performed, with an automatic search of maxima. When maxima have been identified in $f-k$ domain, the phase velocities are simply computed as $v = \frac{2\pi f}{k}$. (Socco & Strobbia, 2004).

A direct example of the processing of a seismogram can be seen in figure 3.2, a).- Corresponds to a shot gather from seismic acquisition , b).- Corresponds to the spectrum in the $(f-k)$ transform discussed previously and the picking process associated to the energy maxima c).- It is associated to the graph of phase velocities against the frequency as discussed . In the shot gather, highly dispersive, multimodal Rayleigh waves are present with also high lateral continuity, that can be observed according to the lateral variations of the gather in Figure 3.2 (a). This flow diagram explained the topics discussed in the processing. Reference: [Strobbia et al., 2010].

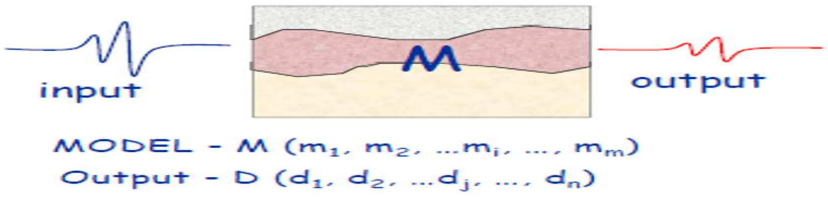

Figure 3.3. Conceptual scheme of a geophysical test

3.2.3 Inversion

In geophysics the term inversion means to estimate a series of parameters of a model from a set of observations (See figure 3.3).The solution of inverse problems is often applied for the interpretation of geophysical data.

For surface wave methods, the inversion supplies the estimated velocity from the dispersion characteristics derived by the data processing, and represents the last step of the method. It is important to address that the surface wave method inverse problem is non linear and mix determined; this makes the solution very sensitive to initial model in local search methods.

The more widely used approach is the linearized iterative least-squares method. But, different approaches can be proposed for the inversion, e.g., a simplified technique which assumes that the shear wave velocity is equal to 110 per cent of the Rayleigh phase velocity to a depth equal to $\lambda/3$ or $\lambda/2$ (Abbiss, 1981) ; the trial and error method by Stokoe et al. (1994) and the Monte Carlo method among others (Maraschini and Foti, 2010).

3.3 Methods of inversion

Usually inversion is performed by assuming an *a priori* value of density (ρ) and Poisson's ratio (or V_P) and inverting just for V_S and layer thickness. There are studies that say that sensitivity to Poisson's ratio is considered poor and so, this is not an unknown of the inversion in most of case. –On the other hand, same studies have also evidenced that a wrong assumption of ν can lead to error in inversion

results.

As stated in chapter 2, for higher modes of Rayleigh wave propagation, the solution of equation (2.5) is not trivial. The solution of an inverse problem is a probability density function of the model space, which can present several local minima. So, the uniqueness of the solution is not guaranteed (Menke, 1989). To find the model associated with the maximum probability, deterministic or stochastic algorithms can be used.

The deterministic algorithm can converge into a local minimum because the model space is not entirely explored (Curtis & Lomax, 2001). Consequently, deterministic algorithms are suitable when *a priori* information is available. When the probability density function presents several local minima, and *a priori* information is not available to constrain the solution, stochastic methods are more suitable because they allow the whole model space to be investigated and avoid linearization (Socco & Boiero, 2008) .

Nevertheless, deterministic inversion algorithms are computationally efficient, whereas stochastic are computationally intensive because of the huge number of models that should be tested to provide a meaningful result. For this reason, stochastic algorithms require efficient forward modeling (Maraschini and Foti, 2010).

3.3.1 Multimodal inversion of surface waves

The issues related to multimodal inversion include dealing with the separation and identification of different modes in the spectrum. This can be done only if many sensors and a long array are available (Foti et al., 2002); whereas when a two station acquisition geometry is considered, only an apparent dispersion curve can be identified (Tokimatsu, 1997).

The major problem in multimodal dispersion curve inversion is mode numbering. A branch of the apparent dispersion curve can derive from the superposition of modes, or some modes may be misidentified in the experimental data set. Zhang & Chan (2003) remarked on the consequences of mode misidentification. If part of the dispersion curve is associated with an incorrect mode number, in particular in the

low-frequency range, the consequent errors are greater than errors due to inaccuracy.

To solve this problem, some authors (e.g. Ganji et al. 1998; Forbriger 2003) compared the experimental apparent dispersion curve with a synthetic apparent dispersion curve or used the full waveform inversion. These approaches are computationally expensive because they require a more realistic simulation of the wave propagation.

An approach for the inversion of multiple modes without the need to number modes was proposed by Ernst (2007) and successively implemented within a deterministic algorithm by Maraschini et al. (2010). This approach uses a misfit function based on the properties of the solution of the forward problem, allowing for a substantial saving of computational costs. In this thesis, we implement the same misfit function within a stochastic algorithm (Maraschini and Foti, 2010) .

3.4 Conclusion on the surface wave method

- Surface waves can be analyze to provide a near surface V_S model
- Usually V_P is not retrieved
- The analysis can be performed in several ways and more critical issue is handling higher modes in the inversion.
- There are several methods that can be used to invert data characterized by higher modes.

Chapter 4

Analysis on a synthetic model: Forward modeling

4.1 Introduction

This chapter presents an analysis of the sensitivity of surface wave modal curves to Poisson's ratio (or V_P). –The objective is to assess if by including higher modes information the sensitivity to P-wave, usually considered very week, can be increased.

To perform the sensitivity analysis a reference 1D velocity model will be used to simulate fundamental and higher modes modal curves. The Poisson's ratio of the reference model is then changed and the new modal curves are compared to the reference ones. Statistical analysis at the comparison results will be presented.

The sensitivity analysis is performed considering different reference models with constant or variable Poisson's ratio with depth.

4.1.1 Algorithm used for simulating the data

In order to solve the eigenvalue problem, we are going to based in the development of the Thomson–Haskell method (Thomson, 1959; Haskell, 1953), which is applicable to a stack of homogeneous layers overlying a half-space with the Dunkin's modification

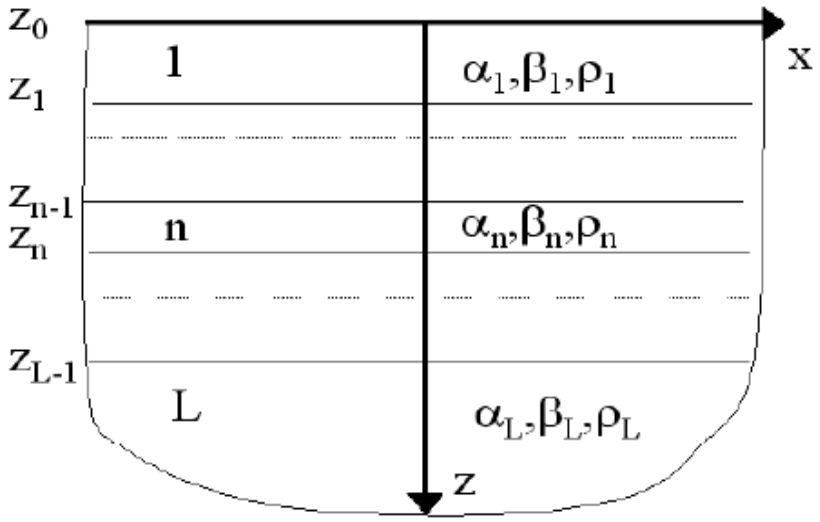

Figure 4.1. A multilayer elastic system (After Strobbia, 2003)

that solve the forward problem of Rayleigh wave propagation in a layered system (Strobbia, 2003) .

Considering a 2D geometry (plane wave equation, fig. 4.1) and using Helmholtz decomposition in the layered system (nth layers) we have the dilatation and shear potentials (Φ_n and Ψ_n) , and applying the Fourier transform potentials with the Rayleigh surface wave conditions (compressional wave velocity from this deductions renamed as (α) is higher than shear wave velocity renamed as (β) and the phase velocity is lower than β), we can express the displacements and the stresses from the potentials (Strobbia, 2003) as:

$$U_x = \frac{\partial \Phi}{\partial x} - \frac{\partial \Psi_y}{\partial z} = ik\overline{\varphi}_n^+ + ik\overline{\varphi}_n^- - n_n\overline{\psi}_n^+ + n_n\overline{\psi}_n^- \tag{4.1}$$

$$U_y = 0 \tag{4.2}$$

$$U_z = \frac{\partial \Phi}{\partial z} - \frac{\partial \Psi_y}{\partial x} = \overline{m\varphi}_n^+ - \overline{m\varphi}_n^- + ik\overline{\psi}_n^+ + ik\overline{\psi}_n^- \tag{4.3}$$

$$\sigma_{xx} = \rho\left(\frac{\partial^2\Phi}{\partial t^2} - 2\beta^2\frac{\partial^2\Phi}{\partial z^2} - 2\beta^2\frac{\partial^2\Psi_y}{\partial t^2}\right) \tag{4.4}$$

$$\sigma_{xy} = 0 \tag{4.5}$$

$$\sigma_{zx} = \rho\left(2\beta^2\frac{\partial^2\Phi}{\partial x\partial z} - 2\beta^2\frac{\partial^2\Psi_y}{\partial z^2} + \frac{\partial^2\Psi}{\partial t^2}\right) \tag{4.6}$$

Where:

- U_x, U_y and U_z are the three scalar functions of displacements
- Φ is the scalar potential of displacement
- Ψ is the vector potential with the three components (Ψ_x , Ψ_y and Ψ_z) such that the displacements satisfy the equation of motion.
- U_y and σ_{xy} are zero since it is considered a 2D geometry of a stress free plane XZ normal to the Y-axis, lying in a elastic medium.
- β is the shear wave velocity
- α is the compressional wave velocity
- k is the wave number
- $\omega = 2\pi f$ is the Pulsatance or angular frequency
- σ is the stress field
- c= is the speed of Rayleigh waves
- The terms $\overline{m}$ and $\overline{n}$ part of the Fourier transform potentials are: $\overline{m} = |\omega|\left(\frac{1}{c^2} + \frac{1}{\alpha_n^2}\right)^{0.5}$

  $\overline{n} = |\omega|\left(\frac{1}{c^2} + \frac{1}{\beta_n^2}\right)^{0.5}$

The terms $\overline{\varphi_n^+}$, $\overline{\varphi_n^-}$, $\overline{\psi_n^+}$ and $\overline{\psi_n^-}$ are the parameters to describe the Fourier Transform:

$\overline{\varphi_n} = A_n e^{m_n(Z-Z_{n-1})} + B_n e^{-m_n(Z-Z_{n-1})} \equiv \overline{\varphi_n^+} + \overline{\varphi_n^-}$

$\overline{\psi_n} = C_n e^{n_n(Z-Z_{n-1})} + D_n e^{-n_n(Z-Z_{n-1})} \equiv \overline{\psi_n^+} + \overline{\psi_n^-}$

Where:

- Φ is the scalar potential of displacement
- $n_n^2 = k^2 - \omega^2/\beta_n^2$
- $m_n^2 = k^2 - \omega^2/\alpha_n^2$
- β is the shear wave velocity
- α is the compressional wave velocity
- $\overline{\varphi_n^+}$, $\overline{\varphi_n^-}$, $\overline{\psi_n^+}$ and $\overline{\psi_n^-}$ are the Fourier Transform potentials of displacements
- Z is the depth of the layer (bottom of the layer)
- Z_{n-1} is the depth of the previous layer (top of the layer)

At any point in the nth layer we can compactly write the above relations between potentials, stresses and displacements (Strobbia, 2003) as:

$S_n(z) = T_n \overline{\Phi_n^z}$ and the inverse relationship as: $\overline{\Phi_n^z} = T_n^{-1} S_n(z)$

Where: $\Phi_n(z)$ is the vector containing the potentials in the nth layer defined as,

$\Phi_n(z) \equiv \left\lfloor \overline{\varphi_n^+}(z), \overline{\varphi_n^-}(z), \overline{\psi_n^+}(z), \overline{\psi_n^-}(z) \right\rfloor$

And the term, $\overline{S}_n(z)$ is the vector containing the displacements and the stresses in the same layer nth.

$\overline{S}_n(z) \equiv \lfloor \overline{u_x^n}(z), \overline{u_z^n}(z), \overline{\sigma_{zz}^n}(z), \overline{\sigma_{zx}^n}(z) \rfloor$

Where: σ_{zz}^n and σ_{zx}^n are the two stresses component in the nth layer.

The propagator matrix $\mathbf{T}$ contains the parameters of displacements and stresses of the relations 4.1 - 4.6:

$$T_n = \begin{pmatrix} ik & -n_n & ik & n_n \\ m_n & ik & -m_n & ik \\ G_n a_n & 2iG_n l n_n & G_n a_n & -2ikG_n n_n \\ 2iG_n l m_n & -G_n a_n & -2iG_n k m_n & -G_n a_n \end{pmatrix} \tag{4.7}$$

Where:

- $a = 2k^2 + \omega^2/\beta_n^2$
- G, is the stiffness
- β is the shear wave velocity
- α is the compressional wave velocity
- k is the wave number
- $\omega = 2\pi f$ is the Pulsatance or angular frequency
- $n_n^2 = k^2 - \omega^2/\beta_n^2$
- $m_n^2 = k^2 - \omega^2/\alpha_n^2$
- i makes reference to the imaginary part

By applying a straightforward calculation, not reproduced here (see Strobbia, (2003) ; Maraschini,(2007)) and applying the boundary conditions. These include: continuity of normal and shear stress across layer interfaces; continuity of horizontal and vertical displacement across layer interfaces; and the vanishing of normal and shear stress at the free surface. It allows to estimate the unknown coefficients (A_n, B_n) and (C_n, D_n) corresponding to the up-going waves at velocities depending on compressional wave velocity (α) and the shear wave velocity (β) (Everett, 2013).

It implies the existence of a linear relationship between the surface displacements $(u1, w1)$ and the bottom layer elastic wave potential coefficients.

$$\begin{pmatrix} 0 \\ 0 \end{pmatrix} = R_{11} \begin{pmatrix} u_1 \\ w_1 \end{pmatrix} \tag{4.8}$$

Where the R_{ij} matrices, each of dimension 2×2, takes into account the physics of elastic wave propagation within the multilayer system, including the boundary conditions at the material interfaces. The eq. (4.8) has a non trivial solution (u_1, w_1) for the surface displacements if and only if the determinant of R_{11} vanishes, that

is, (Everett, 2013)

$$detR_{11} = 0 \tag{4.9}$$

The eq. (4.9) is essentially an implicit equation of the form g(V, f) =0, from the Rayleigh secular equation and $detR_{11}$ is known as the Haskell–Thomson determinant (Everett, 2013). The $detR_{11}$ is the function whose roots give rise to leaking and propagating modes (Strobbia, 2003).

The forward model , i.e., the algorithm which allows to calculate modal dispersion curves and modal displacements for a given soil profile , used for simulating the data is based on the Haskell (1953) and Thomson (1950) matrix methods with the Dunkin (1965) modification. The code used was implemented by Maraschini, (2007) in Matlab language. By considering a multi-layer elastic system like the one shown in fig. 4.1 and the respective Rayleigh wave boundary conditions of the layered medium (stress free surface, continuity at layer interfaces and zero potential at infinity).

The forward operator is the $|\mathbf{T}(v, f, m)| = 0$, since modal curves corresponds to the zero values of the function (F) (Maraschini and Foti, 2010).

$$F = |det(\mathbf{T}(v, f, \mathbf{m}))| \tag{4.10}$$

Where, $\mathbf{T}$ is the Haskell–Thomson matrix (Buchen & Ben Hador,1996),$\mathbf{m}$ is the given model parameters (thickness, V_S , V_P or Poisson's ratio, and density), f are the frequencies, and v are the velocities.

The forward model algorithm simulate the model curves. The input parameters are shear wave velocity (V_S) , compressional wave velocity (V_P) or Poisson's ratio (ν) and density (ρ) and fundamental mode and higher modes are computed.

The logical scheme applied for doing the sensitivity analysis applying several times the forward modeling to different Poisson's ratio or velocity ratios (V_P/V_S) is seen in fig. 4.2.

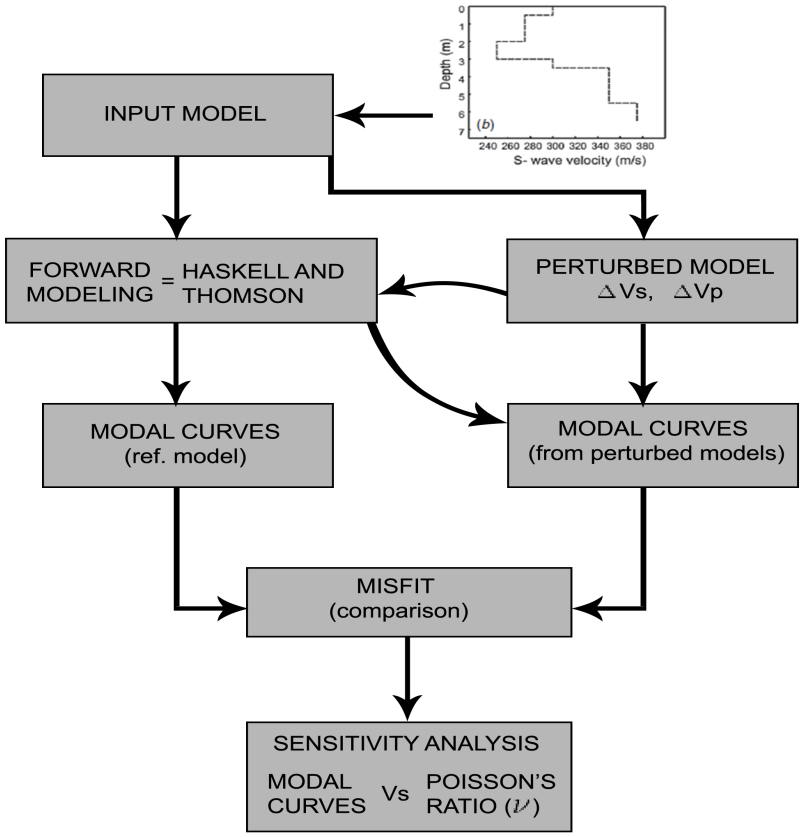

Figure 4.2. Logical scheme applied on the synthetic model for the sensitivity analysis of modal curves

4.2 Synthetic model with initial homogeneous Poisson's ratio in the layered medium

In this section, a synthetic model is used as reference . –The model properties are reported in table : 4.1.

As an initial approximation for the synthetic 1D model (Table: 4.1), the Poisson's ratio (ν) was assumed to be fixed for all layers. The fact of fixing the ν , was because the sensitivity to V_S is much larger. Since the velocity ratio (V_P/V_S) selected was 2, the immediate consequence was that Poisson's ratio took a value equal to 0.33. This value can be considered in shallow granular material in unsaturated conditions.

Table 4.1. Synthetic 1D model used for simulation and sensitivity analysis

Synthetic	Thickness [m]	V_S[m/s]	Density [Kg/ m^3]	Poisson's ratio	$V_P[m/s]$
Layer 1	3	230	1500	0.33	457
Layer 2	7	325	1500	0.33	645
Layer 3	12.5	450	1600	0.33	893
Layer 4	12.5	760	2000	0.33	1509
Half-space	∞	1361	2400	0.33	2702

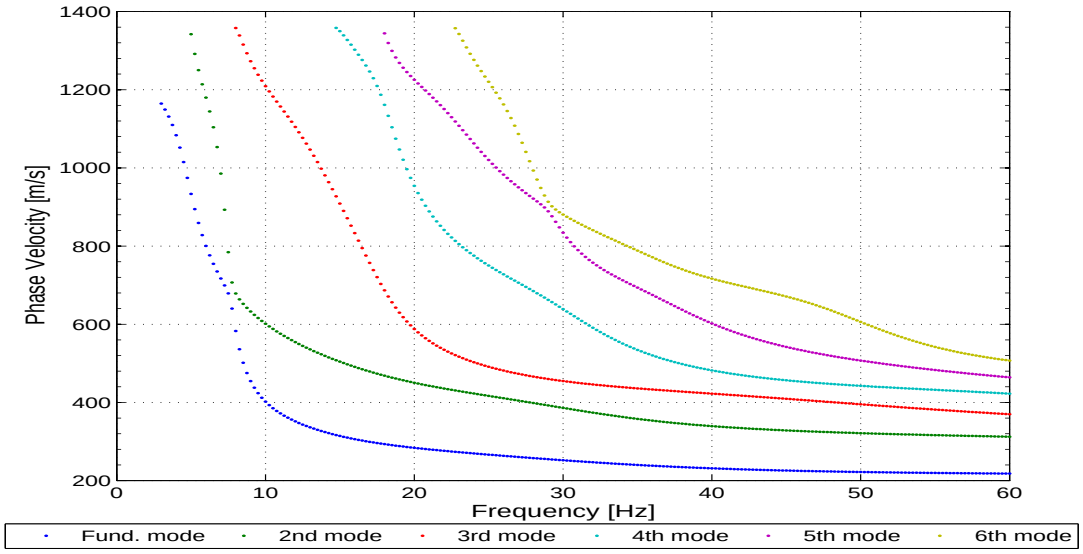

Figure 4.3. Rayleigh wave modal curves for the model of the table 4.1.

4.2.1 Sensitivity analysis

A).- Modal curve for the reference model of table 4.1:

The fig. 4.3 shows the modal curves for the reference model of table 4.1.

B).- Sensitivity analysis by varying the Poisson's ratio simultaneously in each layer.

The Figure 4.4 shows, the modal curves for different Poisson's ratio values. The sensitivity is analyzed by changing the Poisson's ratio (ν) from 0.1 to 0.49 to all the layers simultaneously. A color bar scale helps in associating the different Poisson's ratio (blue=Low ν and yellow= Higher ν) applied for the sensitivity analysis. V_P/V_S

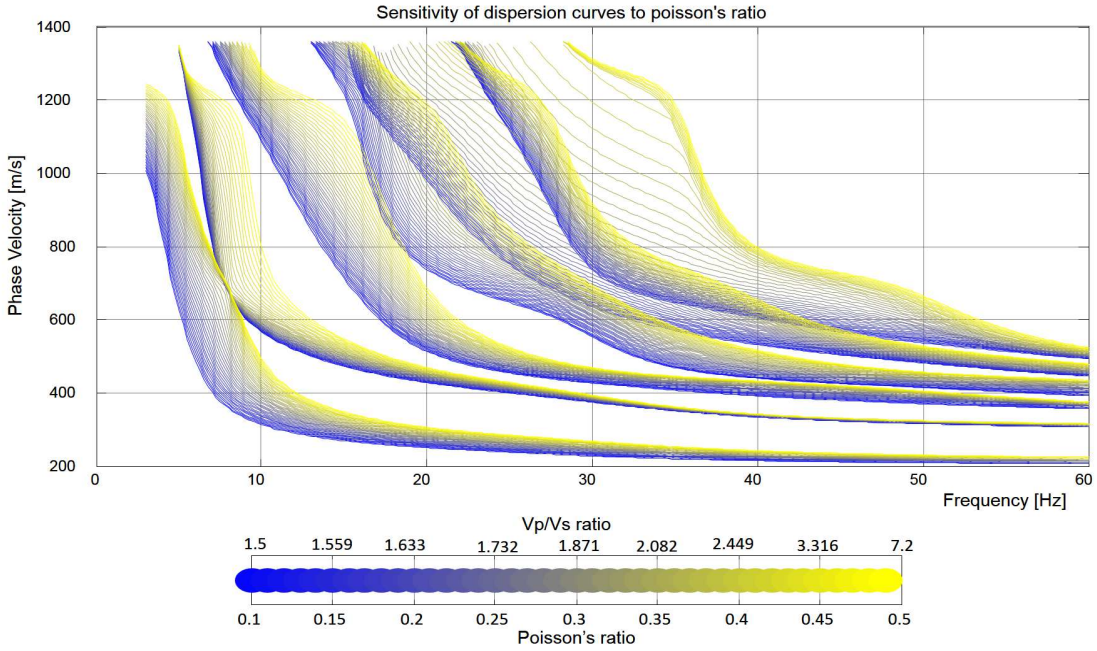

Figure 4.4. Sensitivity of the Rayleigh wave modal curves for the model of table 4.1 with Poisson's ratio varying from 0.1 to 0.49 to all the layers simultaneously.

ratio is also shown on the color bar scale (Just to reference some values of the Poisson's ratio to their equivalent in V_P/V_S ratio) . It should be remarked that as shown in chapter 2 , fig.2.2, the relation between these two parameters is not linear.

The result (fig. 4.4) shows, that when ν varies from 0.2 until 0.40 the fundamental mode and the first higher mode tend to touch themselves in the frequency band from 7.25 Hz to 8.5 Hz. Nonetheless, this behavior change for this two modes in the range of ν higher than 0.40 (value where these two modal curves tend to split again). Additionally, it is possible to observed that the sensitivity of the dispersion curves to ν in the last three modes is increasing in a wider band of frequency compare to just the fundamental mode for instance. This is important, since the higher the variation we see in the modal curves, the higher the sensitivity.

It can be mentioned the fact, that different modes show different sensitivity and that for each mode there are frequency bands which are more sensitive than others.

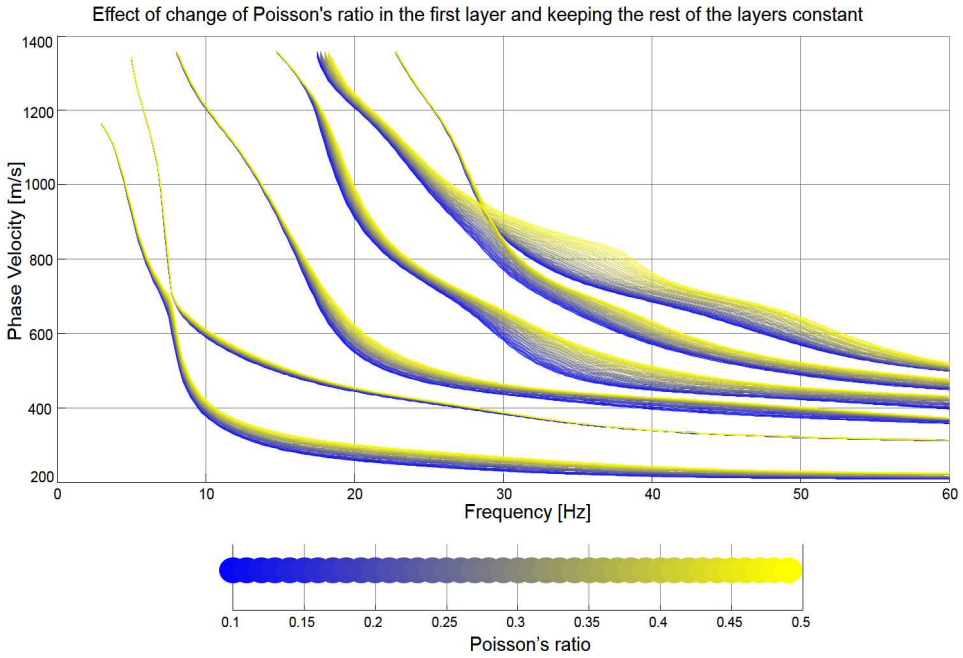

Figure 4.5. Rayleigh modal curves for the model of table 4.1 with Poisson's ratio varying for the first layer from 0.10 to 0.49.

C).- Varying the Poisson's ratio, layer by layer for the model of table 4.1 :

In fig. 4.5 we show the modal curves obtained when the Poisson's ratio is changed from 0.10 to 0.49 for the first layer only and is kept constant for the other layers. The same results are shown for variable Poisson's ratio in the other layers. Figures: 4.6, 4.7, 4.8 and 4.9

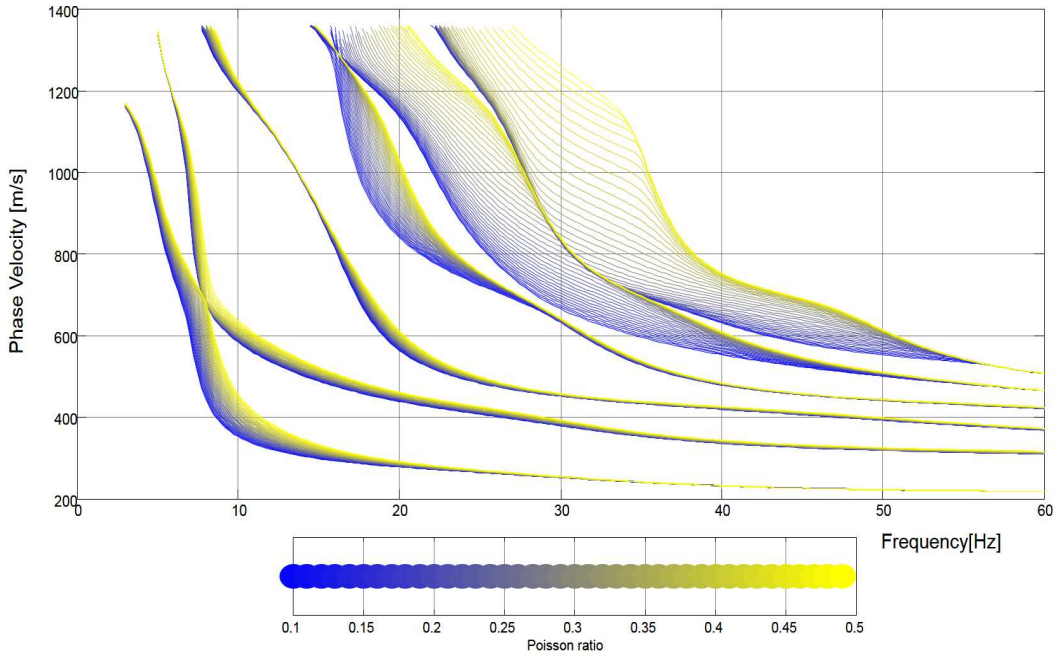

Figure 4.6. Rayleigh modal curves for the model of table 4.1 with Poisson's ratio varying for the second layer from 0.10 to 0.49

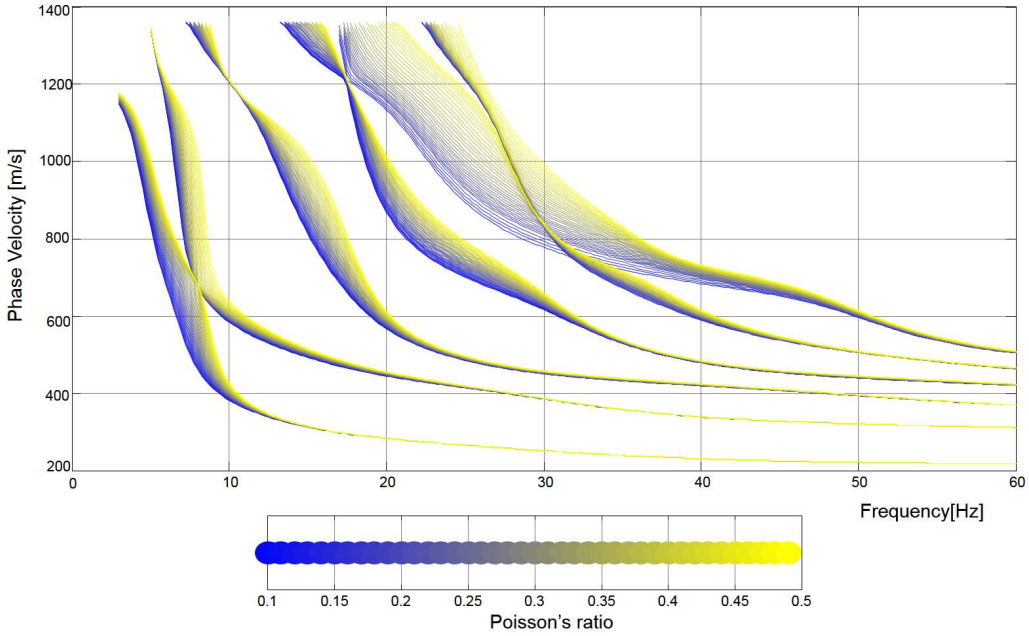

Figure 4.7. Rayleigh modal curves for the model of table 4.1 with Poisson's ratio varying for the third layer from 0.10 to 0.49

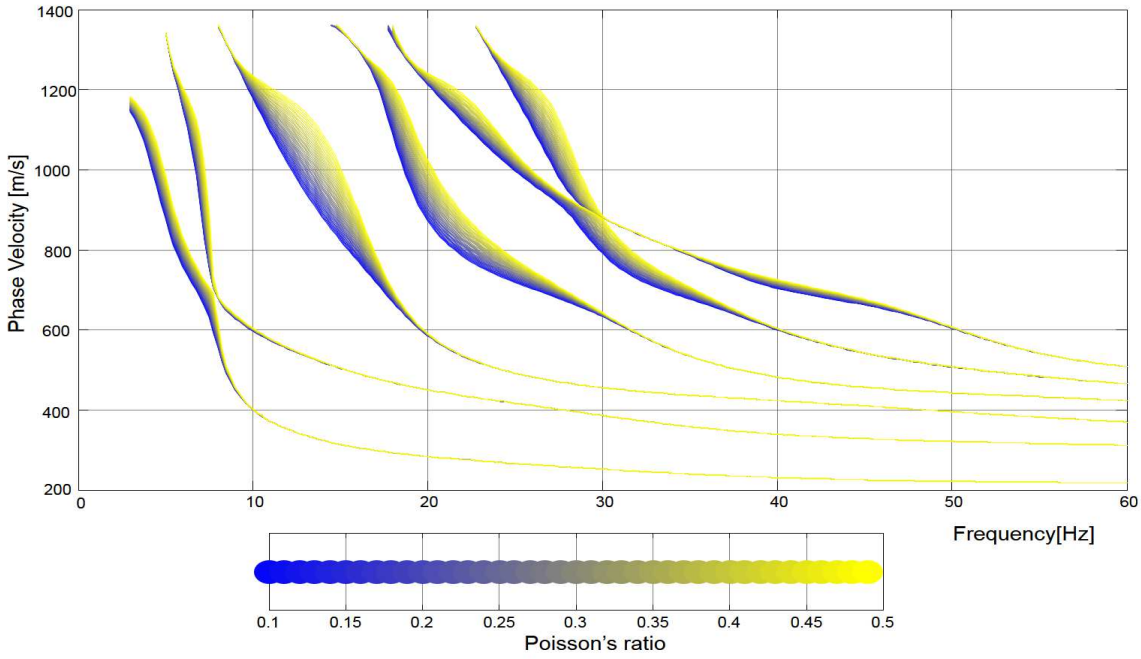

Figure 4.8. Rayleigh modal curves for the model of table 4.1 with Poisson's ratio varying for the fourth layer from 0.10 to 0.49

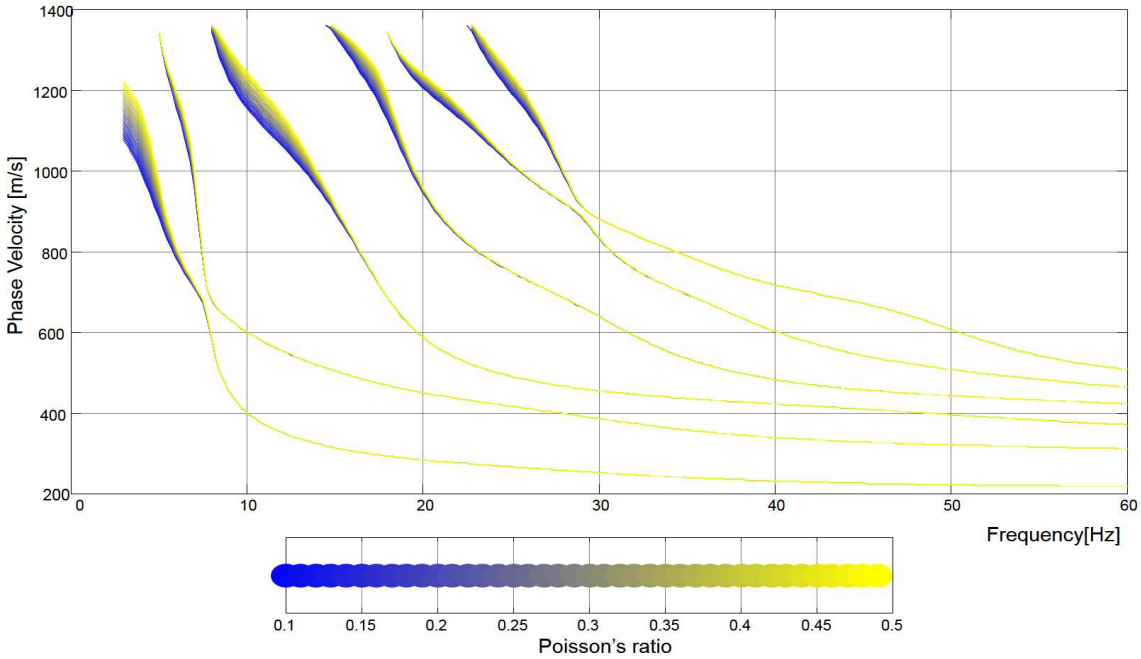

Figure 4.9. Rayleigh modal curves for the model of table 4.1 with Poisson's ratio varying for the Half-space from 0.10 to 0.49

The figures show that different modes present different sensitivity to the change of Poisson's ratio in different layers. In particular, layers 1, 2 and 3 showed significant sensitivity, notably for higher modes 5 and 6. Whereas, the variation of Poisson's ratio in layer 4 and half-space does not affect significantly the modal curves. The different layers affect different frequency bands. Respectively for the higher modes 5 and 6 this band of frequency of sensitivity goes in layer 1 (fig. 4.5) from 25 Hz to 55 Hz, in layer 2 (fig. 4.6) from 18 Hz to 52 Hz, in layer 3 (fig. 4.7) from 17 Hz to 40 Hz, in layer 4 (fig. 4.8) from 25 Hz to 32 Hz (less sensitivity) and half-space (fig. 4.9) from 18 Hz to 25 Hz but is not really appreciable the change.

In consequence , it will be expected to have a much clear distribution on the results of the inversion for the first three layers to retrieve the Poisson's ratio or P-wave velocity of the near surface velocity model. Despite this, for the layer 4 and half-space the answer could be influence to end in a less clear solution.

4.3 Synthetic model with initial heterogeneous Poisson's ratio in the layered medium

The aim of this second model, is to see how is the sensitivity of the dispersion curves to a model where the parameters for the Poisson's ratio or V_P can vary not homogeneously in the layered medium. So, the question is, how much it will be the sensitivity of the dispersion curve to the average Poisson's ratio or V_P . The answer is part of this master thesis.

In order to have a criteria for putting some representative physical values find in the subsoils for V_S , Poisson's ratio and densities. We can keep in mind that in the shallow part of the subsoil, densities range from 1500 -1600 Kg/m^3, exhibit shear wave velocities between 200-375 m/s and Poisson's ratio that goes from 0.2 until 0.3 for soft clays or sandy soils. At deeper depths, the densities due to the compaction of the rocks tend to have higher values from 2000 until 2400 Kg/m^3, with higher shear wave velocities from 700 to 1400 m/s and Poisson's ratio from 0.2 until 0.4 for loose sand or dense soils.

Taking into account some of this values presented before, it is possible to establish a reference set of parameters for the subsoil. A second synthetic model is described (table: 4.2). It consist of four layers plus half-space. The first two layers have density equal to 1500 Kg/m^3, Poisson's ratio equal to 0.3, and V_S 230 and 325 respectively. The third layer has a density equal to 1600 Kg/m^3, Poisson's ratio of 0.3 and V_S of 450 m/s. Finally, the last two layers have densities of 2000 and 2400 Kg/m^3, ν of 0.25 and 0.2 and V_S of 760 and 1361 m/s respectively. (table: 4.2).

Table 4.2. Synthetic model with initial not homogeneous Poisson's ratio

Synthetic Model	Thickness [m]	V_S [m/s]	Density[Kg/ m^3]	Poisson	V_P (m/s)
Layer 1	3	230	1500	0.3	457
Layer 2	7	325	1500	0.3	645
Layer 3	12.5	450	1600	0.3	893
Layer 4	12.5	760	2000	0.25	1316
Half-space	∞	1361	2400	0.2	2223

4.3.1 Sensitivity analysis

For this second analysis, we started from a model with variable Poisson's ratio with depth (Table 4.2). Since the target of this analysis is to assess the possibility of retrieving V_P , we perform the sensitivity analysis with respect to variation of V_P/V_S, instead of Poisson's ratio. The interval in which V_P/V_S can vary is anyway dependent for the possible interval for Poisson's ratio(ν).

The synthetic reference model used to simulate the modal curves is shown fig. 4.10.

The variation of Poisson's ratio between 0 and 0.49 provides a possible range for average V_P/V_S from 1.41 to 7.14. For each layer, we have then increased the V_P/V_S from the starting value (table 4.2) to the maximum value with step of 0.1 and for each obtained model, we have computed the modal curves. See fig. 4.11, which expresses the sensitivity analysis respect to the change in the average velocity ratios V_P/V_S in all the layers simultaneously, for the different Rayleigh modal curves.

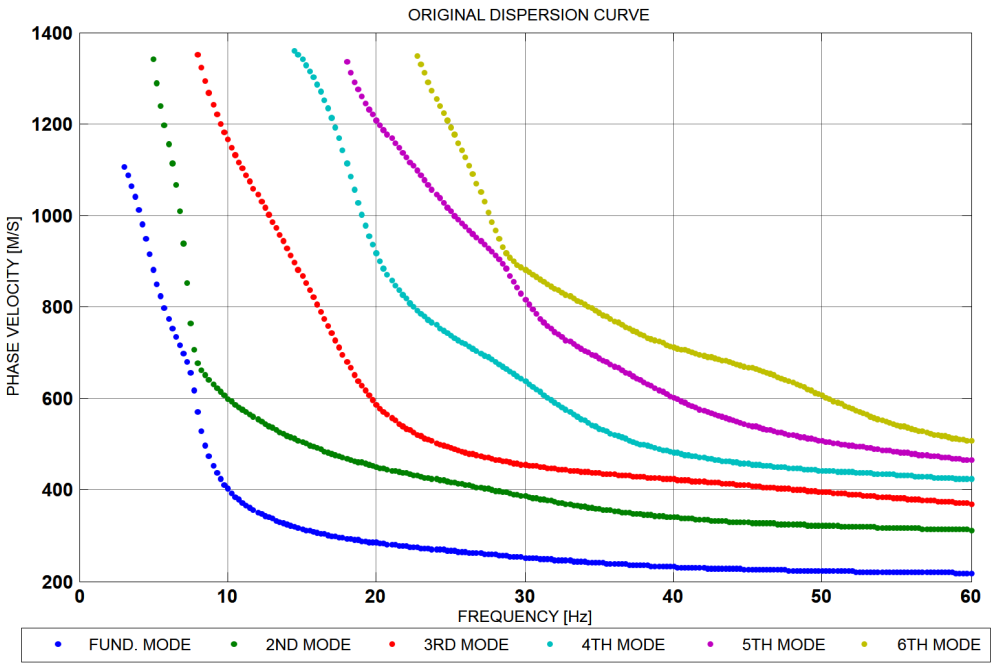

Figure 4.10. Dispersion curve for the model of table 4.2

Since the V_P/V_S is different for each layer, we represent the results associating to each model the average value of V_P/V_S of all the layers.

We show the results in different way to analyze the sensitivity to V_P/V_S:

Fig. 4.11 shows, the different modal curves for the different values of velocity ratios V_P/V_S (from 1.864 to 6.964) . There is evidence of sensitivity notably below 25 Hz for the first three modes, and for the last three modes starting from 50 Hz. In general, taking into account the first three modes, we can say that there is a change in the phase velocity particularly at low frequency.

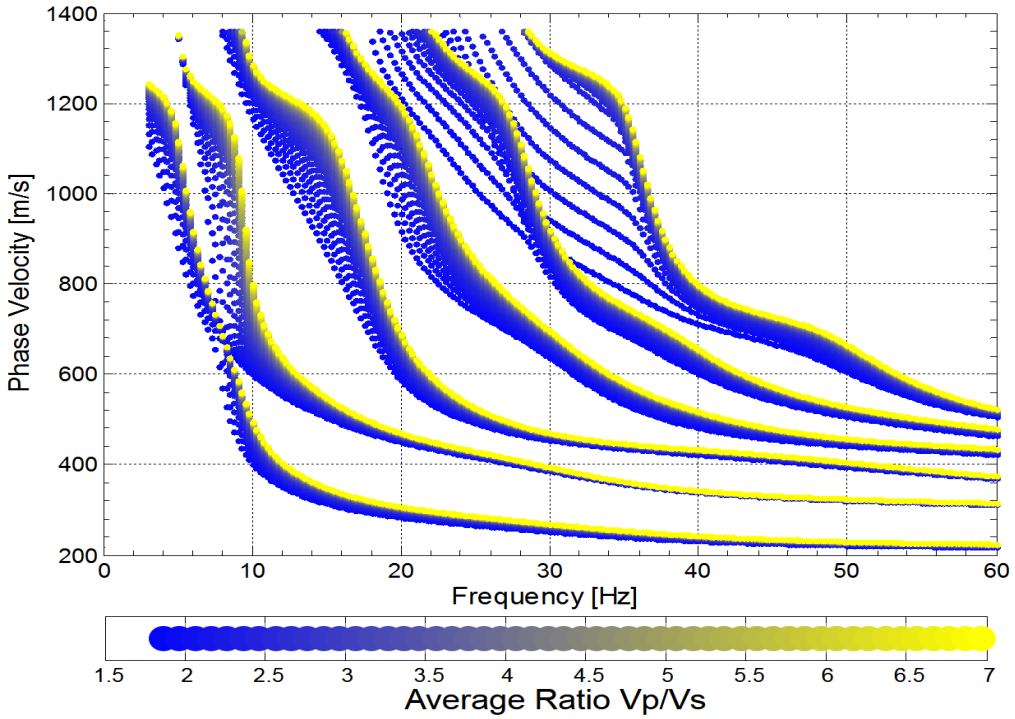

Figure 4.11. Sensitivity of Dispersion curves by changing V_P/V_S in all the layers simultaneously . Reference model of table: 4.2

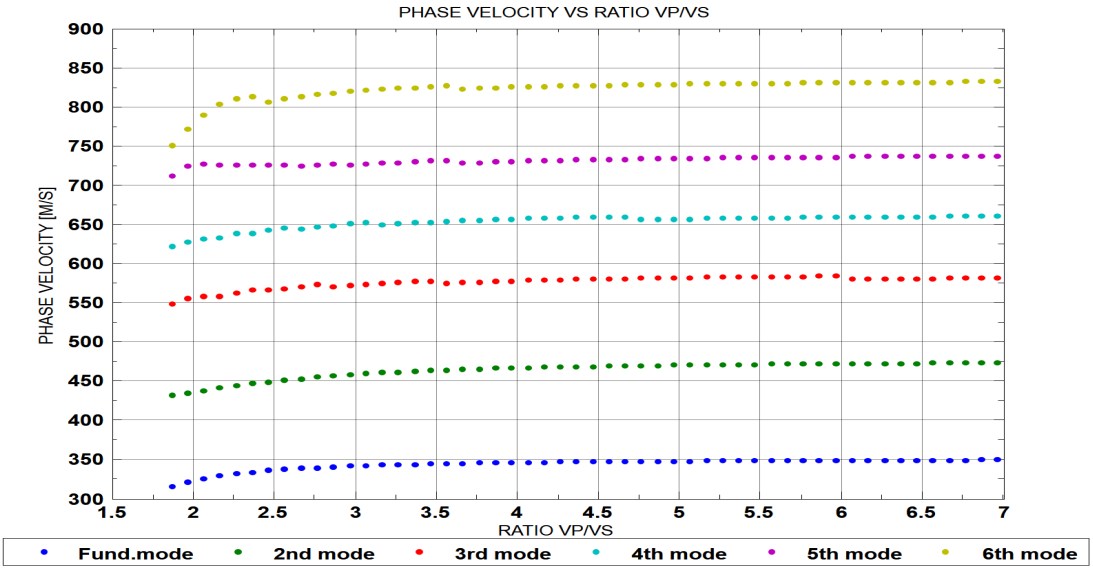

Figure 4.12. Average phase velocity for each mode plotted with respect the average ratio V_P/V_S.

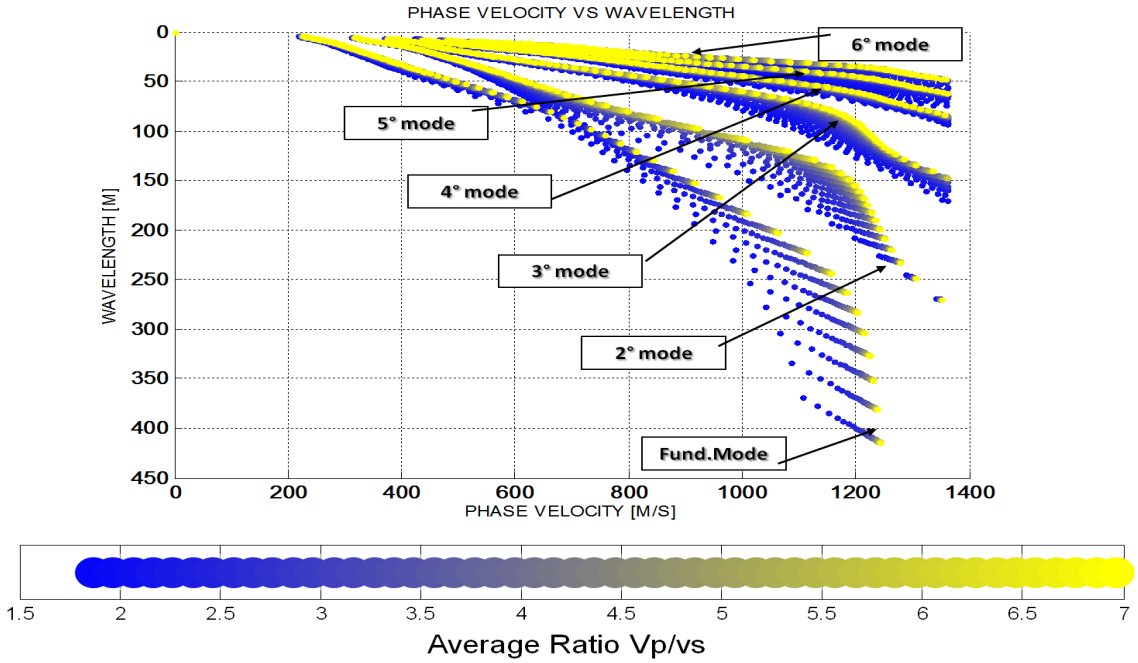

Figure 4.13. Phase Velocity over the wavelength corresponding to each modal curve and their respective average value of V_P/V_S.

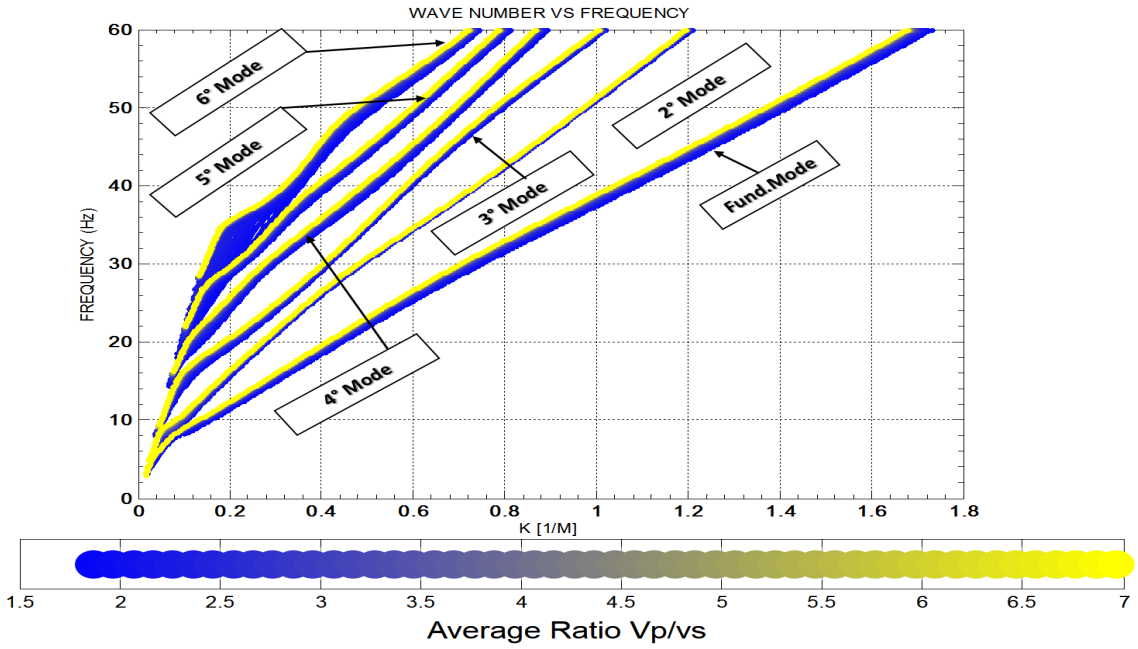

Figure 4.14. Diagram showing the relationship between the wave number [1/m] and frequency-[Hz], this respectively for each average ratio V_P/V_S.

Fig. 4.12 shows, the variation of the average phase velocity for each mode vs V_S/V_P. This result shows that for low values of V_P/V_S (below 3.5) there is a clear shift in the modal curve and the sensitivity is higher.

Fig. 4.13 shows, the modal curve phase velocity represented as a function of wavelength. This is interesting because the wavelength is related to the investigation depth and hence fig. 4.13 shows sensitivity to V_P/V_S at different depths. For short wavelength (high frequency band) there is week variation in the phase velocity as was pointed out from figure 4.11, while at long wavelengths (low frequency band) , around 75 meters there is a wider change respect to the surface wave velocity.

Fig. 4.14 shows, the same modal curves of fig. 4.11 plotted in $f-k$ domain- This picture shows the poor sensitivity in this domain and this is important in the view of processing for the extraction of the dispersion curves which which is performed in $f-k$ domain.

To provide a clear picture of the sensitivity of different modes we have computed the relative difference between the phase velocity of consecutive modal curves to the fundamental mode.

The results are shown in fig.4.15 , where is evident that the dispersion curves are sensitive to the change in the average V_P/V_S ratio, particularly under a range of frequencies. –Approximately from 40 Hz to 5 Hz depending on the mode.

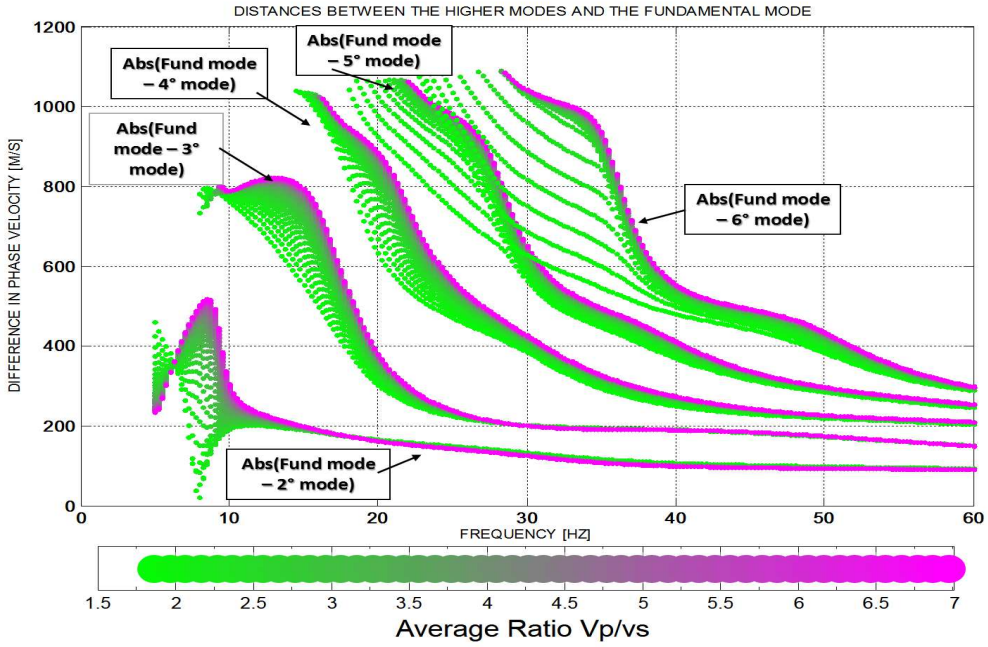

Figure 4.15. Distances of each higher mode respect to the fundamental mode accordingly to each average ratio V_P/V_S.

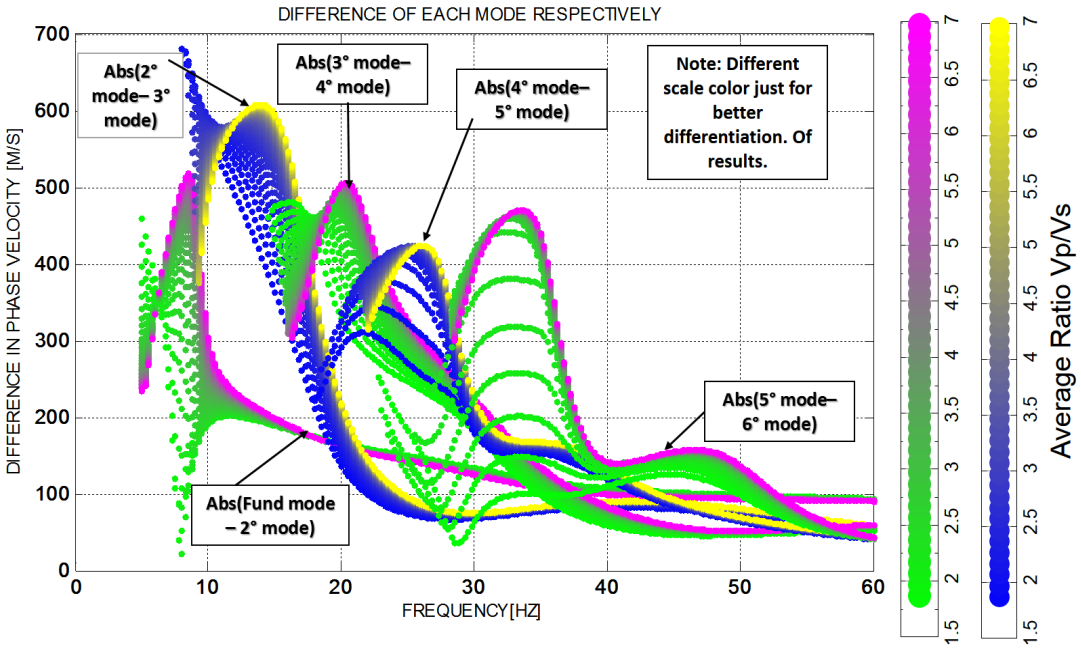

Figure 4.16. Distances between successive modes expressed respectively for each ratio average V_P/V_S.

To provide a clear picture of the sensitivity of different modes we have computed the relative difference between the phase velocity of consecutive modal curves.

Fig. 4.16 shows, the distances between successive modes. The set of curves correspond to differences between consecutive modes, i.e., 1st higher mode and fundamental mode, 2nd higher mode and 1st higher mode and respectively until reaching the difference between the 5th higher mode and the 4th higher mode.

It can be seen from fig. 4.16 that the sensitivity changes significantly from one mode to another and that different modes are sensitive in different frequency bands.

The use of the two scales within figure 4.16, was just a matter of change of the set of scale color to get a better and easier differentiation of the results.

The plots of fig. 4.11, fig. 4.15 and fig. 4.16 can be seen in the Annex A. (Sensitivity to the Poisson's ratio of the synthetic model of table 4.2) as a function of change of the average Poisson's ratio. A similar analysis can be used for those results of Annex A. Just a matter of visualization of results: or Poisson's ratio (V_P) or velocity ratio (V_P/V_S).

Chapter 5

Monte Carlo multimodal Inversion of synthetic data

5.1 Introduction

After analyzing the sensitivity to the Poisson's ratio (and/ or velocity ratios (V_P/V_S)) on the Rayleigh modal curves including higher modes, we now test the effect of this sensitivity on the inversion results.

To do this , we consider the synthetic model curves of Fig. 4.10 (Table: 4.2) and we invert them with a Monte Carlo approach. –The M.C. approach is used because it allows the model space to be widely investigated and the solution space to be explored providing a clear picture of the resolution of retrieved final models. Moreover, by considering a large number of possible models, a statistical analysis of the results is possible.

The Monte Carlo algorithm is based on a forward operator which has been described in chapter 4, proposed by Maraschini, (2007) and developed in Matlab code. The new misfit is based in the Haskell and Thomson determinant (Maraschini, et.al., 2010) and a second misfit is used corresponding to the root mean square deviation between dispersion curves ($RMS_{Distance}$).

5.1.1 Approach for Monte Carlo multi-modal inversion

The solution of the inverse problem is resolved using a forward operator. From a mathematical point of view, the model for surface wave inversion consist typically of a stack of homogeneous linear elastic layers. The matrix of the observed data ($\mathbf{D}^{obs}$) contains the velocity–frequency (v, f) couples of the observed dispersion curve:

$$\mathbf{D}^{obs} = \begin{bmatrix} v_1^{obs} & f_1^{obs} \\ ... & ... \\ v_N^{obs} & f_N^{obs} \end{bmatrix} \tag{5.1}$$

Where, N is the number of observed data points. The vector $\mathbf{m}$ contains the model parameters of the layers (thickness, V_S , V_P or Poisson's ratio, and density).

The determinant of the Haskell–Thomson matrix $\mathbf{T}$ (Thomson, 1950; Haskell, 1953) is a function of frequency and velocity:

$$F = |det(\mathbf{T}(v, f, \mathbf{m}^*))| \tag{5.2}$$

Where, $\mathbf{T}$ is the Haskell–Thomson matrix (Buchen & Ben Hador,1996), $\mathbf{m}^*$ is the given model parameters, f are the frequencies, and v are the velocities.

The function $|det(\mathbf{T}(v, f, \mathbf{m}^*))|$ can be defined as a surface in the velocity–frequency domain. This function (F) values are zero ($|det(\mathbf{T}(v, f, \mathbf{m}^*))| = 0$), corresponding to the modal curve of the model $\mathbf{m}^*$. The determinant of $\mathbf{T}$ depends on the model $\mathbf{m}^*$ and on the point (V, f); consequently, $|\mathbf{T}(v, f, \mathbf{m}^*)| = 0$, represents the forward operator (Maraschini and Foti, 2010).

The classical misfit function minimizes the geometric distance between the real and synthetic dispersion-curves (eq. 5.3) :

$$S(\mathbf{m}^*) = \left\{ \sum_{i=1}^{N} \left[w_i \left| V_i^{obs} - g(\mathbf{m}^*, f_i^{obs}) \right| \right]^{\iota} \right\}^{1/\iota} \tag{5.3}$$

Where w_i represents the weight of the ith point; $g(\mathbf{m}^*, f_i^{obs})$ represents the forward operator, which calculates the velocity value of a given mode (chosen by the

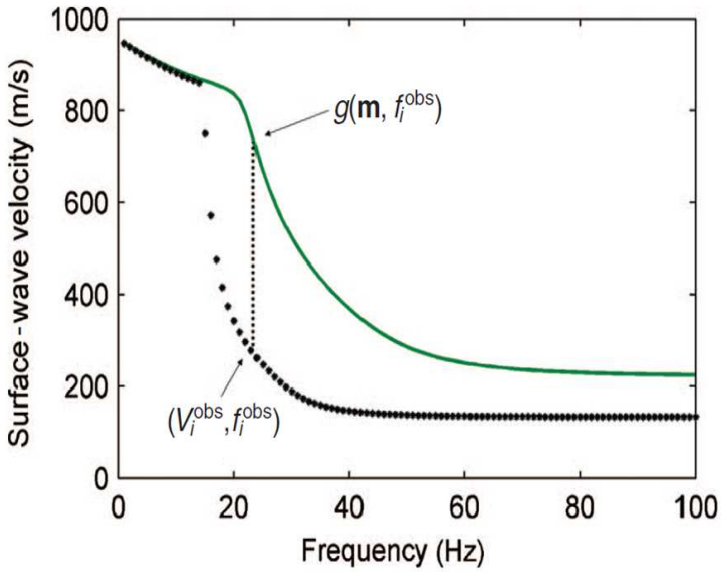

Figure 5.1. Calculation of the classical misfit function. The green line represents the synthetic dispersion curve, and the black dots represent the experimental data (After Maraschini, et al., 2010).

user) of the dispersion curve at the ith frequency; and ι is the norm. This approach requires mode numbering. The principle of the calculation for the classical misfit is shown in fig. 5.1. For each frequency, the corresponding distance is the difference between the velocities of the synthetic dispersion curve and the experimental dispersion curve.

However, this classical misfit function needs more computational time which is not appropriate. Particularly for stochastic inversion approaches. That is the reason, why the proposed misfit function for the master thesis, referred to as the determinant misfit function, is the norm of the vector containing the value of the **T** surface evaluated at the experimental data points. This new misfit for multimodal inversion of surface waves was established and used by Maraschini, et al. (2010):

$$S(\mathbf{m}^*)_{H.T} = \left\{ \sum_{i=1}^{N} \left[w_i \left| \mathbf{T}(V_i^{obs}, f_i^{obs}, \mathbf{m}*) \right| \right]^{\iota} \right\}^{1/\iota} \tag{5.4}$$

The misfit function (eq: 5.4) used for this master thesis was developed by Maraschini, et al. (2010). This misfit presents two important advantages. First

of all, the approach is inherently multi-modal, so, it allows all the modes of the experimental dispersion curve to be considered, without the need to establish initial assumptions to which mode each data point belongs to (Maraschini et al., 2010).

The second advantage is the computational cost, which is strongly reduced compare to the classical misfit based on the distance between the observed and the dispersion curves of the model $\mathbf{m}^*$ and since, dispersion curve calculation requires a cost expensive zero search, i.e., for each frequency of the observed dispersion curve a zero search on velocity (or wavenumber) is required. For the classical misfit, the zero search procedure requires several evaluations of the Haskell–Thomson matrix for each frequency (depending on accuracy and soil complexity). On the contrary, the misfit adopted for this master thesis developed by Maraschini, et al. (2010) requires for the evaluation of the misfit (eq. 5.4), a single evaluation of the Haskell–Thomson matrix determinant for each frequency, and consequently reduces the computational time. The calculation of the determinant misfit function is shown in fig. 5.2.

The Monte Carlo approach consists in random sampling the model space and then by computing the determinant misfit of all the models ($S(\mathbf{m}^*)_{H.T}$), we are going to be able to reconstruct the solution space. In order to select acceptable models, it is necessary to have a second misfit criteria. Since, the determinant misfit function is fully multimodal and efficient from computational time, since it just computes the Haskell and Thomson determinant values in correspondance to the data points and does not require the zero search that is necessary to compute the synthetic dispersion curves . However, this algorithm is strongly non linear because the data points can fall in different modes.–misidentification of modes (Maraschini et al., 2010). So, we make an *a posteriori* refinement to select the right solutions as those whose fundamental data points fall in the fudamental mode also in the inversion.

The *a posteriori* refinement is made only on a limited number of models (the best fitting curves) and is based on the computation of a different misfit funtion that is a distance between the data points and the synthetic dispersion curve.

The root-mean-square deviation (RMSD) or root-mean-square error (RMS) is going to be used as a measurement of the differences between the dispersion curves predicted by the forward operator within the Monte Carlo inversion approach for the determinant misfit and the values actually observed or experimental. The

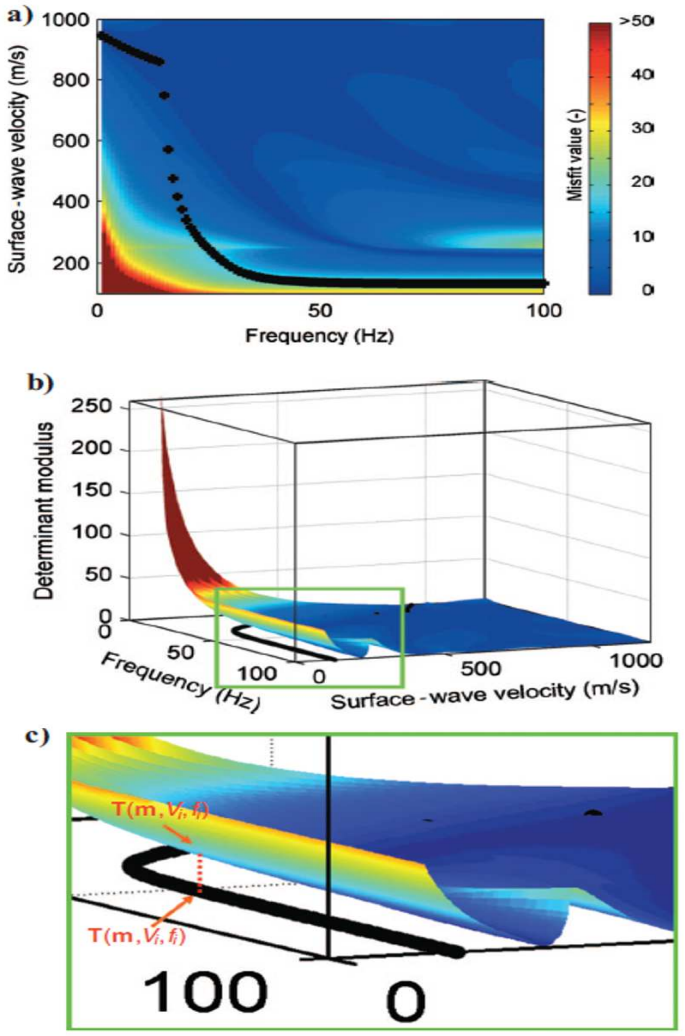

Figure 5.2. Calculation of the determinant misfit function. The colored surface represents the absolute value of the Haskell-Thomson matrix determinant of the synthetic model. The black dots represent the experimental data. For each experimental point, the corresponding distance is the value assumed by the surface at the same $V - f$ pair: (a) 2D view, (b) 3D view, (c) close-up of 3D view. (After Maraschini, et al., 2010)

$RMS_{Distance}$ is going to account as a measure of how well is the accuracy of the solution between dispersion curves. It can be expressed mathematically as:

$$RMS_{Distance} = \sqrt{\frac{\sum_{i=1}^{N} |V_{inv}(f_i) - V_{exp}(f_i)|^2}{N}} \tag{5.5}$$

Or, considering the uncertainties associated with the data, the weighted RMS distance between dispersion curves can be defined as:

$$RMS_{Distance_W} = \sqrt{\frac{\sum_{i=1}^{N} |V_{inv}(f_i) - V_{exp}(f_i)|^2}{N\sigma_u^2}} \tag{5.6}$$

Where :

- σ_u: It is the uncertainty associated with the data (Supposed to be equal to 5% for the exploration seismic data)
- $V_{inv}(f_i)$: It is the phase velocity obtained from the theoretical dispersion curve at each frequency.
- $V_{exp}(f_i)$: It is the phase velocity obtained from the observed or experimental data at each frequency.
- N: Corresponds to the number of predictions.

Since, the $RMS_{Distance}$ misfit is computationally more consuming in time, because each theoretical dispersion curve for each model needs to be calculated, we are going to use just the 1 % of the best models from the determinant misfit to finally retrieve the best 20 profiles according to the lower root- mean -square deviation (Eq. 5.5 for the synthetic data and Eq. 5.6 for the experimental exploration dataset).

5.2 Data input for the Monte Carlo multimodal approach

The inversions are performed on the thickness ($\mathbf{d_i}$) , on the s- wave velocity (V_S) of each layer and half space and Poisson's ratio (or V_P), assuming a priori the values for the density (ρ) which are going to be fixed during the simulations. The synthetic reference model is the one from table: 4.2.

The number of profiles for the Monte Carlo inversion are two million random samples. By keeping constant the density, and varying the shear wave velocity from a minimum and maximum value (V_{smin} and V_{smax}) and the $\mathbf{d_i}$ between a minimum

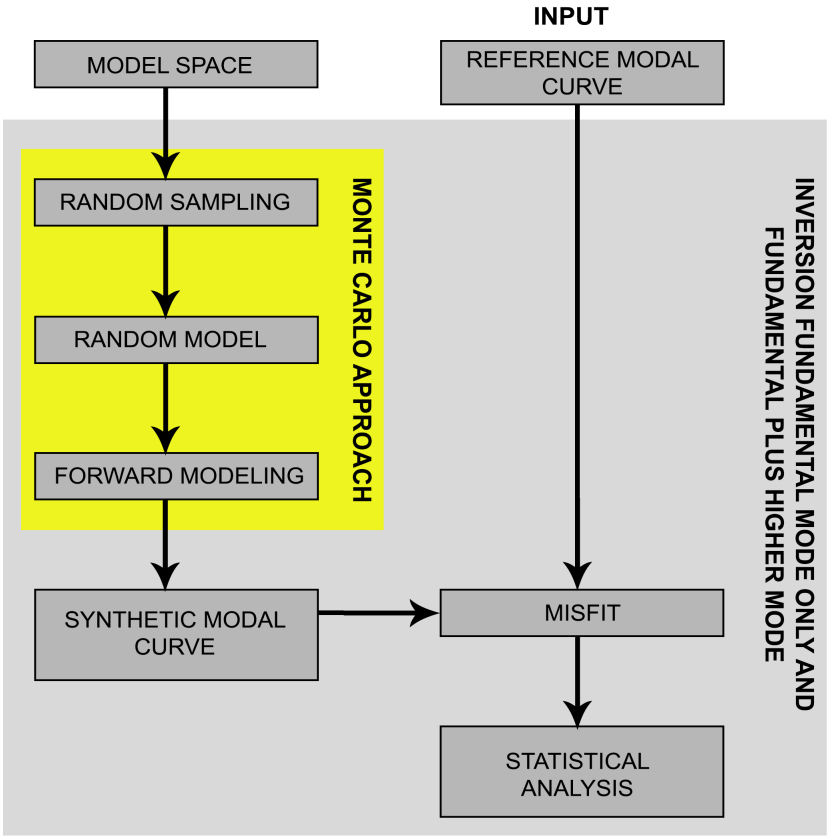

Figure 5.3. Logical scheme applied on the Synthetic model for the inversion

and maximum thickness (H_{min} and H_{max}). – The range of the values will be assumed to be half and double of the respective, thicknesses ($\mathbf{d_i}$) and shear wave velocities (V_S) of the values from table 4.2 . Furthermore, the Poisson's ratio (ν) is going to be changed between a minimum and maximum value (ν_{min} and ν_{max}) , which will correspond to the range from 0.05 until 0.49.

The logical scheme used for the inversion of the synthetic model can be seen in fig. 5.3.

5.3 Results of the Monte Carlo multi-modal inversion related to the synthetic data

5.3.1 Estimation of the shear wave velocity (V_S) of the layered medium

The shear wave velocities (V_S), were satisfactory estimated through the Monte Carlo multi-modal inversion for fundamental and higher mode fitting. The results, are showed after explaining, how the Monte Carlo multi-modal inversion works for the synthetic model.

For the inversion, the use misfit is the values of the Haskell and Thomson determinant (eq. 5.4) and these synthetic modal curves are computed *a posteriori* to show the results. In figs. 5.4 , 5.5 and 5.6 . We show the fitting of the modal curves of the 20 best fitting models. It can be noticed that when inversion is performed with fundamental mode only, the higher modes are not matched.

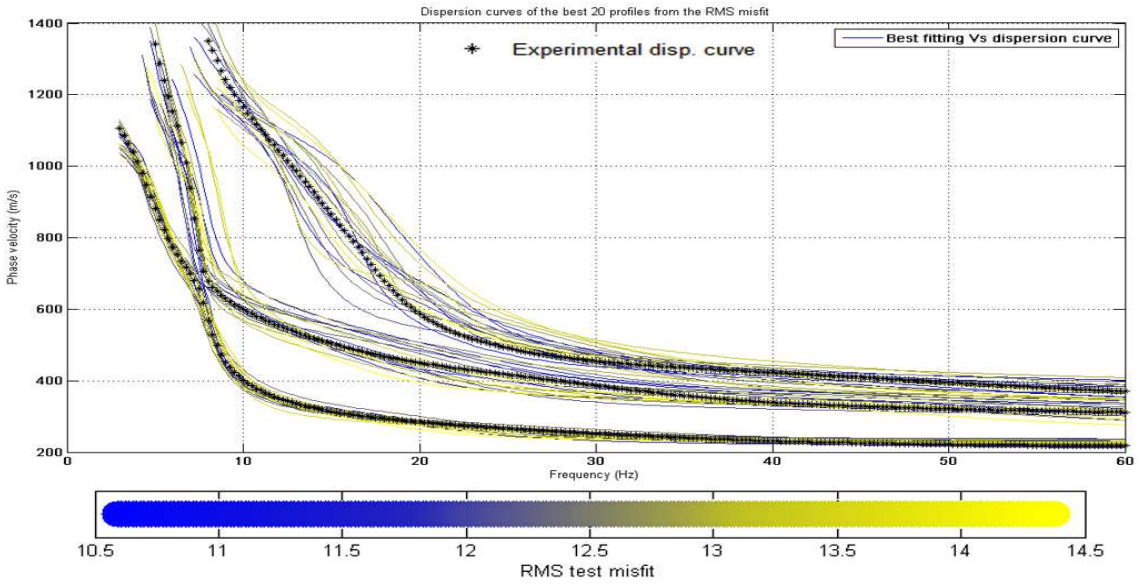

Figure 5.4. Misfit of the modal curves for the 20 best fitting models. –Fundamental mode inversion.

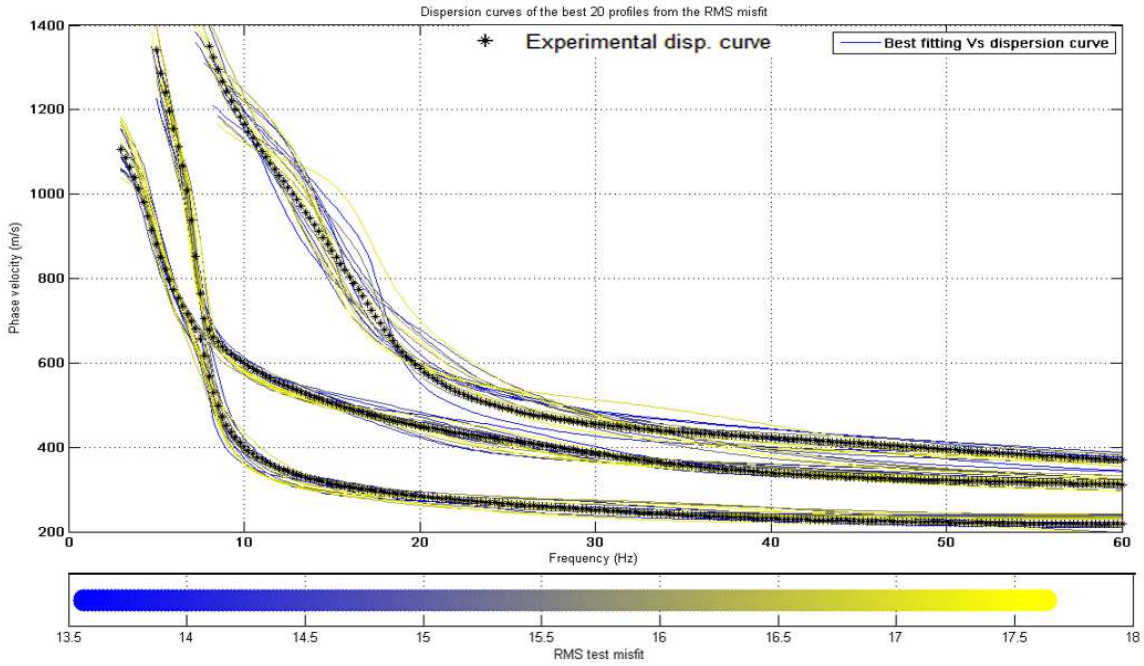

Figure 5.5. Misfit of the modal curves for the 20 best fitting models. –Fundamental and first higher mode inversion.

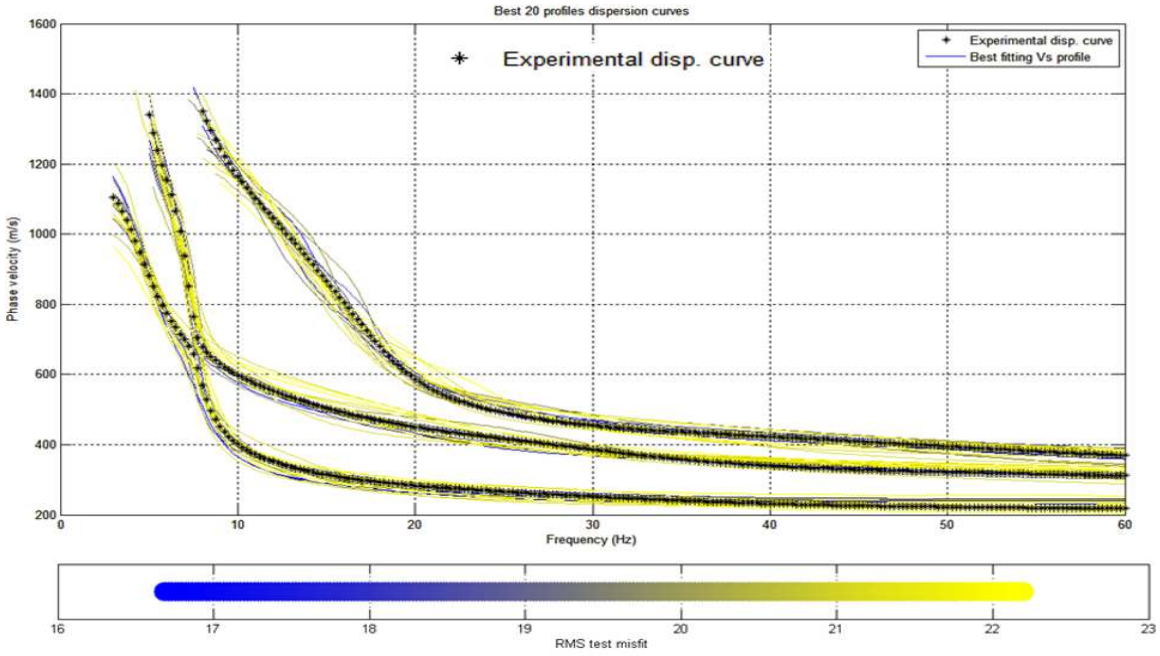

Figure 5.6. Misfit of the modal curves for the 20 best fitting models. –Fundamental, first and second higher mode inversion.

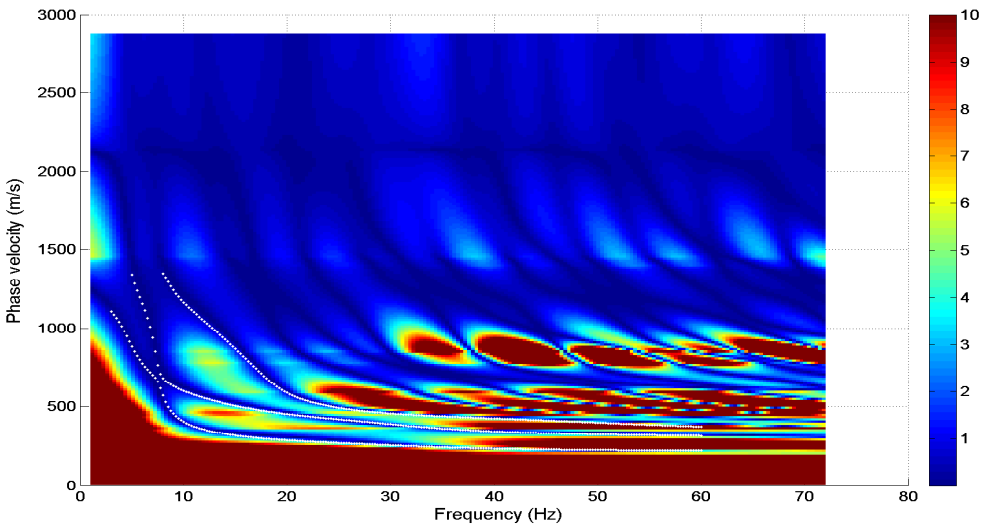

Figure 5.7. Haskell–Thomson matrix determinant for the best fitting model out of 2 million iterations. –Fundamental, first and second higher mode inversion and keeping: V_S, thickness and ν variable.

Fig. 5.7, shows the determinant misfit for the best fitting profile model. Then, in fig. 5.8, there is depicted the 100 best fitting profiles according to this determinant misfit.

In the fig. 5.8, is possible to distinguish two different sets of solutions that equally fit the data. This happens because with the Haskell and Thomson determinant misfit there is the fitting of the different theoretical curves.

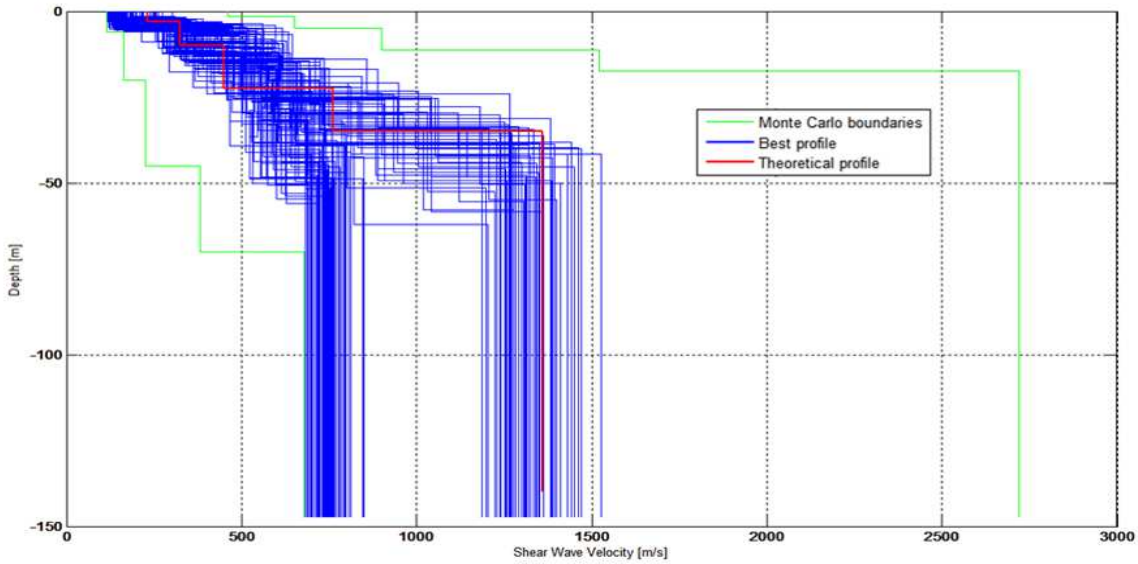

Figure 5.8. Best fitting models obtained after the Haskell and Thomson determinant misfit

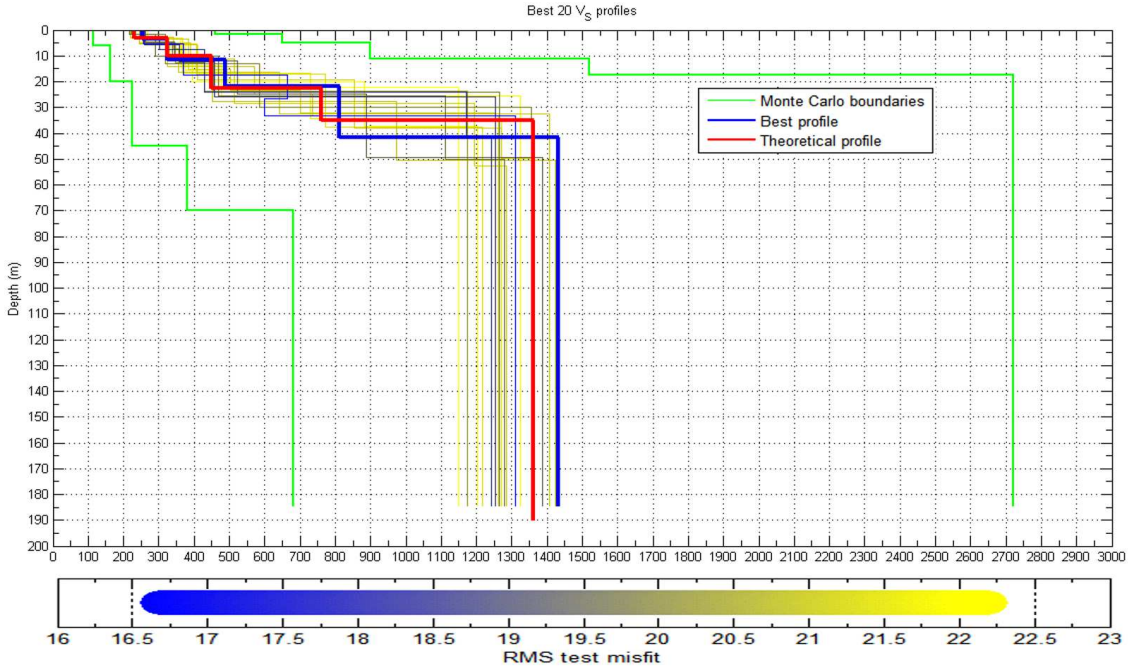

Figure 5.9. Best fitting models after refinement with dispersion curve distance misfit

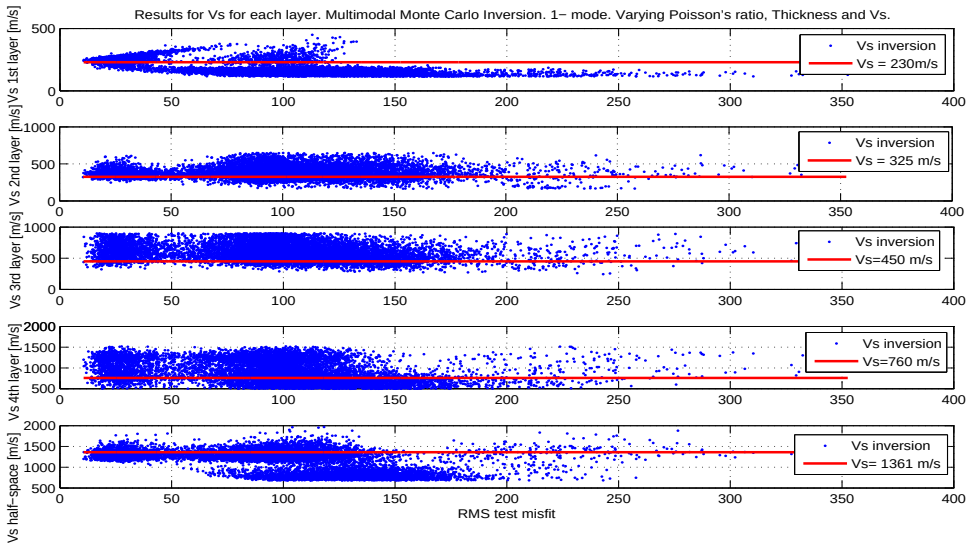

Figure 5.10. Results for the Monte Carlo Inversion taking 1-mode and varying Vs, Poisson's ratio and thickness. Estimation of Vs for each layer

One set of solution is obtained by fitting the wrong modes (fundamental mode is matched with higher modes and higher modes are matched with wrong higher modes). The second misfit is computed by imposing the fundamental mode data point to fit fundamental mode of the synthetic, 1st higher mode with 1st higher mode and so on.

The result of the 20 best fitting profiles according to distance RMS misfit (eq: (5.5) can be seen in fig. 5.6 and the V_S profile in fig. 5.9. The best profiles in blue have been selected according to the lower distance RMS misfit. The results, are compared with the theoretical profile which is expected in red.

We computed the distribution of the RMS misfit results respect to the shear wave velocity for the Monte Carlo multimodal inversion for the inversion with different modes. The results can be seen in figs. 5.10 , 5.11 and 5.12. In general , the agreement for fundamental and different modes inversions were consistent.

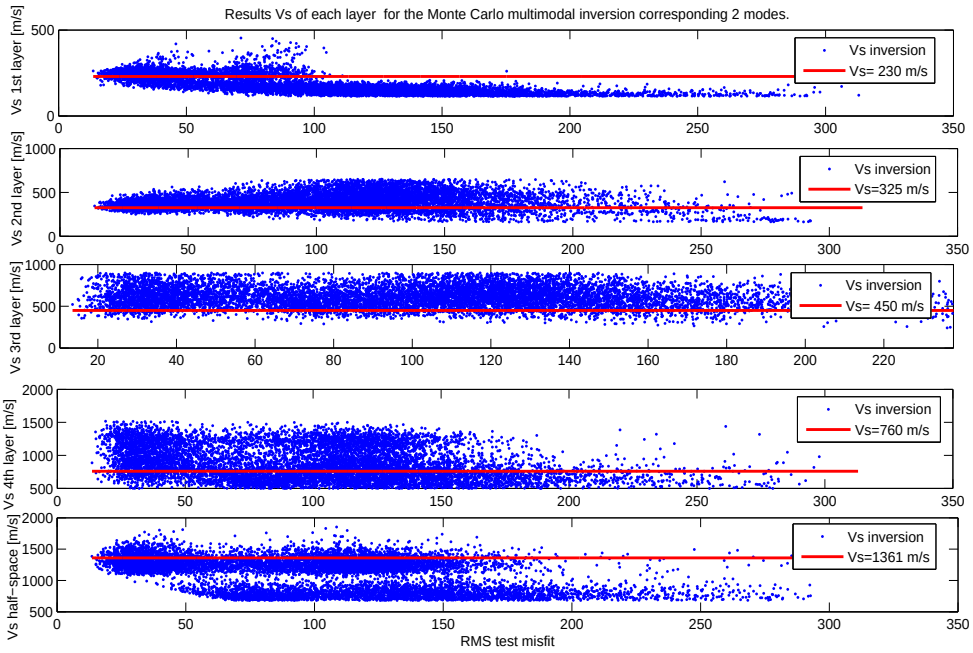

Figure 5.11. Results for the Monte Carlo Inversion taking 2-modes and varying Vs, Poisson's ratio and thickness. Estimation of Vs for each layer

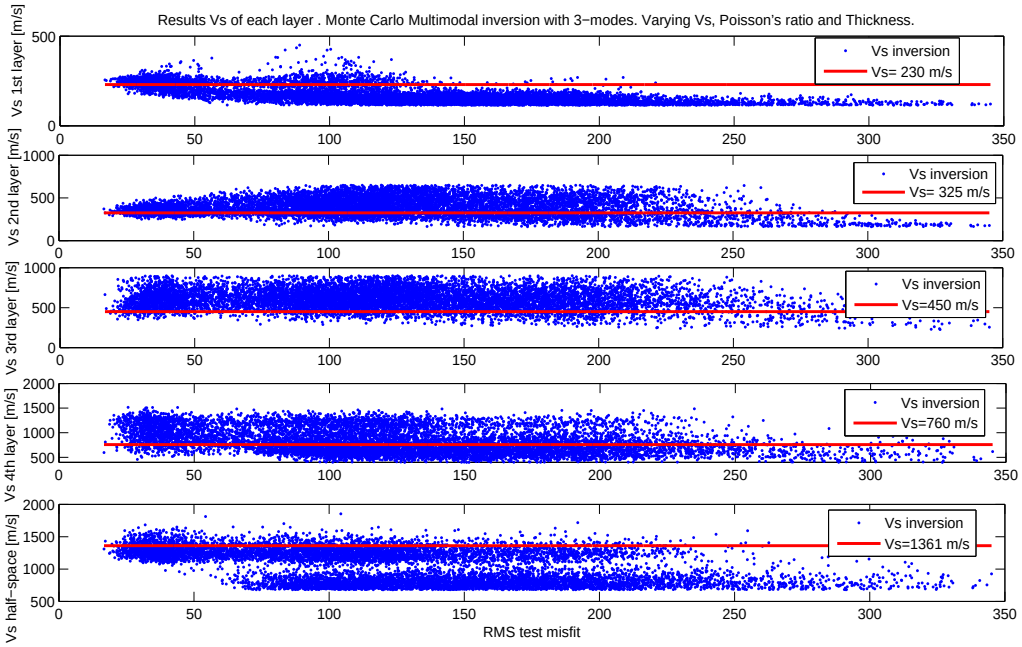

Figure 5.12. Results for the Monte Carlo Inversion taking 3-modes and varying Vs, Poisson's ratio and thickness. Estimation of Vs for each layer

5.3.2 Estimation of V_P or Poisson's ratio (ν) of the layered medium for a model space parameters with given thickness and density

A statistical analysis was performed to evaluate the sensitivity of higher modes to V_P , with given thickness of the layered medium.

Since the input parameters for the Monte Carlo multi-modal inversion (See section 5.2) , were selected with a random uniform distribution, the V_P is expected to have a log-normal distribution. In fact, when the product of many independent random variables each of which is positive, provides a variable with log normal (Weisstein, E. W., 2013). The median is the statistical parameter chosen as the data is biased within a range of p-wave velocity within the inversion result.

In this test the layer thickness was fixed and only V_S and V_P where considered unknowns. To assess the probability of estimating V_P , the results where statistically analyzed. The distribution of the V_P values of the best fitting profiles can be fitted with a log-normal distribution (here just the histograms are shown) and the median was estimated as the estimate of V_P .

In figures from 5.13 to 5.17, we show the distribution and the median of the V_P for all the layers. In each plot we compare the results of the inversion performed with fundamental mode only, with fundamental plus 1st higher mode and fundamental plus 1st and 2nd Higher modes. The medians are compared with the true values. It has been calculated by a statistical analysis code that all the V_P distributions fitted to a log-normal distribution (These results are not shown in this work for simplicity).

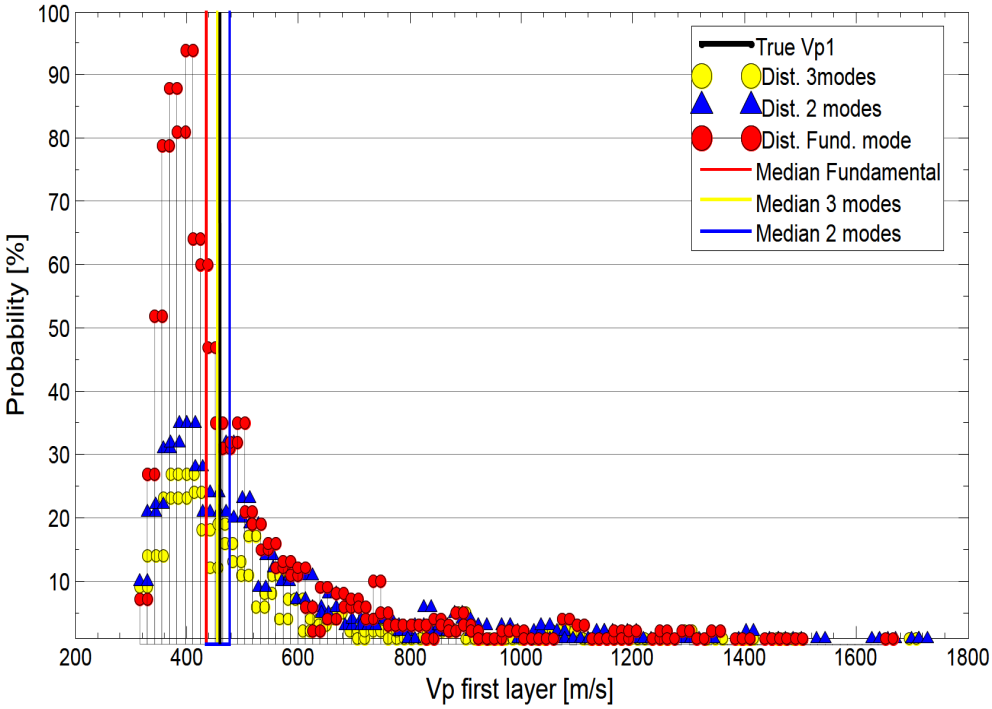

Figure 5.13. Histogram with the distribution of V_P for the first layer for fixed thickness showed for different modes.

Additionally, the statistical mode as a measure of central tendency, can be used to corroborate the results. Since the mode, represents the most frequent value in a given amount of data points, the histograms can be used to see the most recurrent value of V_P . For instance, the mode in 4th layer, (fig. 5.16), corresponding to the inversion with 3 and 2 modes (yellow and blue dots), is closer to the true V_P (black line) compared with the one of the fundamental mode (red dots). The same behavior is observed in fig. 5.17. Meanwhile, the value of the mode, appeared to be very similar for the distribution of V_P in figs. 5.13, 5.14 and 5.15 for fundamental mode, first and second higher mode inversion results.

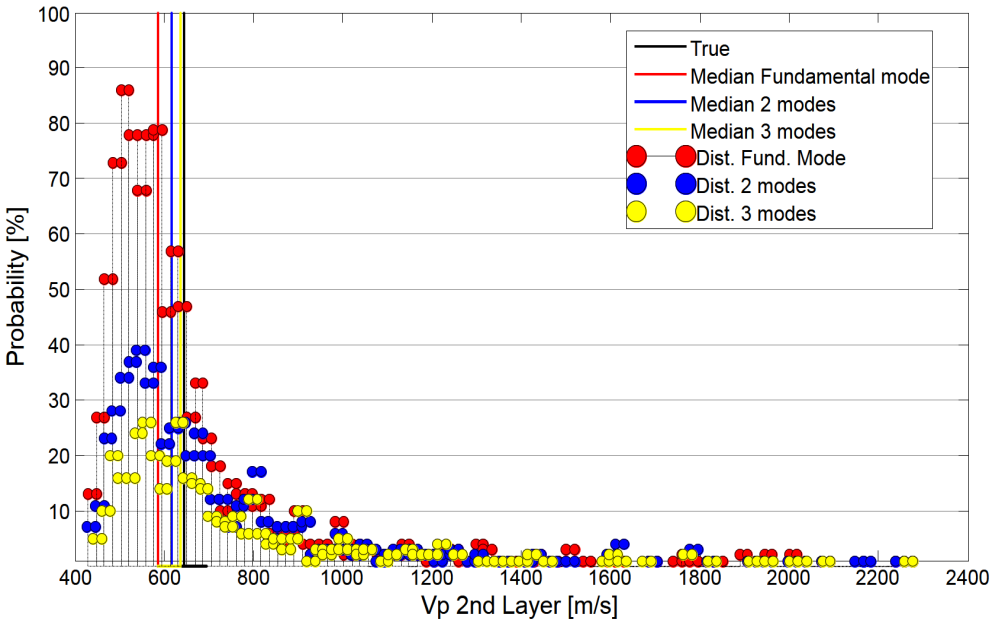

Figure 5.14. Histogram with the distribution of V_P for the second layer for fixed thickness showed for different modes.

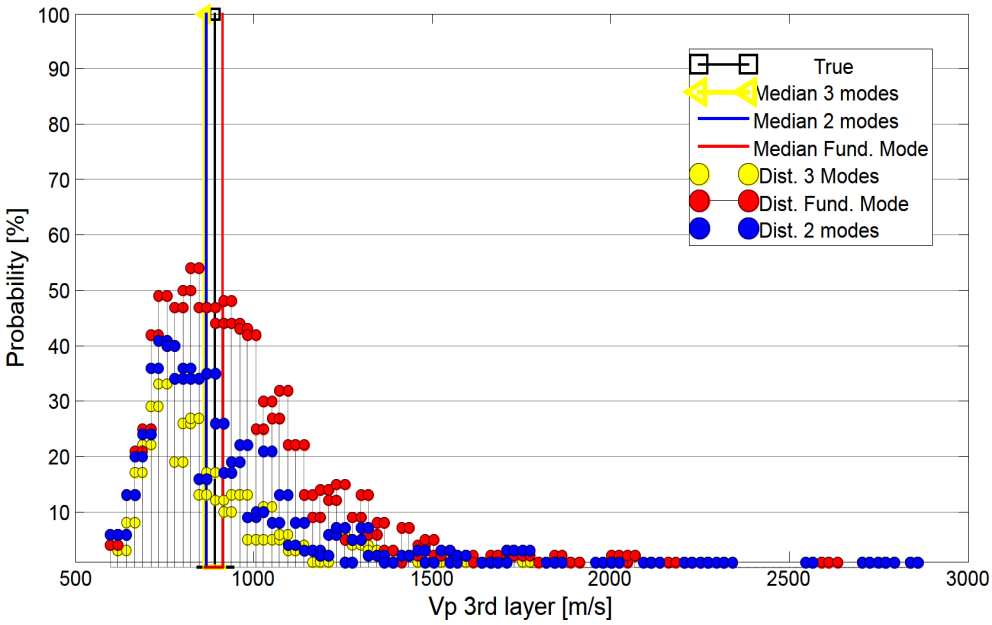

Figure 5.15. Histogram with the distribution of V_P for the third layer for fixed thickness showed for different modes.

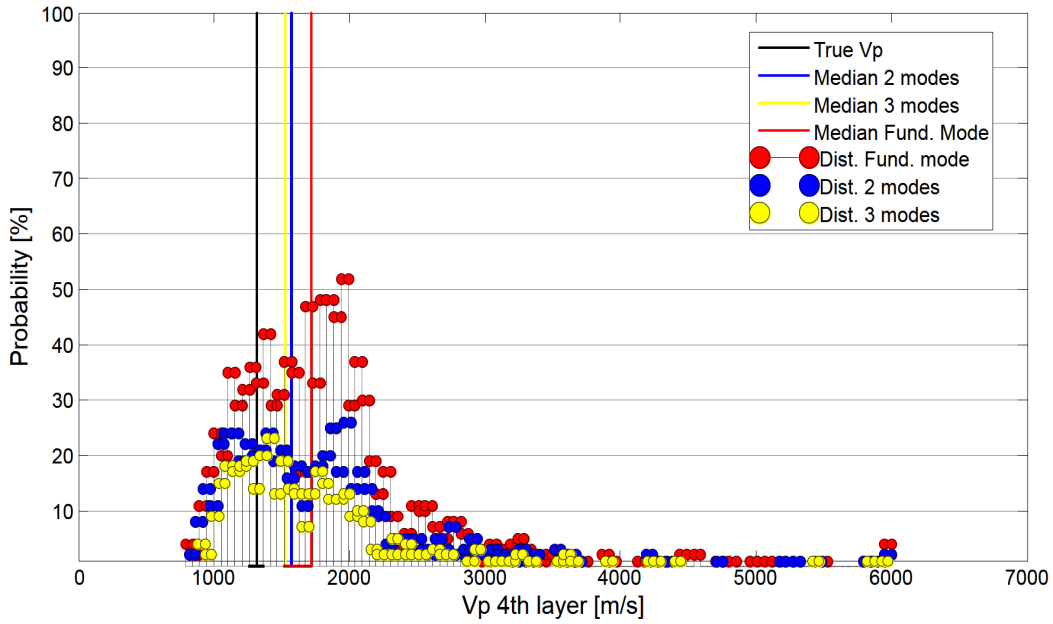

Figure 5.16. Histogram with the distribution of V_P for the fourth layer for fixed thickness showed for different modes.

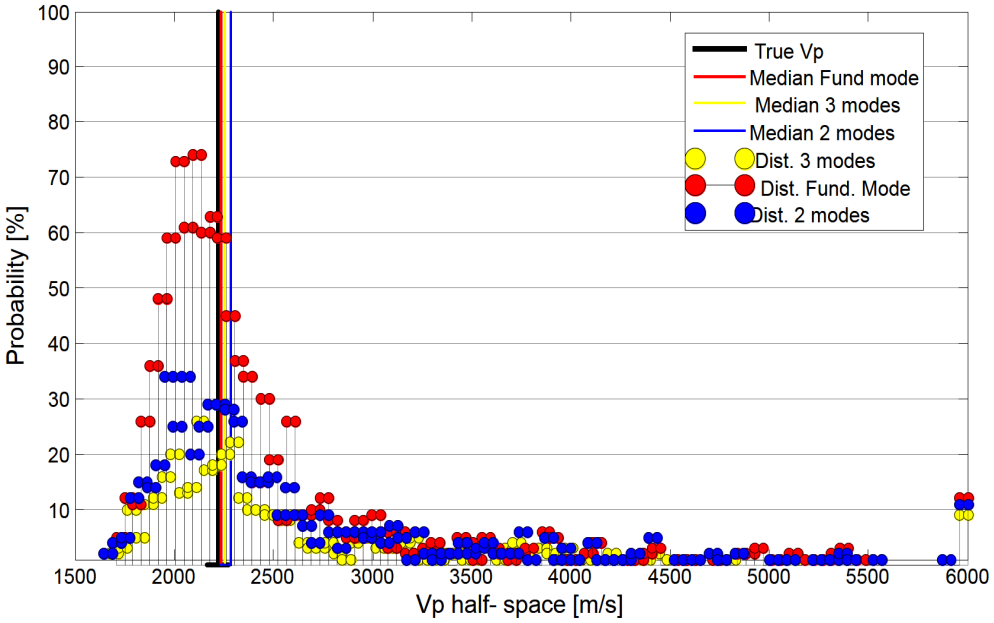

Figure 5.17. Histogram with the distribution of V_P for the half-space for fixed thickness showed for different modes.

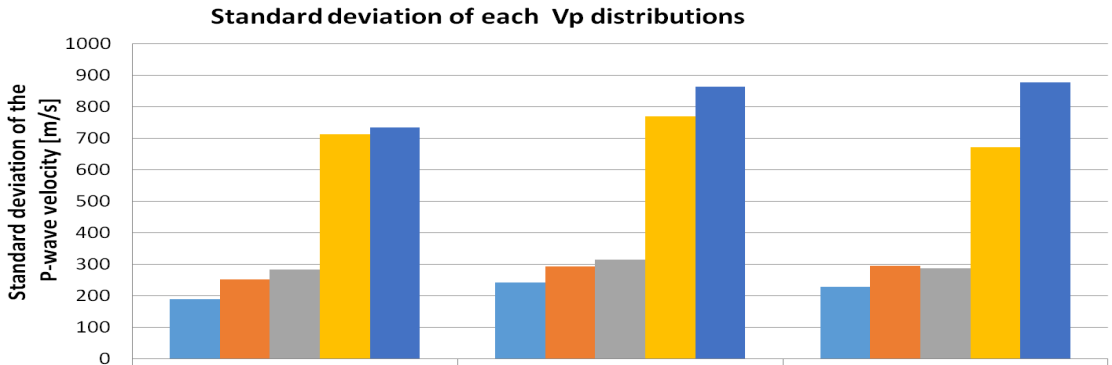

	Matching fundamental mode	Matching two modes	Matching three modes
1st Layer	190,1965552	241,7933409	229,5715975
2nd Layer	252,7191606	294,1698606	294,8260066
3rd Layer	283,8664051	315,5796704	287,9755617
4th Layer	713,6696144	769,5569546	670,9010299
Half-space	733,5658207	864,0184722	877,0257854

Figure 5.18. Comparison of the standard deviation respect the addition of higher modes to the Monte Carlo multimodal inversion for fixed thickness model (Misfit distance RMS higher than 30 was not considered for the analysis)

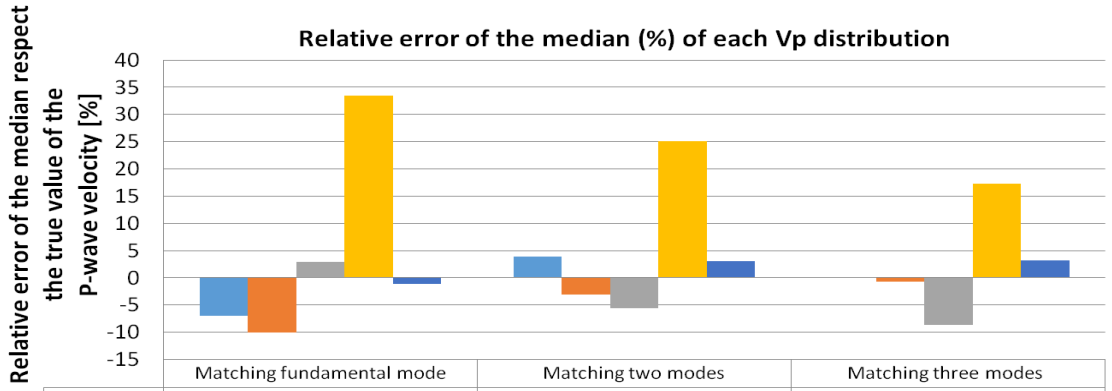

	Matching fundamental mode	Matching two modes	Matching three modes
1st Layer	-7,039478801	3,868821549	0,079107421
2nd Layer	-9,994845683	-3,138177879	-0,666969097
3rd Layer	2,934259486	-5,597973063	-8,658077584
4th Layer	33,47169248	25,10225326	17,35228629
Half-space	-1,078729153	3,022644261	3,225174446

Figure 5.19. Comparison on the addition of higher modes to the Monte Carlo inversion for a model where the thicknesses are fixed. (Misfit distance RMS higher than 30 was not considered for the analysis)

The fig. 5.19, indicates that the V_P is somehow better retrieved with the addition of higher modes, by considering the median. Note that in order to make

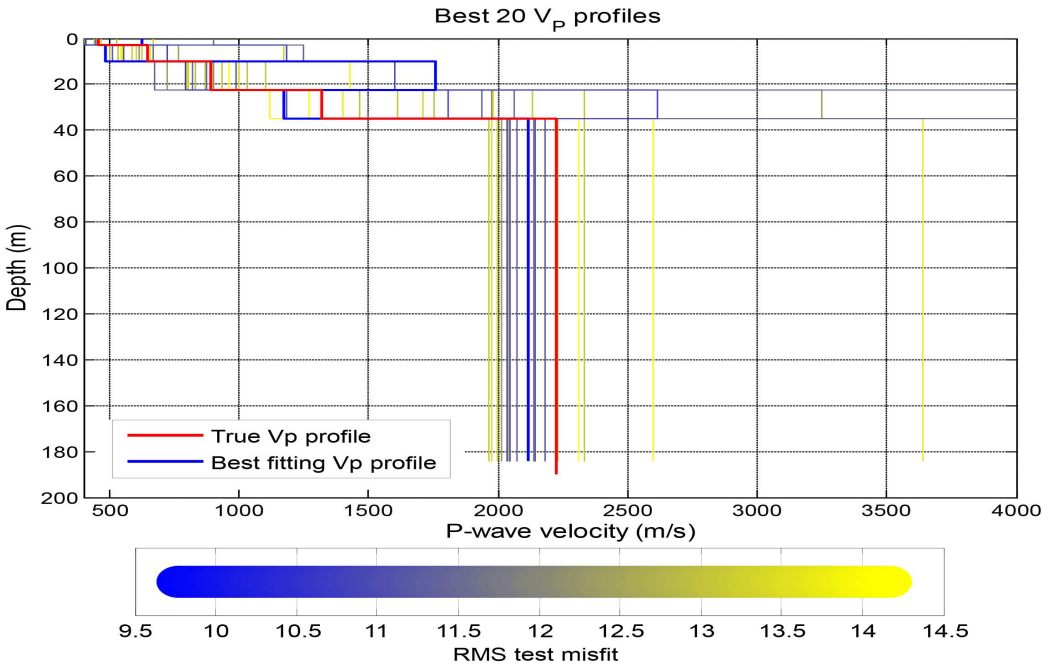

Figure 5.20. V_P profile of the misfit of the modal curves for the 20 best fitting profiles for the fundamental mode inversion . Fixed thickness

the comparison between the modes appropriate a misfit in the distance RMS (eq:5.5) higher than 30 was not considered for the statistical analysis for all the inversion with different modes. Besides, fig. 5.18 , shows that the standard deviation respect the V_P distribution is similar for the fundamental mode, the first and second higher mode inversion.

Additionally, the V_P of the 20 best misfit fitting profiles of the modal curves are shown, for fundamental mode in fig. 5.20 , for two modes in fig. 5.21 and for three modes in fig. 5.22.

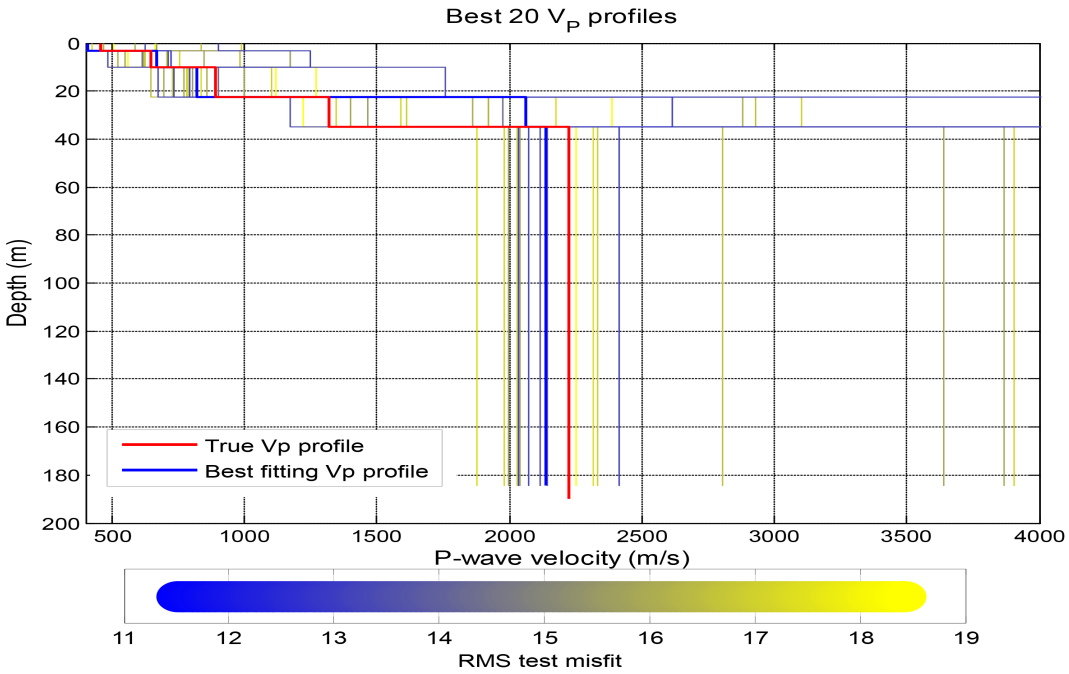

Figure 5.21. V_P profile of the misfit of the modal curves for the 20 best fitting profiles for the fundamental and first higher mode inversion . Fixed thickness

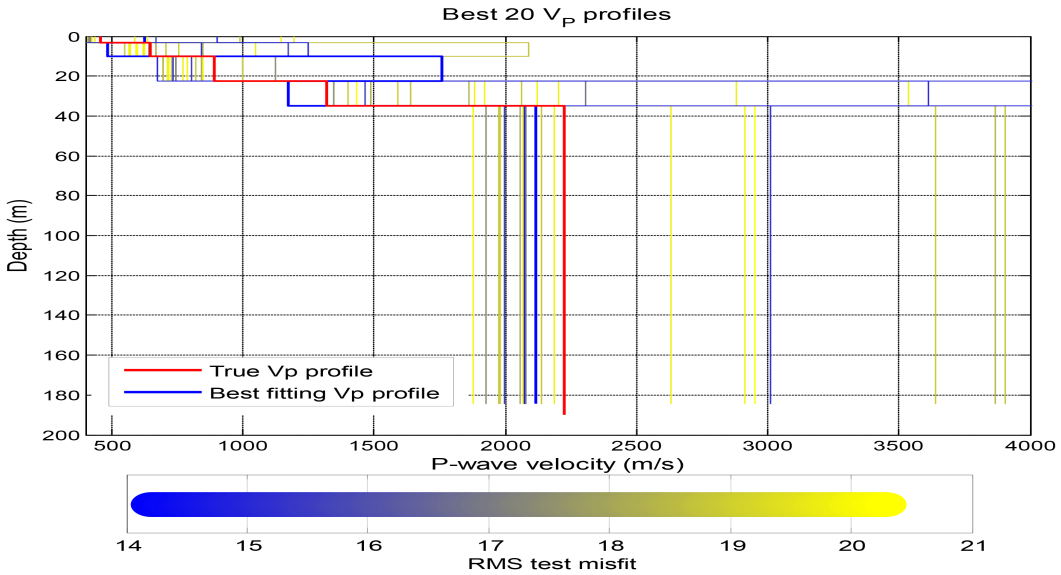

Figure 5.22. V_P profile of the misfit of the modal curves for the 20 best fitting profiles for the fundamental mode and first and second higher inversion . Fixed thickness

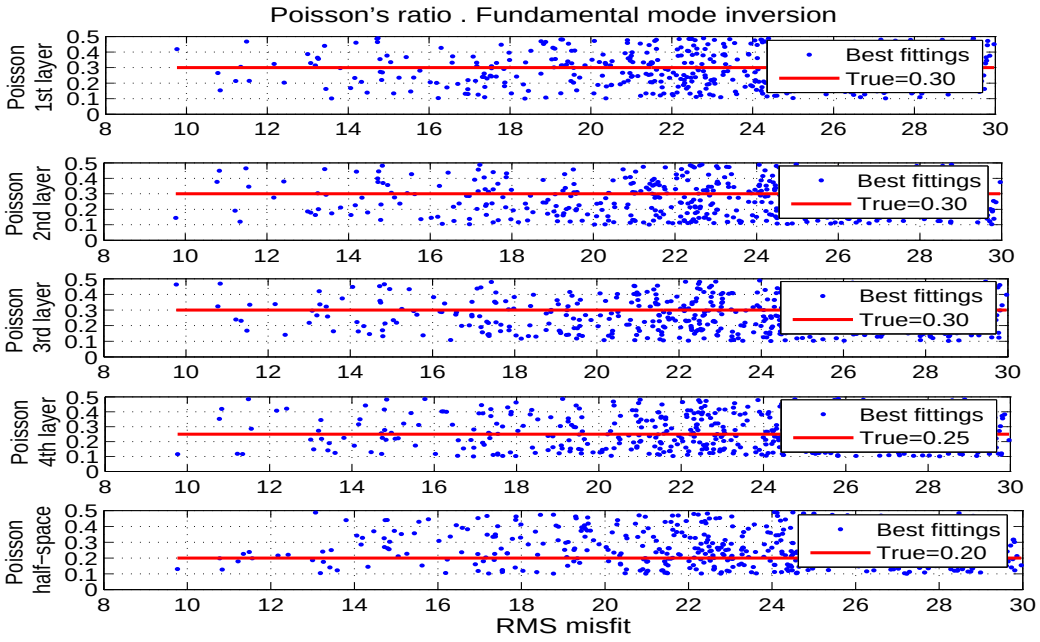

Figure 5.23. Poisson's ratio of the misfit of the modal curves for a RMS lower than 30. Fundamental mode inversion. Fixed thickness

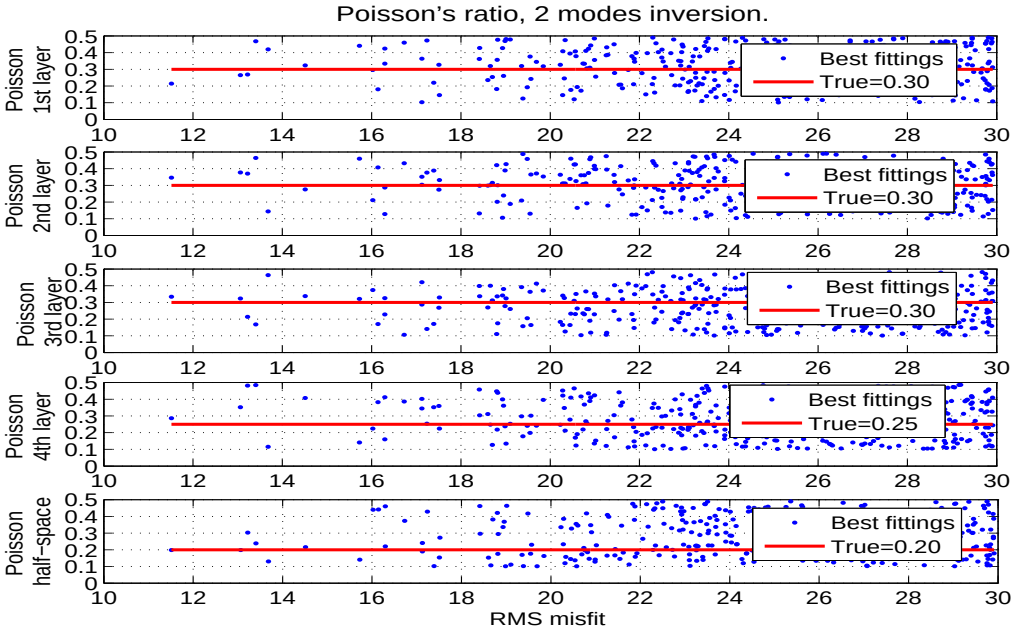

Figure 5.24. Poisson's ratio of the misfit of the modal curves for a RMS lower than 30. Two modes inversion. Fixed thickness

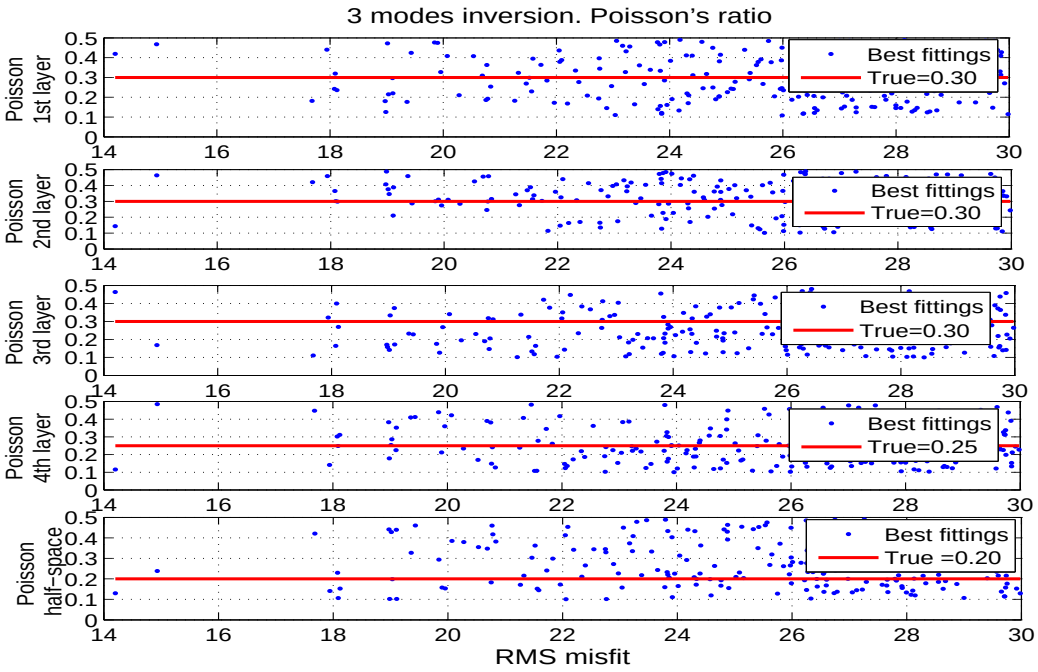

Figure 5.25. Poisson's ratio of the misfit of the modal curves for a RMS lower than 30. Three modes inversion. Fixed thickness

Meanwhile, the Poisson's ratio (ν), can be seen in the successive plots. In fig. 5.23 is depicted for fundamental mode inversion, in fig. 5.24 for two modes inversion and in fig. 5.25 for three modes inversion.

5.3.3 Estimation of the compressional wave velocity (V_P) or Poisson's ratio (ν) of the layered medium with fixed thickness , density and V_S

The final step, was to redefine the model parameters space for the Monte Carlo multimodal inversion, by fixing the layer thickness and V_S from the previous steps, in order to retrieve better the results for the V_P .

The fig. 5.26 , shows the V_P for the 20 best fitting profiles, for the fundamental mode inversion, in fig. 5.27 for two modes inversion and in fig. 5.28 for three modes inversion.

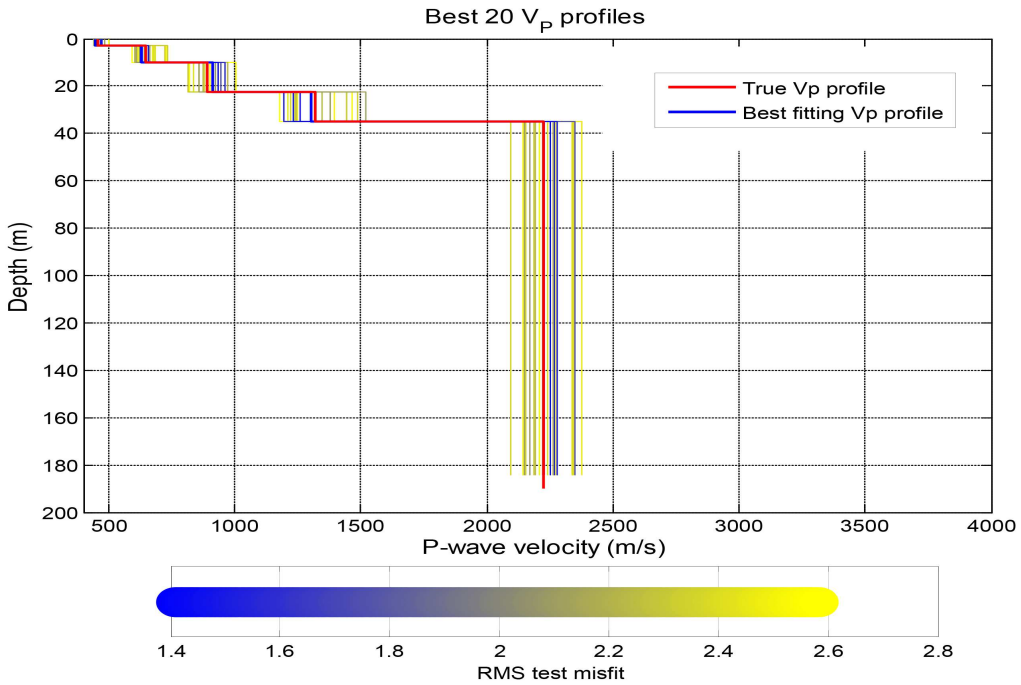

Figure 5.26. 20 V_P best fitting profiles for fundamental mode inversion. Fixed thickness ans V_S

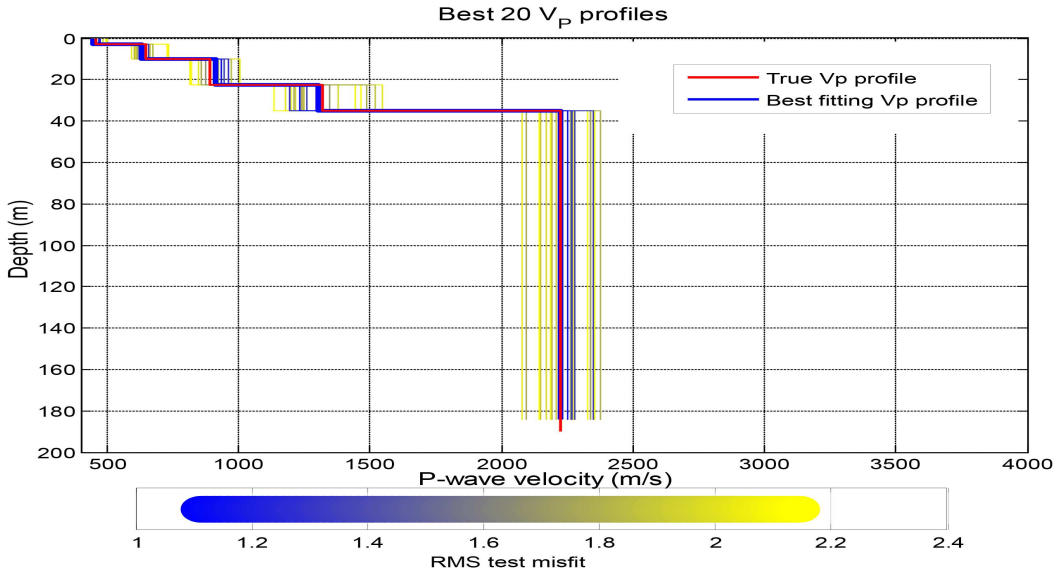

Figure 5.27. 20 V_P best fitting profiles for fundamental mode plus 1st higher mode inversion. Fixed thickness ans V_S

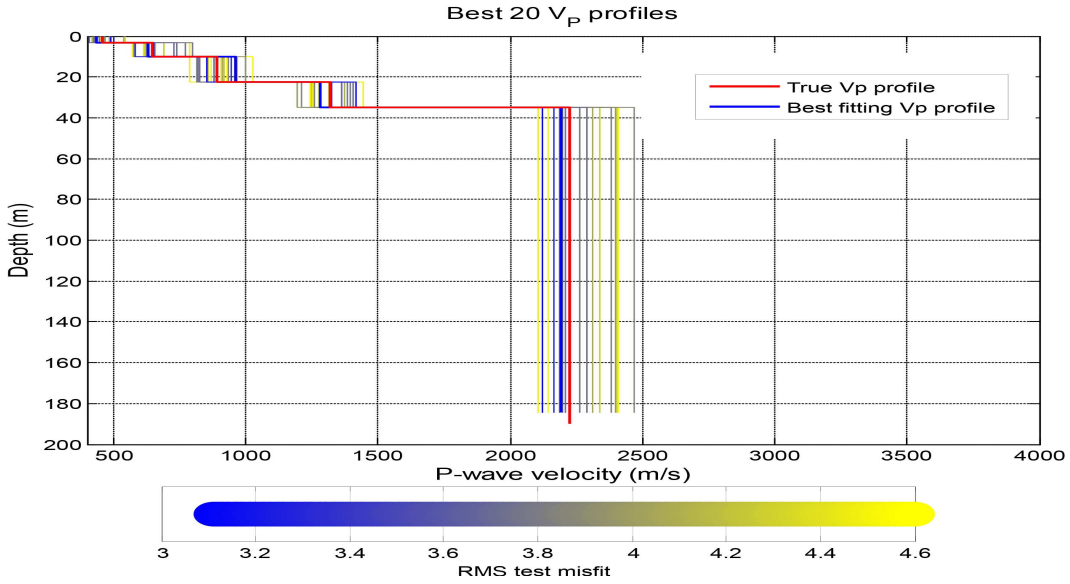

Figure 5.28. 20 V_P best fitting profiles for fundamental mode plus 1st higher mode and 2nd higher mode inversion. Fixed thickness ans V_S

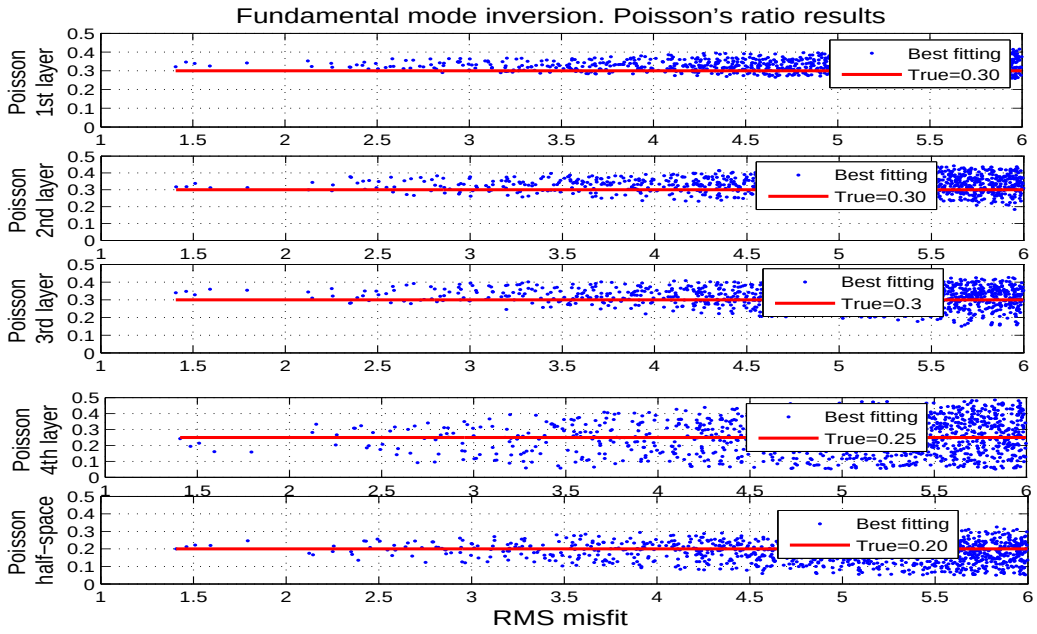

Figure 5.29. Poisson's ratio. Fundamental mode inversion. Fixed thickness and V_S

Furthermore, the fig. 5.29 express the relation to the Poisson's ratio obtained from the fundamental mode inversion of the best fitting models of the distance RMS misfit. Then, for two mode inversion is shown in fig. 5.30 and finally, for three modes inversion in fig.5.31.

The fig. 5.32, shows the summary of the results of the Poisson's ratio for each layer and different modes, with fixed thickness and V_S . The mean value was used in this opportunity instead of the median as the statistical parameter, we have to take into account that in this opportunity the final solution of the Poisson's ratio is not a log-normal distribution and the values are not biased (skewed). So, the mean represents an appropriate and simple statistical measure to make the comparison. Besides, the standard deviation is shown, in fig. 5.33.

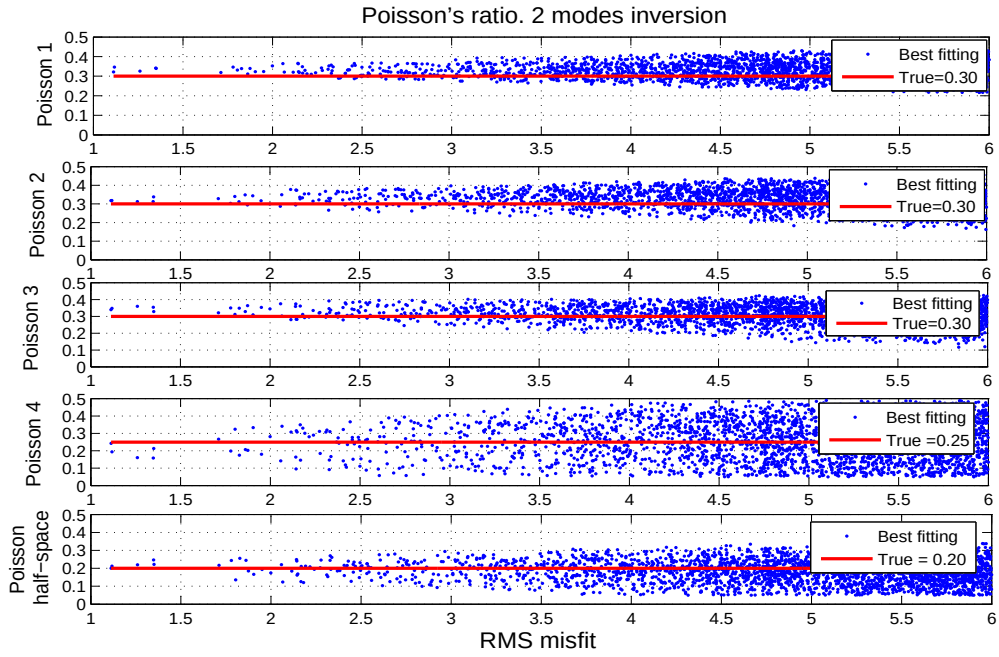

Figure 5.30. Poisson's ratio. Two modes inversion. Fixed thickness and V_S

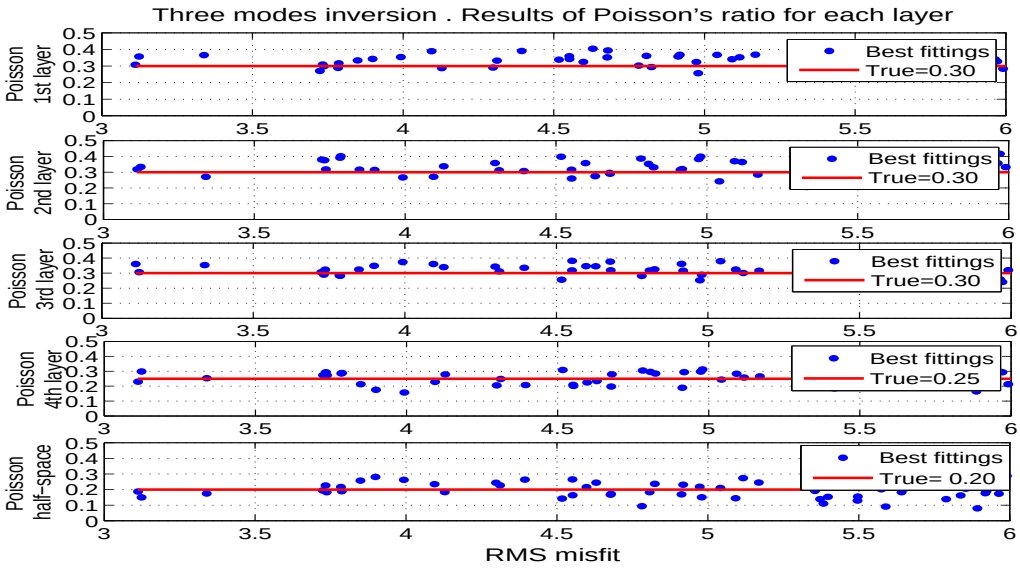

Figure 5.31. Poisson's ratio. Three modes inversion. Fixed thickness and V_S

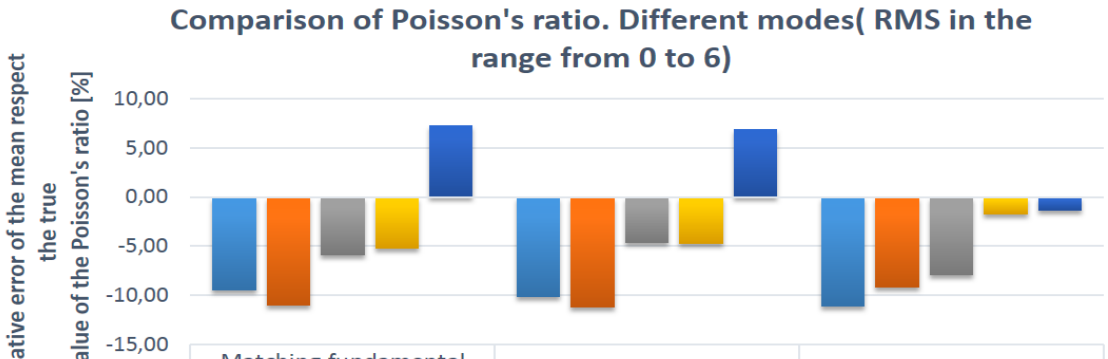

	Matching fundamental mode	Matching two modes	Matching three modes
1st Layer	-9,53	-10,16666667	-11,13333333
2nd Layer	-11,00	-11,23333333	-9,233333333
3rd Layer	-5,9	-4,7	-8
4th Layer	-5,28	-4,76	-1,72
Half-space	7,3	6,9	-1,35

Figure 5.32. Comparison of the mean Poisson's ratio to the Monte Carlo Multimodal Inversion for different modes . With fixed V_S and thickness.

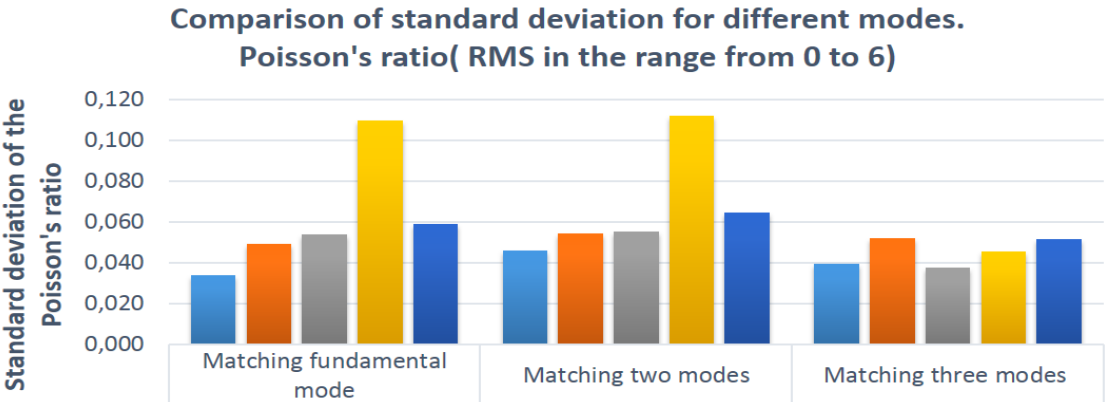

	Matching fundamental mode	Matching two modes	Matching three modes
1st Layer	0,034	0,046	0,040
2nd Layer	0,049	0,054	0,052
3rd Layer	0,054	0,055	0,037
4th Layer	0,110	0,112	0,045
Half-space	0,059	0,065	0,052

Figure 5.33. Comparison of the standard deviation of Poisson's ratio to the Monte Carlo Multimodal Inversion for different modes . With fixed V_S and thickness.

It can be seen from fig. 5.32, that the Poisson's ratio is well retrieved in the first three layers. Additionally, the last two layers (4th layer and half-space), seem to be improved by the inversion with three modes . Moreover, the final standard deviation, was also lowered by adding the third mode to the inversion. See figure 5.33.

The results of V_P seen in fig. reffig:Vp1modesHconstantVsfixed , fig.5.27 and fig. 5.28 agree with the true values of V_P .

5.4 Conclusion on the synthetic data

The results show that the best way to estimate the ν or V_P of the layered medium is to follow a step- by step inversion. First , V_S and thickness of the layers have been estimated. Then,the V_S and layer thickness were fixed for the inversion. Additionally, improvement inversion results have been evidenced by adding modes to retrieve V_P or ν . See figs. 5.19 , 5.18, 5.32 and 5.33. Particularly, for deeper layers (4th layer and half-space of table 4.2).

Nonetheless, the results obtained during the inversion process with fixed thickness (fig. 5.20 , fig.5.21 and fig. 5.22) , show that the sensitivity of V_P or ν obtained within the forward modeling to higher modes was still not enough to give an accurate solution, due to be much higher sensitive to V_S , hence the first run provides the V_S model and the second run is performed with fixed V_S and provides V_P .

Chapter 6

Application to real data. Analysis of Ground Roll from a seismic record

6.1 Introduction

Here we show the application of the inversion strategy proposed in chapter 5 to a field data. An exploration seismic record is processed to extract thedispersion curves and inverted to estimate both V_S and V_P profile.

6.2 Methodology applied to the data

The scheme of the workflow applied to the field dataset is shown in fig.6.1.

The main steps of the inversion are:

1. Analysis of the data in phase velocity vs pseudo-depth (fig.6.9) and definition of an initial model (layered model) but smoothed (with high number of layers).

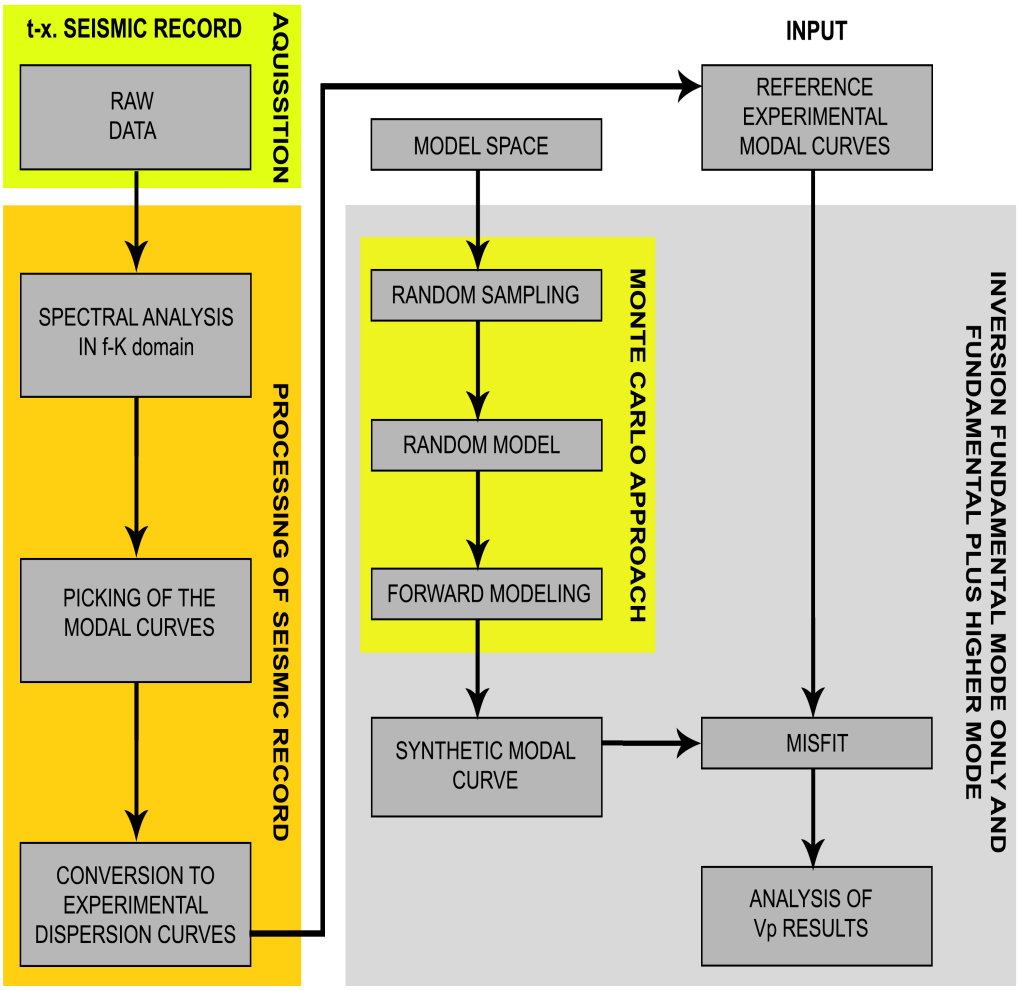

Figure 6.1. Logical scheme applied to the seismic exploration field dataset for the inversion

2. Definition of the model parameters space for a Monte Carlo multi-modal inversion based on the model of step 1.

3. Analysis of Monte Carlo inversion results (step 2) to find the zones of high gradients of velocity, that could be linked to a true interface.

4. Redefinition of the initial model on the bases of the results at point 3, according to a minimum parameterization.

5. Monte Carlo multimodal inversion with 1 million simulations, with fundamental mode and with higher modes.
6. Redefine the initial model on the bases of the results from step 5. Monte Carlo multimodal inversion with fixed V_S and thickness of each layer with 500 thousand simulations.
7. Compare the results with fundamental and first higher mode.

6.3 Data: Quality and content of surface waves

Table 6.1. Acquisition parameters for field data

Sampling rate[s]	Record length [s]	Time samples	# of Traces	Trace spacing [m]
0.004	14.504	3626	1280	30

The records made vertical components measured by tri-axial receivers of 5.5Hz. The horizontal components were not considered. Nonetheless, the possibility to have data H -in line and H-cross line offers additional potential for the study. The raw seismic exploration data are seen in fig. 6.2 and the seismogram of one shot gather is shown in detail for fig. 6.3.

The analysis of the data shows that:

- It is present a considerable amount of Ground Roll with an optimal signal-to-noise- ratio.
- There is enough separation between the Ground Roll and direct and refracted P-waves. This makes possible to isolate in a simple way the seismic events for an easier interpretation.
- The high content in low frequency allows a high investigation depth to be reached
- The spatial spacing is coarse and produces spatial aliasing. Considering that the events of interest are well separated from the body waves. It was possible to recover the aliased signal by enlarging the range of the analyzed wavenumber.

In fig. 6.2 , we show the raw seismic exploration data. The plot was make for time samples vs trace number. In order to get the y-axes in time (seconds), it is just a matter of taking the sampling rate given in table 6.1 and multiplying by each time sample. The offset can be calculated from the trace number and the respective spacing between traces given in table 6.1. So on, in fig. 6.3 , it has been built the plot of offset (meters) vs time(milliseconds),which represents the first right shot gather from the fig. 6.2 and contains surface and body waves.

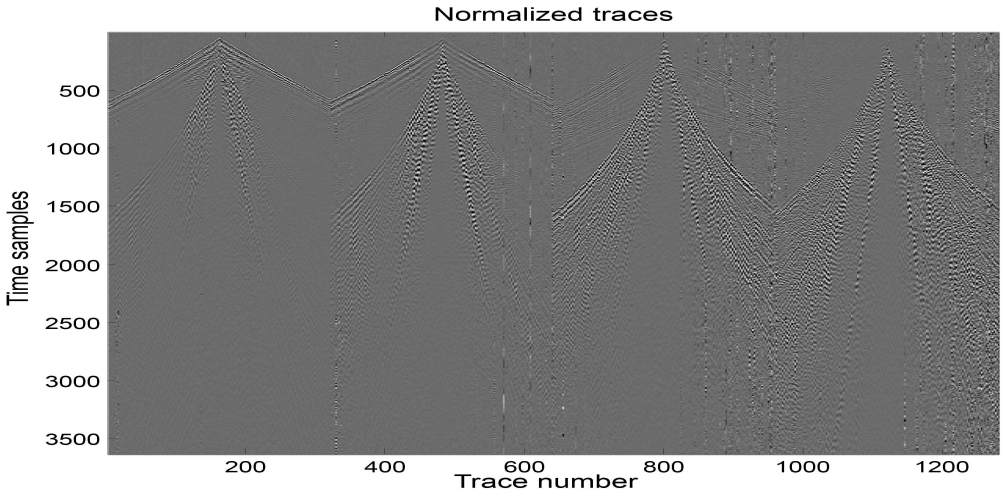

Figure 6.2. Raw seismic data

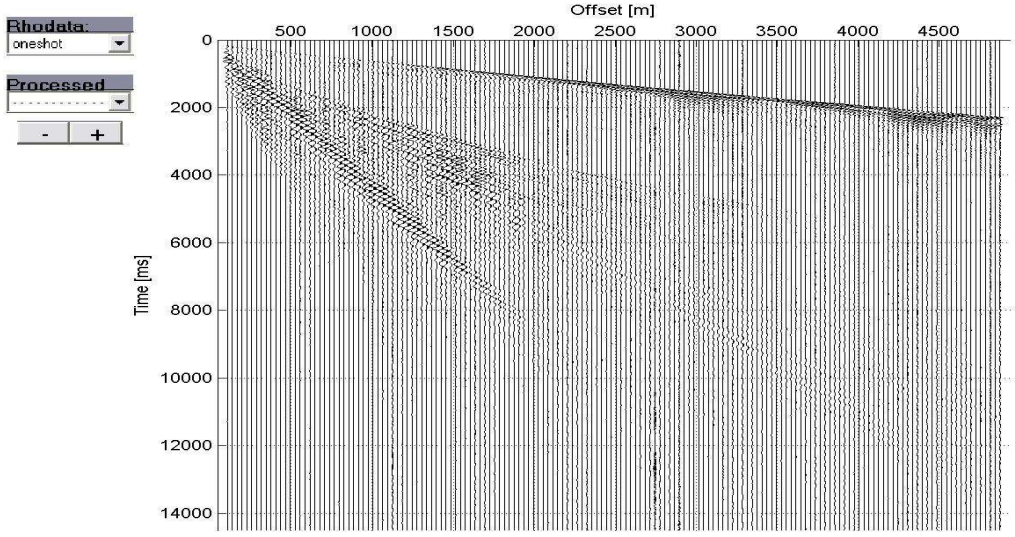

Figure 6.3. Seismogram first right shot point gather of fig. 6.2 (measurements of vertical components). Not muting of body waves

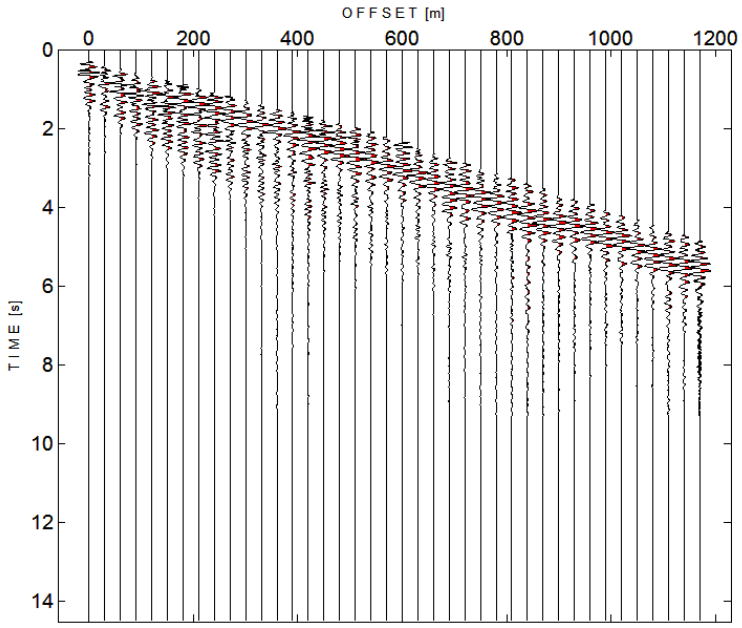

Figure 6.4. First 40 traces with muting of the body waves of fig. 6.3

6.4 Processing: from the record to the dispersion curves

To extract the dispersion curves a $f-K$ processing was performed. Before extracting the dispersion curves the data were windowed in offset domain to reduce the risk of lateral variations beneath the receiver spread. A windowing of the record was applied in groups of 40 traces (dividing the seismogram in 8 parts for the first shot gather of fig. 6.2) , e.g., fig. 6.4 (where the offset refers to the first channel and not to the source).

The dispersion curves obtained per each group of 40 traces, were associated each of them to the position of the center of the window.The dispersion curves were estimated by picking the maxima of the normalized $f-k$ spectrum (fig. 6.8). Then, the curves were represented in a phase velocity vs frequency (fig. 6.5).

The curves in fig.6.5, represent the fundamental mode curves from the first shot gather of fig. 6.2. They evidence that:

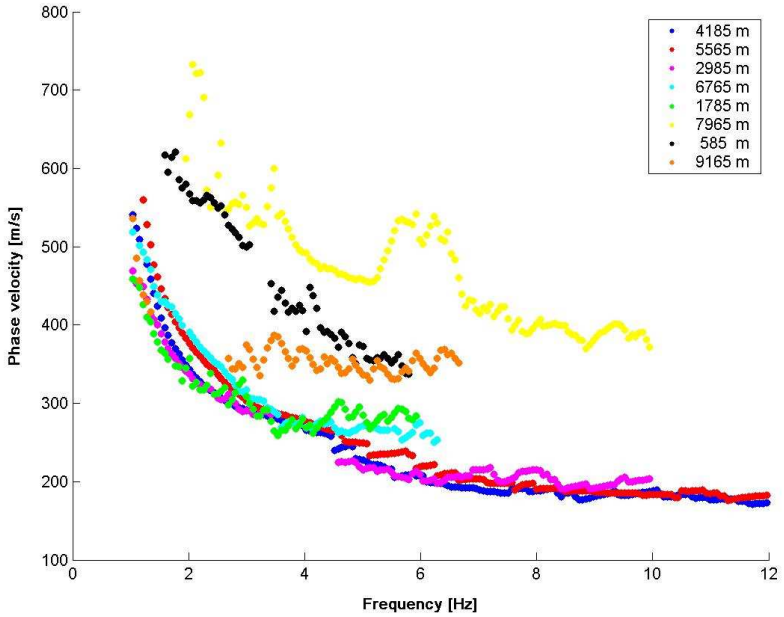

Figure 6.5. Fundamental mode curves derived from dividing the first shot gather of the seismogram of fig.6.2 in 8 parts and associating each of them to the position of the center of the window

1. A reduction of the content at high frequency respect to the part of the record farther from the source which makes more difficult to solve the first meters of the subsoil .

2. A very similar behavior in the central part of the record, meanwhile there is a worst result in the fundamental mode curves located at larger offset. This is influence for the fact of a not favorable signal to noise ratio.

The approach 1D used for processing and inversion for very long offset increases the risk on the data to be more influence by lateral variations of the seismic properties.

Due to the poor quality of the modal curves obtained in the far offset (See fig. 6.5), it has been decided to invert only the curve referred to the shortest offset of the right first shot point gather of fig. 6.3, which corresponds to the first 40 traces shown in fig. 6.4.

The analysis of the spectrum $f - k$ obtained from fig. 6.4 can be seen in fig.

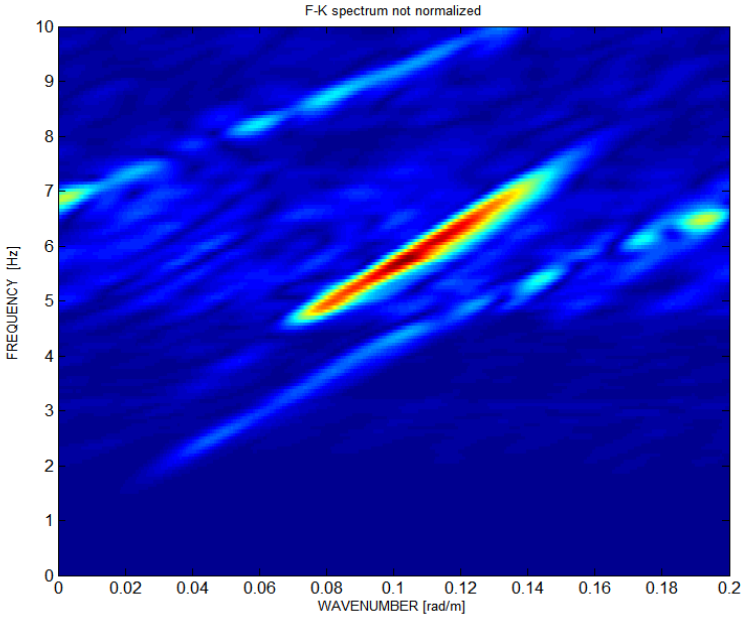

Figure 6.6. Spectrum $f-k$ of the seismogram of fig. 6.3.

6.6 and normalized in fig. 6.8 and then in fig. 6.7 just zoomed . These were used to recover the aliased part of the signal. Meanwhile, the final picking for obtaining the experimental dispersion curves are shown in fig. 6.8.

1. It is possible to follow the dispersive events, fundamental mode and higher modes, because they separate very clearly in the $f-k$ domain shown in fig. 6.7, without applying muting of the body waves.

2. The aliased frequency can be recovered from the normalized $f-k$ spectrum shown in figure 6.8 as stated before .

In general, the quality of the data is and allows an accurate recovery of the information of the dispersive events associated to the propagation of the pseudo-Rayleigh waves. In particular is important to underline that the high spectral resolution due to the larger offset permits to isolate very well the contribution of the different modes of vibration allowing recovering the fundamental mode and also the higher modes for the Monte Carlo multimodal inversion. (See fig. 6.8).

To get a preliminary idea on the depth of penetration that can be reached, it

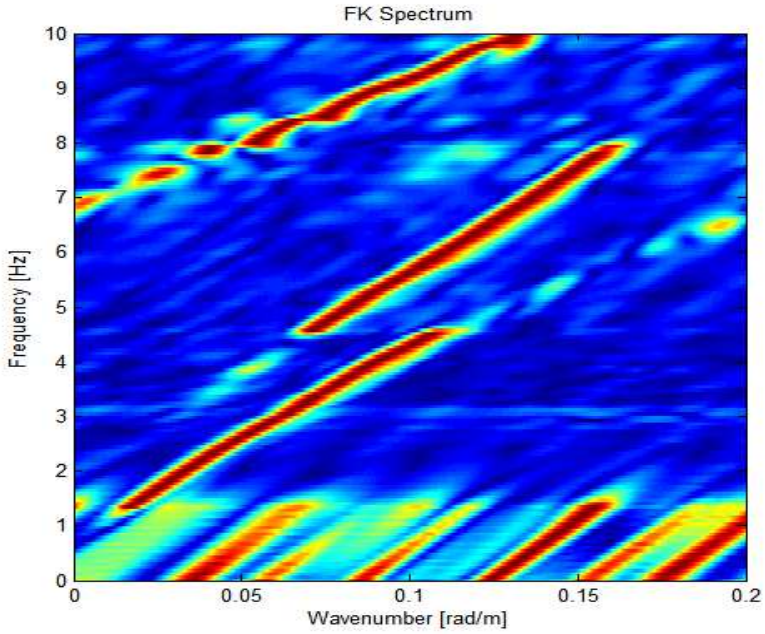

Figure 6.7. Zoom of the normalized $f - k$ spectrum of fig. 6.3.

was used a representation of the curves in the plane of phase velocity vs pseudo-depth (fig. 6.9) for the central part of the record from the first shot point gather of fig. 6.2 , where the pseudo-depth is assumed to be approximately one third (1/3) of the λ . Such assumption, is based in the fact that the vertical displacements associated to the propagation of the fundamental mode corresponding to the Rayleigh waves for a homogeneous and isotropic half-space reaches a depth around the wavelength and has its maximum at a depth close to $\lambda/3$.

In consequence, it can be hypothesize that in the data acquisition, the properties of the material are going to be sensitive at this depth. Obviously, this is not applicable to a layered medium as the one presented in the thesis , nonetheless the representation of $\lambda/3$ can be used, as an instrument to make a preliminary and roughly estimation of the investigation depth. So, it can serve as a reference for the construction of an initial model consistent with the data for the inversion process.

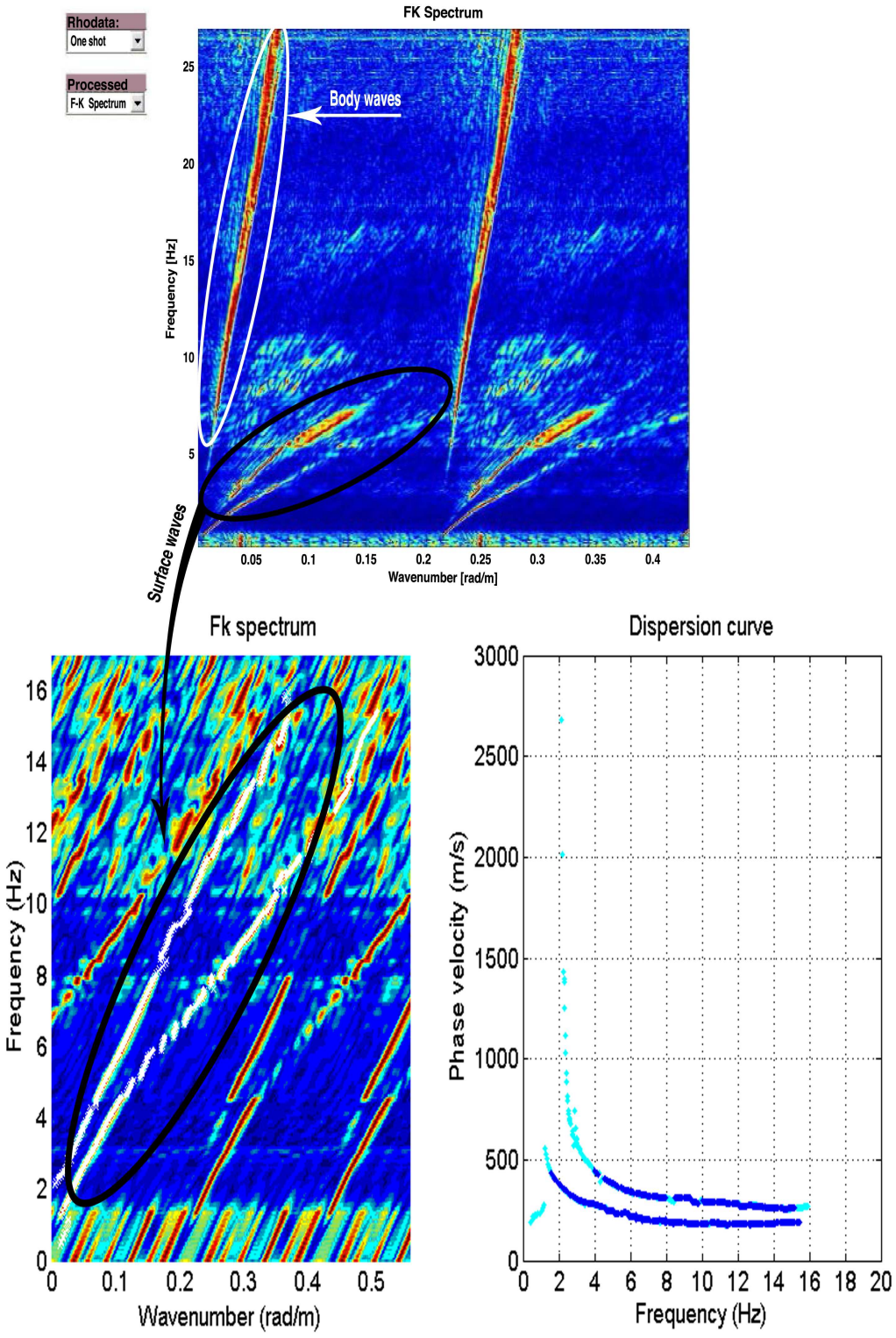

Figure 6.8. Picking to obtain the experimental dispersion curves.

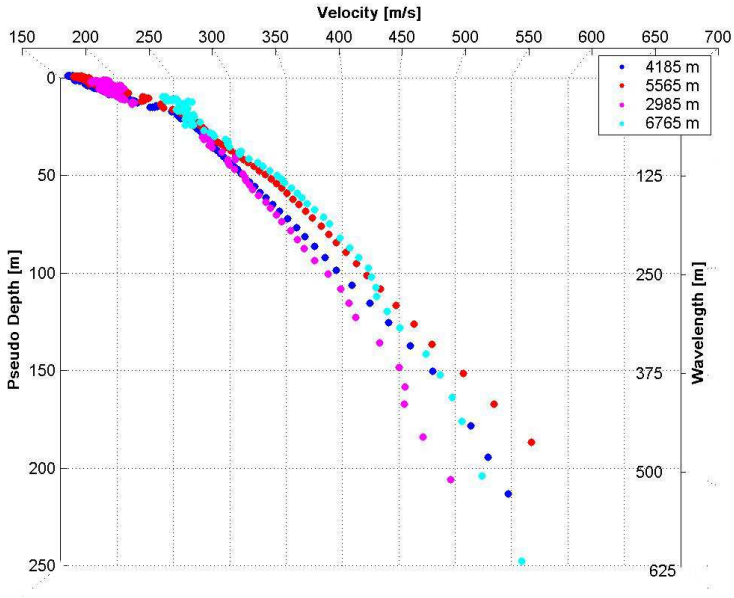

Figure 6.9. Fundamental mode obtained from the central part in λ-v domain

The good quality of the data has been confirmed on the processing phase. Consequently, it was possible to estimate with more accuracy the fundamental and the higher modes of the pseudo-Rayleigh waves in a wide range of frequency. The analysis of the curves 6.9, shows that the record from seismic exploration field dataset , allows to recover a lot of information to a considerable depth (Approximately around 150 meters) , but there has to be mentioned a lot of noise in the first 10 meters with makes them difficult to resolve. See Figures: 6.6 , 6.7 and 6.8.

6.5 Results of the Monte Carlo multimodal inversion on the seismic exploration data

Table 6.2, shows the model parameters space used for the Monte Carlo multimodal inversion, according to the criteria at point 3 and redefining the initial smoothed model (step 4) .

Table 6.2. Model parameters space according to step 4

Parametrization	Thickness [m]	V_S [m/s]	Density[Kg/ m^3]	Poisson	V_P [m/s]
Layer 1	10-20	190-300	1800	0.10-0.49	285-1357
Layer 2	30-70	190-600	1800	0.10-0.49	285-4285
Layer 3	70-100	350-700	1800	0.10-0.49	525-4999
Half-space	∞	500-1000	1800	0.10-0.49	750-7141

6.5.1 Results for V_S , layer thickness and V_P for fundamental mode inversion. Step 6

Fig. 6.10 , is the plot of the Haskell and Thomson matrix determinant for the Monte Carlo multimodal inversion. The deep blue color represents the zero of the function which theoretically contains the modal curves. Meanwhile, the white dots take into account the experimental dispersion curves retrieved from the picking of fig. 6.8.

Fig. 6.11 , shows the 20 best fitting curves for fundamental mode inversion. There is evidence of a good fitting of the Monte Carlo approach respect to the experimental dispersion curves obtained from fig.6.8.

Further, in fig. 6.12 has been depicted the 20 best fitting V_S profiles according to the distance weighted RMS misfit, for the fundamental mode inversion. There has been a good agreement of the V_S compare with the values from fig.6.16 for two modes inversion. However, the V_S of the half-space seems to be overestimated with just fundamental mode.

Whereas, the fig. 6.13 shows the 20 best fitting V_P profiles, for fundamental mode inversion. The V_P results seem not so well established for the last two layers

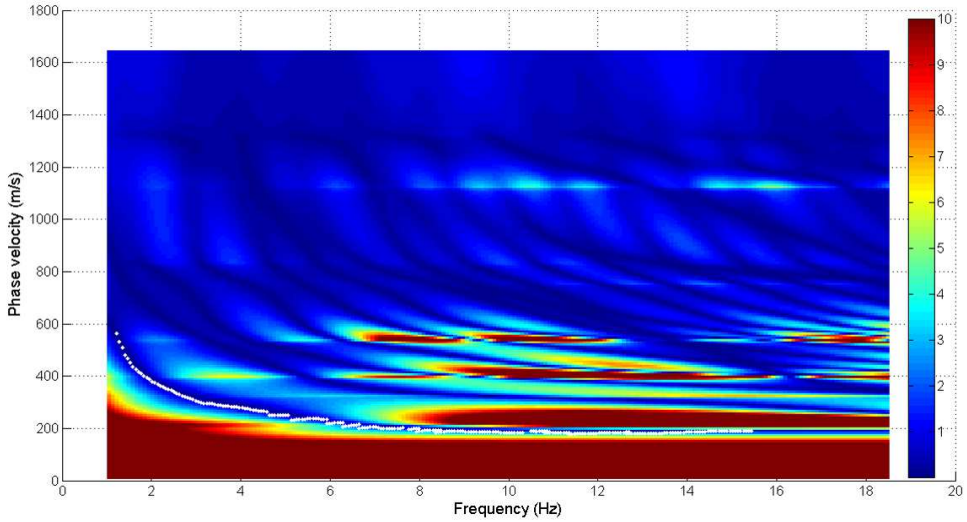

Figure 6.10. Best fitting model from the Haskell and Thomson determinant misfit. Fundamental mode inversion

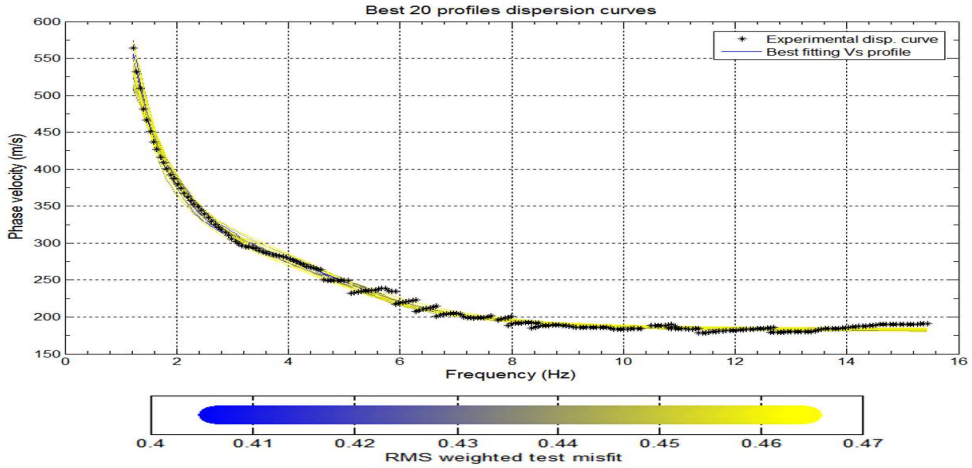

Figure 6.11. Best 20 fittings of the dispersion curves. Fundamental mode inversion. Input data of table 6.2. According to the distance weighted RMS (Equation:5.6)

(4th layer and half-space) because of the scattered of the inversion solution.

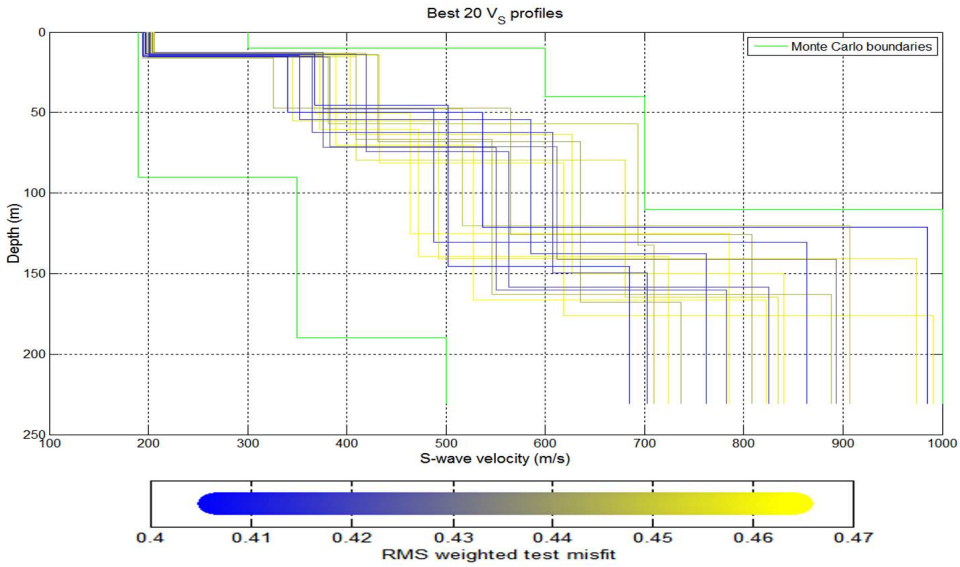

Figure 6.12. V_S profiles for the best fittings. Fundamental mode inversion. Input data of table 6.2. According to the distance weighted RMS (Equation:5.6)

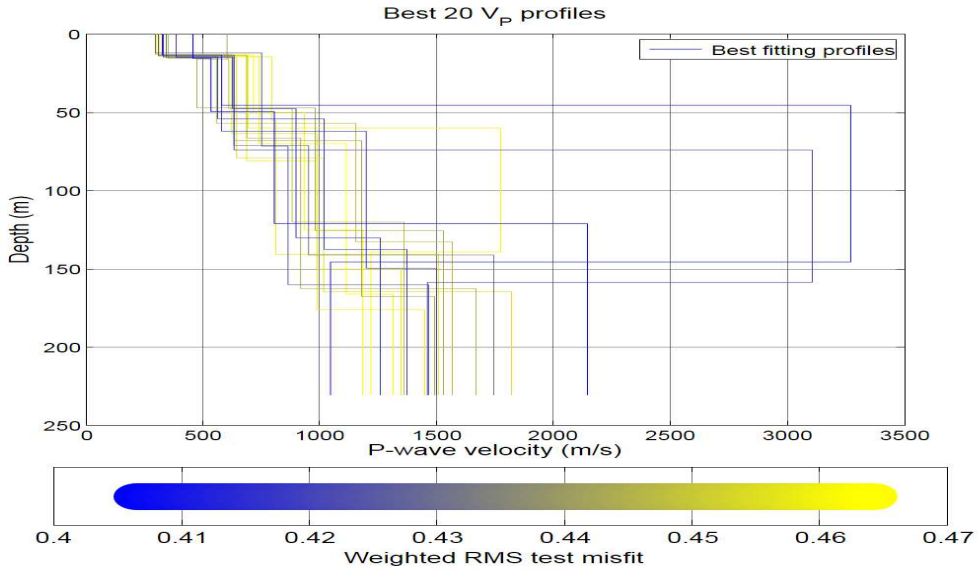

Figure 6.13. V_P profiles for the best fittings. Fundamental mode inversion. Input data of table 6.2. According to the distance weighted RMS (Equation:5.6)

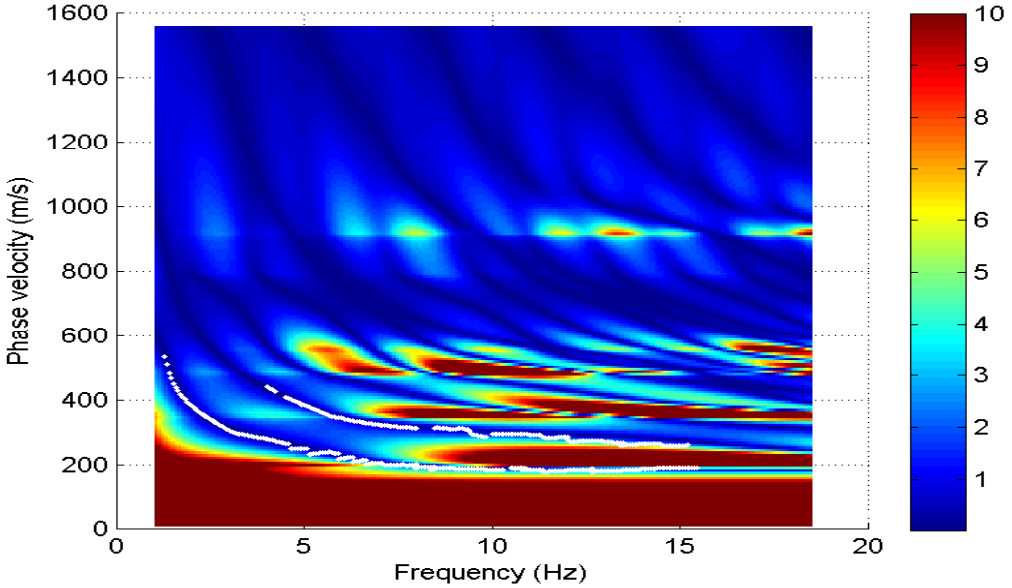

Figure 6.14. Best fitting model from the Haskell and Thomson determinant misfit. Two modes inversion

6.5.2 Results for V_S , layer thickness and V_P for two modes inversion. Step 6

Fig. 6.14 shows the best fitting model from the Haskell and Thomson determinant misfit for two modes inversion. The deep blue color refers to value of the determinant misfit close to zero. Secondly, fig. 6.15 represents the 20 best fitting dispersion curves for fundamental and first higher mode. There is evidence of a good fitting of the experimental data with the inversion model.

Fig. 6.16, expresses the 20 best fitting V_S profiles by fundamental and first higher mode inversion. The best results are colored in blue. Furthermore, a similar plot has been built for V_P . The results from 6.17 are less dispersed compared with the one found in fig. 6.13.

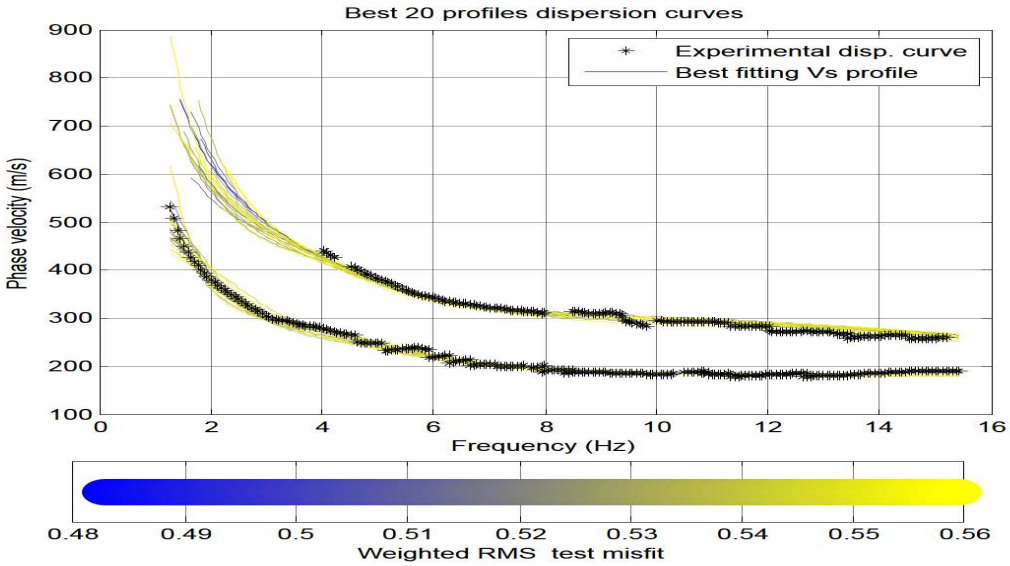

Figure 6.15. Best 20 fitting of the dispersion curves. Fundamental and first higher mode inversion. Input data of table 6.2. According to the distance weighted RMS misfit (Equation: 5.6)

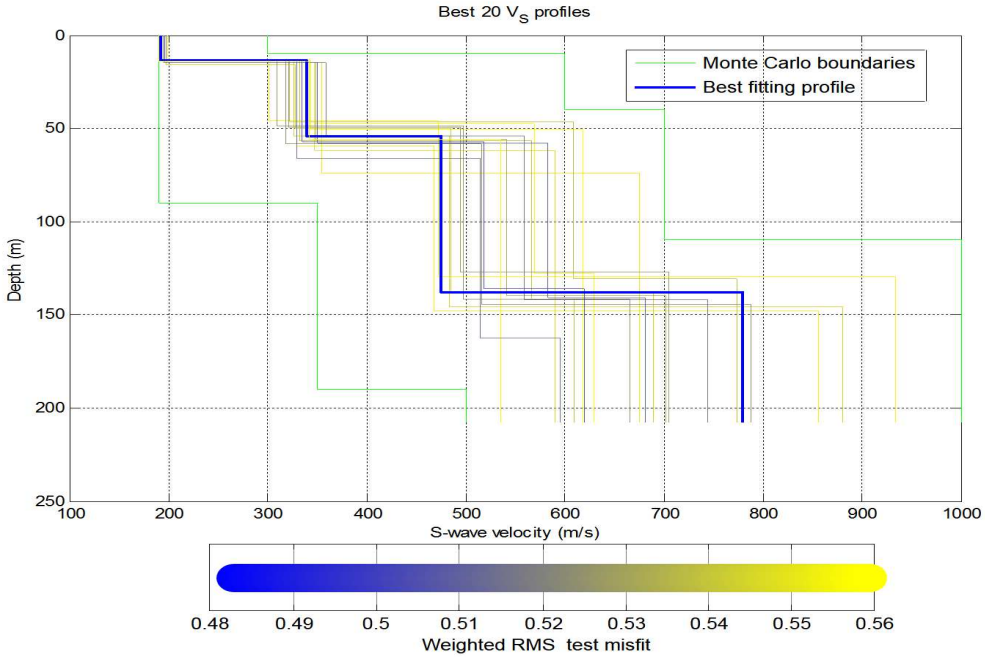

Figure 6.16. 20 V_S of the best fitting profiles. Fundamental and first higher mode inversion. Input data of table 6.2. According to the distance weighted RMS misfit (Equation: 5.6)

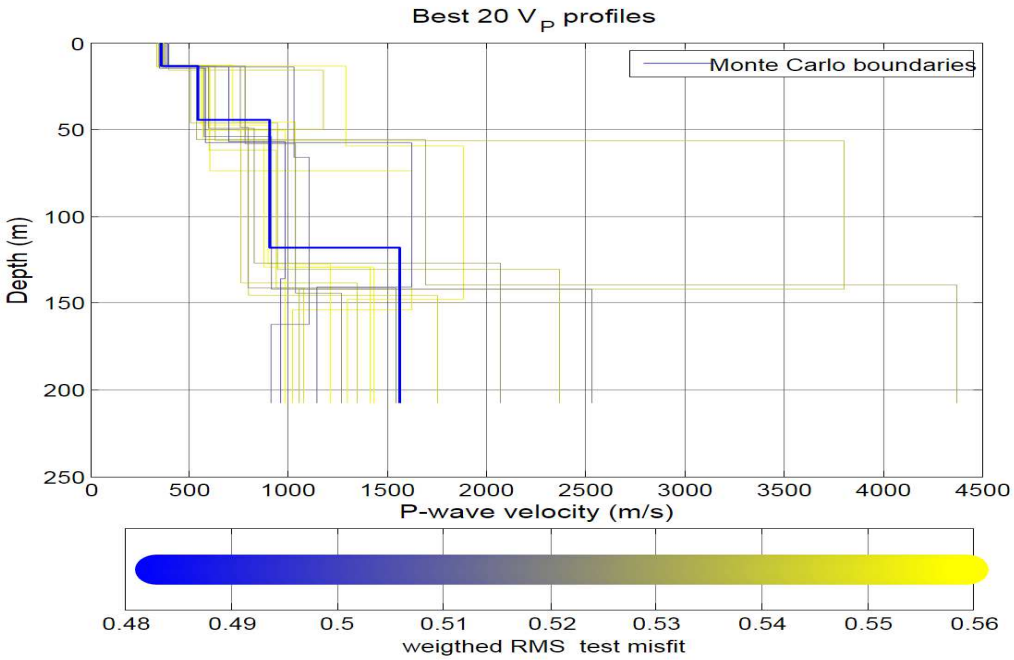

Figure 6.17. Misfit of the 20 best fitting V_P profiles. Fundamental and first higher mode inversion. Input data of table 6.2. According to the weighted RMS (Equation: 5.6)

6.5.3 Summary results from step 6

The final results for two modes inversion according to a minimum parametrization criteria (Table 6.2) evidenced the present of four layers: The first layer to a depth of 13 meters with shear wave velocity (V_S) of 192 m/s , the second layer which is from 13 m until 44 meters with a velocity of 339 m/s, the third layer from a depth of 44 m until 118 m with a velocity of 475 m/s and the last layer where it is not possible to evidence the bottom (half-space) the velocity arrived to 779 m/s. These results were obtained also with fundamental mode inversion. Nonetheless, the results for V_S (Figs. 6.16) were less well resolved for the half-space with fundamental mode inversion, compare with two modes inversion . Also, see comparison tables : 6.3 and 6.5.

Respect V_P , for the first Monte Carlo multimodal inversion. The summary is shown in table 6.4. For this particularly, exploration seismic dataset with, in contrast to the results for the synthetic inversion. There is considerably difference ,

by using fundamental mode compare with two modes inversion with the exception of the second layer. See figs. 6.13 and 6.17.

Table 6.3. Comparison of the V_S referenced to fundamental mode and then the addition of the first higher mode. Taken the best fitting profile

Results	Vs 1-mode [m/s]	Vs 2-modes [m/s]	Vs difference 1-mode [m/s]
Layer 1	195	192	3
Layer 2	340	339	1
Layer 3	537	475	62
Half-space	985	779	206

Table 6.4. Comparison of the V_P referenced to fundamental mode and then the addition of the first higher mode. Taken the best fitting profile

Results	Vp 1-mode [m/s]	Vp 2-modes [m/s]	Vp difference 1-mode [m/s]
Layer 1	457	355	102
Layer 2	532	545	13
Layer 3	804	905	101
Half-space	2144	1563	581

Table 6.5. Comparison of the layer thickness referenced to fundamental mode and then the addition of the first higher mode. Taken the best fitting profile

Results	H, 1-mode [m]	H, 2-modes [m]	H, difference 1-mode [m]
Layer 1	16	13	3
Layer 2	31	34	3
Layer 3	71	74	3
Half-space	∞	∞	∞

6.5.4 Results for V_P or Poisson's ratio for fundamental mode inversion. Step 7 and 8.

Fig. 6.18 shows the distance weighted RMS of the 20 best fitting V_P profiles. The blue lines represent the best fitting profiles and the misfit is expressed below in a linear color scale. In addition, fig. 6.19, covers the results of the Poisson's ratio for each layer. The blue dots, represents each of the points retrieved by the Monte Carlo multimodal inversion by fixing the thickness and the V_S of the model parameters space of table 6.2.

It can be seen that the half-space is not retrieved by the inversion. In contrast , the V_P of the first layer was well established. For the second and third layer, there was a strange behavior. At looking through the graph of fig. 6.19 , it can be observed that for these two layers, the Poisson's ratio is just following the lower limit of the model space parameters of table 6.2. In consequence, even the results appeared as not scattered in fig. 6.18, the two values may be not correct according

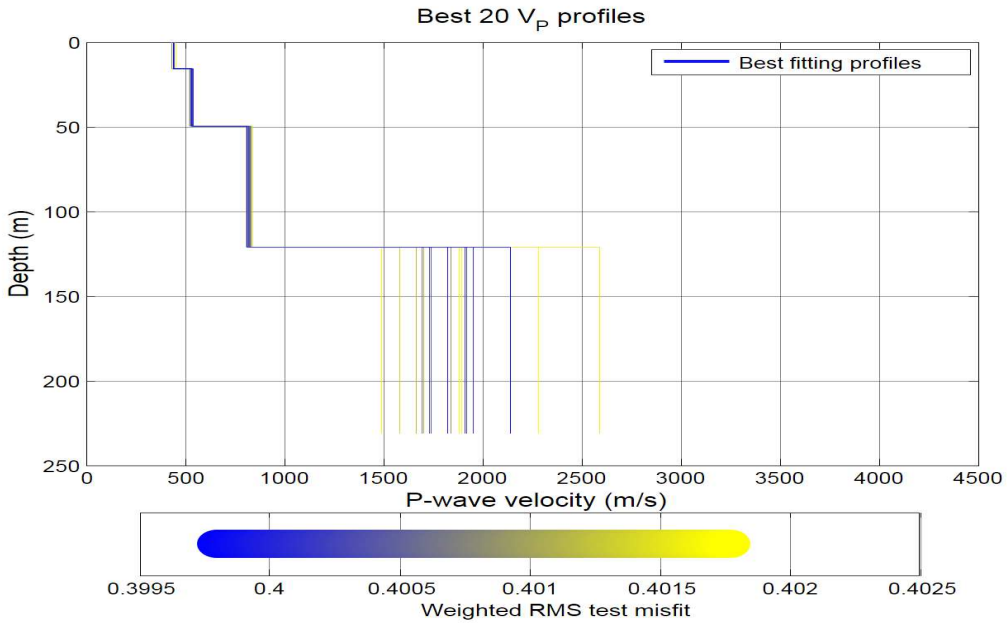

Figure 6.18. 20 best V_P fitting profiles. Fundamental mode inversion. By fixing the V_S and layer thickness of the model parameters space . According to the distance weighted RMS (Equation: refeq:weightedRMS)

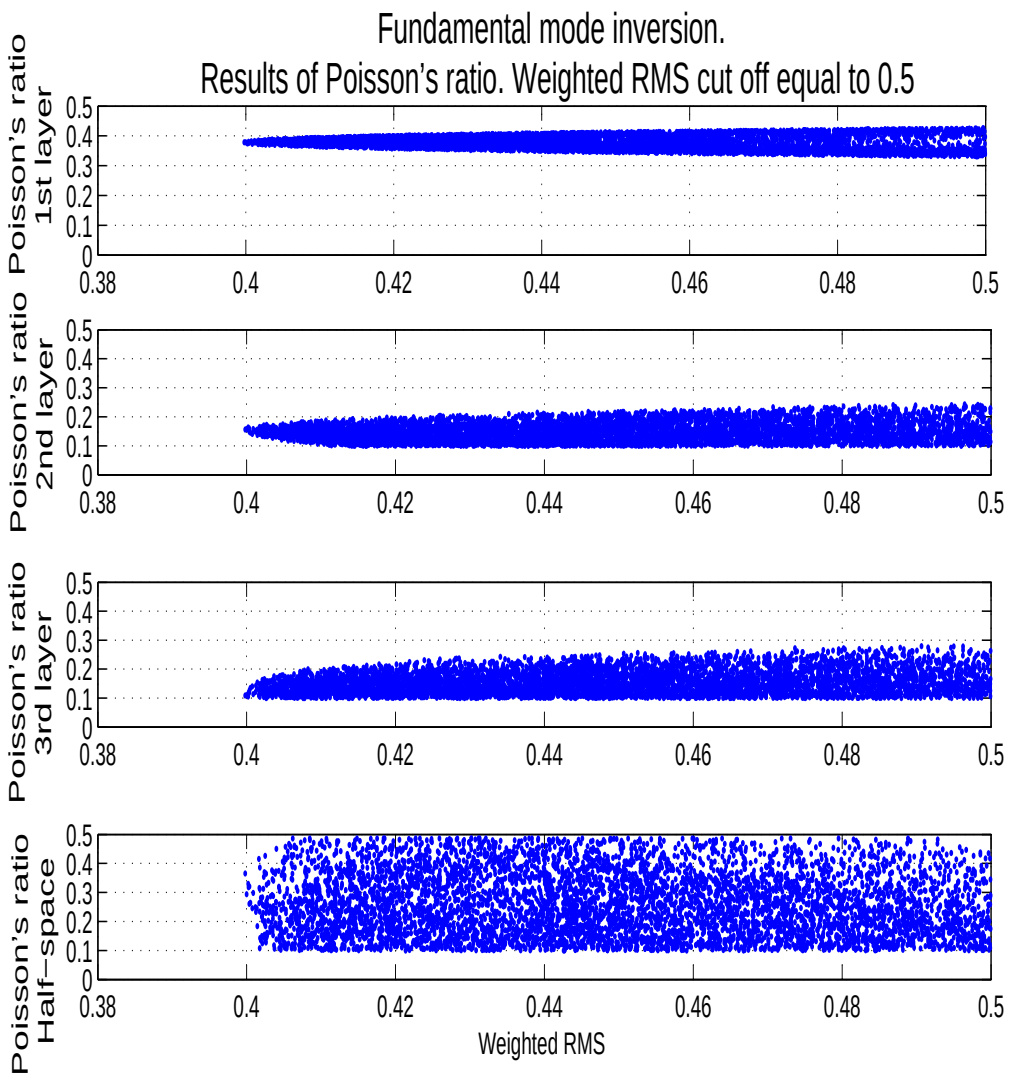

Figure 6.19. Best Poisson's ratio fittings from the distance weighted RMS misfit. Fundamental mode inversion. By fixing the V_S and layer thickness of the model parameters space

to this assumptions in which the data is following the trend of the lower limit with not sensitivity at all.

6.5.5 Results for V_P or Poisson's ratio for fundamental and first higher mode inversion. Step 7 and 8

Fig. 6.20, presents the misfit of the 20 best fitting V_P profiles for two modes inversion, by fixing the V_S and the thickness of each layer. The blue colors , represents in the color scale the best fittings according to the weighted RMS. It can be analyzed that the first three layers seems to be properly resolved. Even though, for the half-space there was not found too much sensitivity.

Likewise, fig. 6.21, shows the results of the misfit of the best fitting Poisson's ratio according to the distance weighted RMS for two modes inversion. Similarly, the Poisson's ratio (ν) seems to be well established for the first three layers. Despite this, the ν of the half-space does not present sensitivity to higher modes.

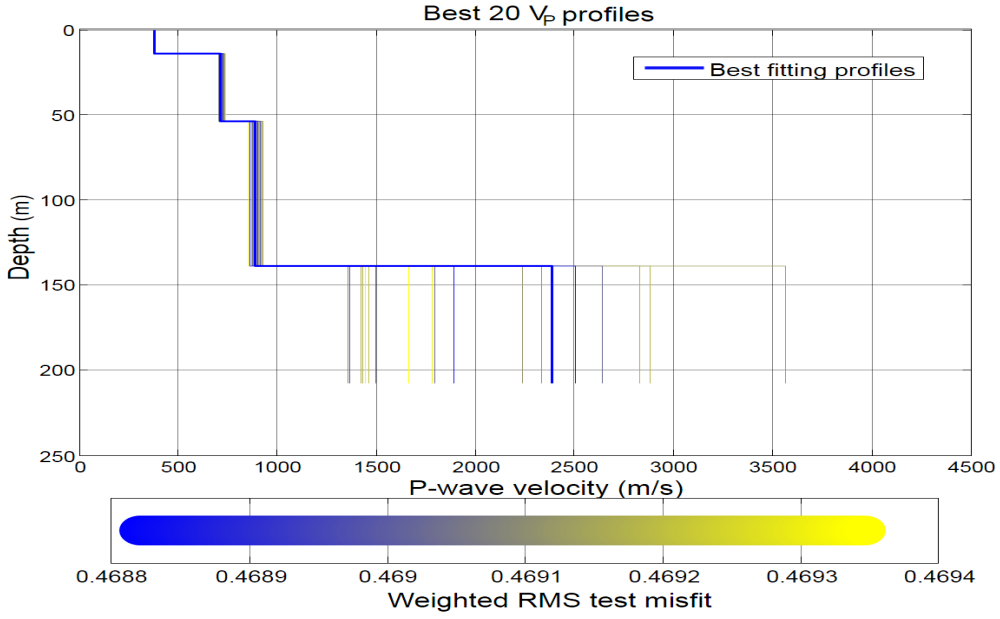

Figure 6.20. 20 V_P best fitting profiles from the weighted distance RMS misfit. Fundamental and first higher mode inversion. By fixing the V_S and layer thickness of the model parameters space.

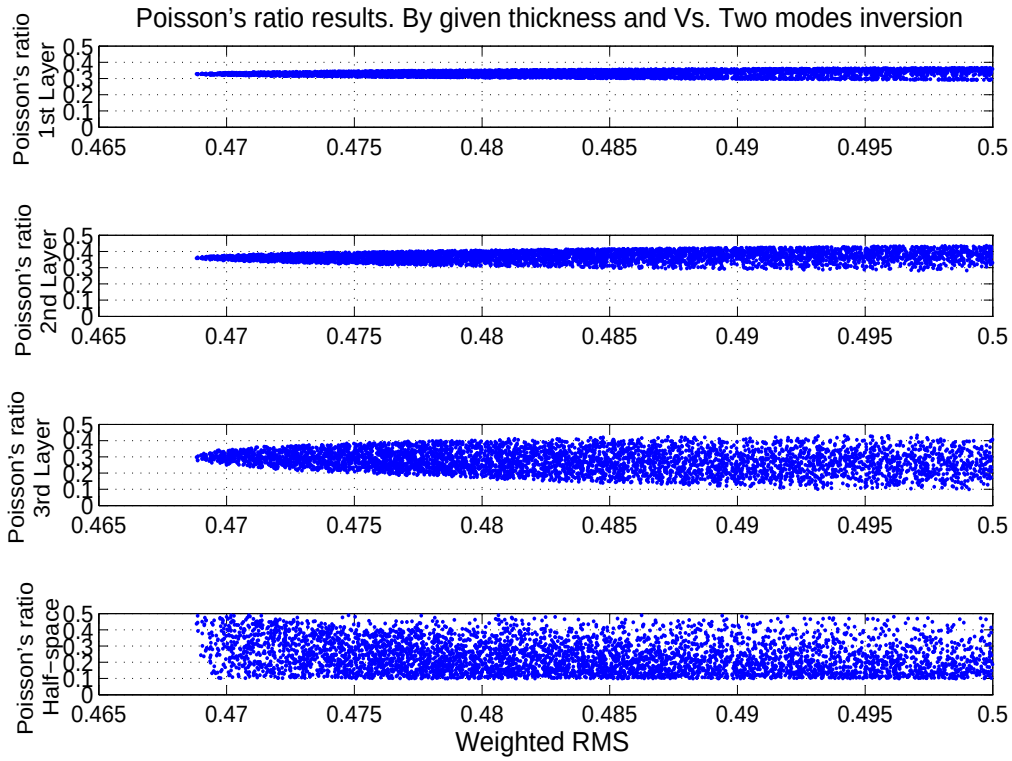

Figure 6.21. Poisson's ratio for the best fittings. Two modes inversion. By given the V_S and layer thickness of the model space parameters

6.5.6 Summary and comparison of the results of V_P or Poisson's ratio. Step 9.

From table 6.6, it can be seen that the Poisson's ratio (ν) of the first layer was retrieved by using the fundamental or two modes Monte Carlo multimodal inversion approach by given the layer thickness and the V_S of the model parameters space of table 6.2. The result obtained for ν seems in agreement with values from the Poisson's ratio of typical soils in the case of two modes inversion for the first three layers. In contrast, for fundamental mode inversion, the second and third layer (see fig. 6.19) , presented values of Poisson's ratio that contrast the results of the Monte Carlo multimodal inversion for two modes of fig. 6.21 and seem to follow the trend of the lower limit set to the Monte Carlo space parameters (equal to 0.10, see table

6.2) . The Half-space did not present sensitivity to fundamental or either higher modes.

Due to the fact, that velocity is link to the elastic properties of the material through the Poisson's ratio. The results of V_P , are affected for the results from ν of table 6.6. So, the results obtained for the Monte Carlo multimodal approach for the second and third layer respect to V_P with fundamental mode inversion (table 6.7), are also doubtful (or in discussion since the solution tends in the whole range to the lower limit set to the Monte Carlo multimodal inversion). Meanwhile, the first layer has been well resolved in terms of V_P for both: one and two modes respectively. (See table 6.7).

Finally, the half-space was not well resolved for one and two modes inversion. See tables: 6.6 and 6.7 and figs. 6.18 to 6.20.

Table 6.6. Comparison of the Poisson's ratio referenced to fundamental mode and then the addition of the first higher mode. Taken the best fitting profile from distance weighted RMS

Results	Poisson, 1-mode	Poisson, 2-modes	Poisson, 1-mode error [perc.]
Layer 1	0.378	0.328	15.24
Layer 2	0.156	0.358	56.42
Layer 3	0.109	0.297	63.30
Half-space	0.365	0.437	16.48

Table 6.7. Comparison of the P-wave velocity referenced to fundamental mode and then the addition of the first higher mode. Taken the best fitting profile from the distance weighted RMS

Results	V_P 1-mode [m/s]	V_P 2-modes [m/s]	V_P, 1-mode error [perc.]
Layer 1	441	380	16.05
Layer 2	533	715	25.45
Layer 3	811	892	9.10
Half-space	2138	2386	10.39

Chapter 7

Conclusion

The reason for studying surface wave analysis is to provide a near surface velocity model to be used for correcting seismic reflection data. In particular, after analyzing the main features of surface wave propagation and the processing steps used to analyze surface wave signals to retrieve near surface S-wave velocity model, this work has focused on the possibility to extract also P-wave information by adding the contribution of higher modes of propagation to the processing workflow. The idea that including higher modes of propagation could provide a significant sensitivity to P-wave velocity was originated in a previous study (Bergamo and Socco, 2013) regarding surface wave analysis in homogeneous granular materials and it is here extended to layered systems.

To assess the possibility to retrieve the compressional wave velocity (V_P) from surface wave analysis by adding higher modes to inversion, a sensitivity analysis has been performed in the first part of the thesis by considering a synthetic layered velocity model, which has been used to simulate fundamental and higher modes of propagation. A parametric study with extensive simulations (three hundred seventy one total simulations) showed that Rayleigh wave modal curves present a sensitivity to the Poisson's ratio (or V_P/V_S ratio), particularly in the low frequency band.

After analyzing the sensitivity of surface wave higher modes to model parameters, with particular attention to Poisson's ratio, through extensive forward simulations, we have explored the effects of including higher modes in the inversion

by using a Monte Carlo approach. Inversion is the process through which the parameters of a reference model are estimated from experimental data. In our case we have used a synthetic dataset in order to have a benchmark for the results. The inversion algorithm used for this part of the work is a multimodal Monte Carlo inversion developed by Maraschini et al (2010). To assess the benefit of including the higher modes in the estimation of P-wave velocity the synthetic data were inverted first with fundamental mode only and then with higher modes. The Monte Carlo inversion is based on a random sampling of model parameters (layer thickness, S-wave velocity and Poisson's ratio of each layer) with uniform probability density function. In other words, the random models are generated by randomly selecting a value for each model parameter within a selected range of variation. For each generated model (two million random samples for each run) the surface wave modal curves are computed with a forward operator and are compared with the synthetic data. The comparison is made through the computation of a misfit and the different models are ordered according to the misfit. The selection of accepted models that are considered the solution of the inverse problem can be made with several inference techniques. In our case, we have performed a statistical analysis of the results. This analysis indicated that the V_P was better retrieved with the addition of higher modes with respect to fundamental mode only. The evidence of this increased sensitivity was obtained by analyzing the posteriori probability density function of the retrieved model parameters, focusing particularly on Poisson's ratio and V_P (Figures 5.13 to 5.19). Nonetheless, the results obtained during the inversion where not sufficient to provide the best model of V_P (Figures 5.20 to 5.22). Therefore, a strategy for inversion has been defined using a step by step Monte Carlo multimodal inversion to retrieve the whole set of model parameters. By keeping the value of the V_S and layer thickness constant during the inversion it was possible to estimate the final V_P profile. Additionally, the final results were improved by using higher modes for deeper layers (half-space) compared to using fundamental mode only.

The step-by-step inversion defined by analyzing synthetic data was then applied to a real data from an exploration acquisition on land. The data contain a significant amount of coherent noise (ground roll) which is mainly related to the propagation of surface waves. Not only the surface waves are very energetic in a

wide frequency band (from 2[Hz] to 15[Hz]), but through frequency-wavenumber processing, it was possible to recognize well separated modes of propagations. Several processing steps were applied to retrieve optimal dispersion curves and, after extracting the dispersion curves in $f-k$ domain, a preliminary idea on the depth of penetration was achieved by plotting the phase velocity vs wavelength. It was estimated that the investigation depth reached approximately 150 meters. Finally, the inversion with Monte Carlo multimodal approach was performed both with fundamental mode only and then with the first higher mode (one million random samples for each run). The results for the V_S of the model were better retrieved for two modes inversion, particularly in deeper and thicker layers. Besides, three interfaces were found associated with the top of the layers, even by using fundamental or first higher mode inversion. In addition, the V_P of the final model, was better retrieved from the two modes inversion for the second and third layer. However, the half-space did not show sensitivity to any of the modes of propagations.

Thanks to the combined sensitivity of fundamental mode and higher modes to P-wave, we were able to depict information of the P-wave (or Poisson's ratio) of the layered model (Figures 5.26 to 5.28). When three modes inversion was used in the final step of the inversion strategy, the Poisson's ratio was achieved with a lower degree of uncertainty for the synthetic model compare to just using fundamental mode inversion, particularly for the deeper layers. (Figures 5.29 to 5.33).

The analysis performed on synthetic and real data (Table: 6.7) have shown that the inclusion of higher modes may increase the sensitivity to V_P during surface wave inversion. The importance of this result is related to the possibility to retrieve a near surface V_S and V_P model by using a part of the seismic signal which is usually considered noise. The near surface velocity models will be useful for near surface effect removal in hydrocarbon seismic exploration data, to provide reliable velocity model for pre-stack migration algorithms, to model and remove the ground roll, to optimize acquisition design. The obtained results are promising but deserve further investigation. In particular, different ways of defining the velocity model (velocity functions instead of layered media), inclusion of some constraints coming from body waves analysis and the analysis of leaky modes of surface waves are foreseeable further development of the present work.

Annex A

Sensitivity to the Poisson's ratio of the synthetic model of table 4.2

For the propagation velocity is known that at high frequency band (short wavelength) propagates in thin top layers while the low frequency band (long wavelength) propagates in the thicker layers. Intuitively, it can be predicted that the P-wave velocity according to this statement, is going to be more sensitive under a specific value of frequency.

Due to the fact, that the relation between the Poisson's ratio and the V_P/V_S is not linear. Now, in this Annex there has been proposed to make the same graphics of chapter 4, section 3 (but in a scale based directly on the sensitivity over the average Poisson's ratio) .

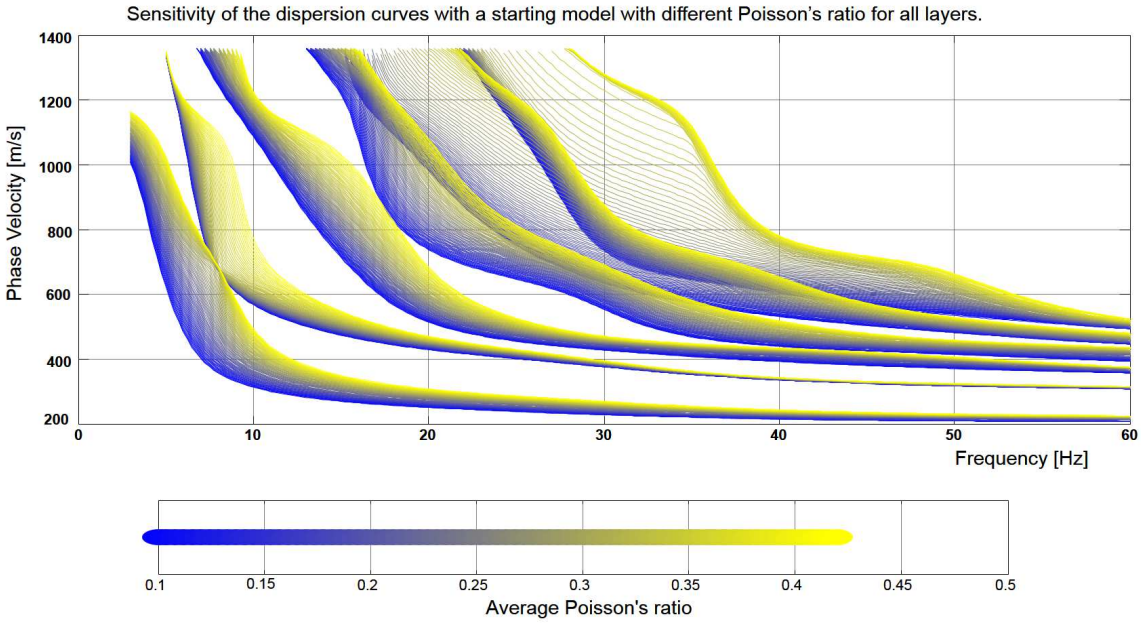

Figure A.1. Behavior of the dispersion curves for a model of five layers with different Poisson's ratio and varying them for a given consecutive rate. Obtained from table 4.2

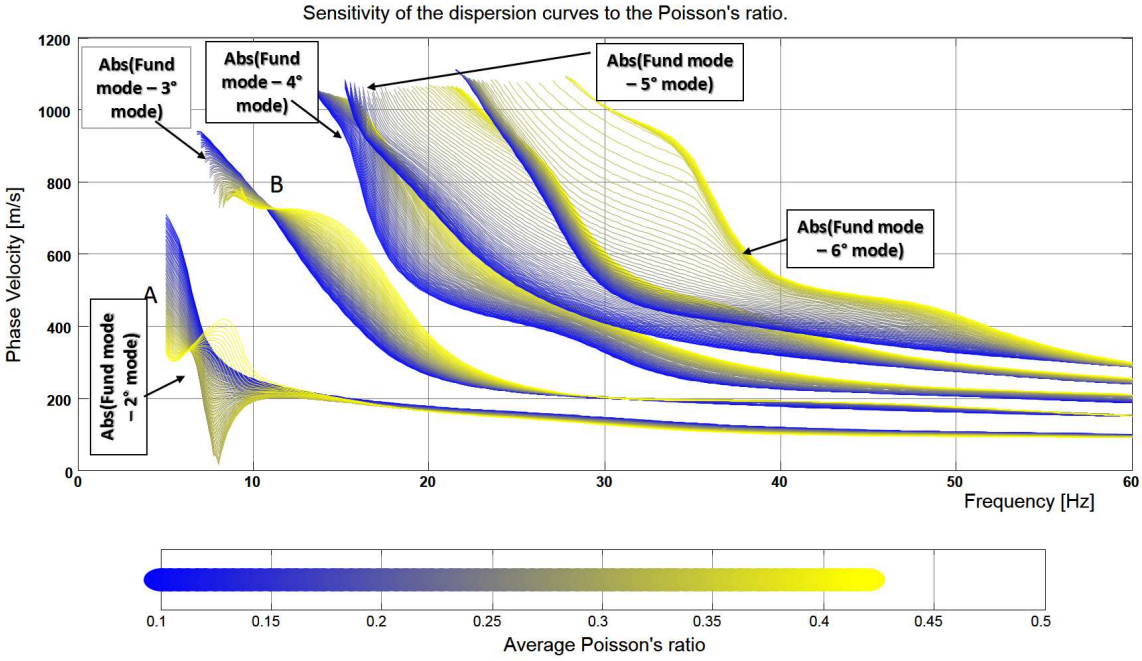

Figure A.2. Differences of each of the higher modes to the fundamental mode for the average Poisson's ratio changes. The reference is made from Table 4.2

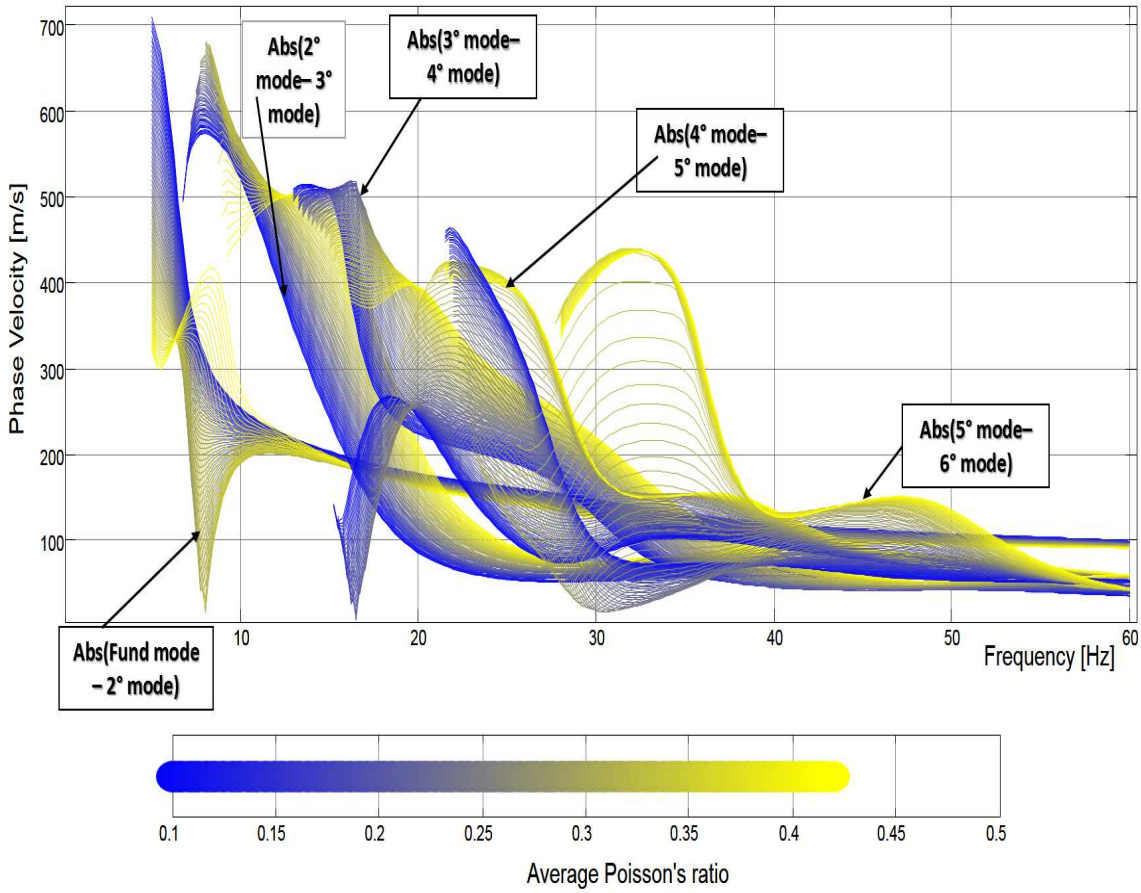

Figure A.3. Differences respect to successive modes according to the change in the average Poisson's ratio. The reference is made from Table 4.2

Annex B

Typical mass densities of basic soil types

This appendix presents some information of properties related to the soils

Table B.1. Typical mass densities of basic soil types. Density Units. [g/m^3]

	Poorly graded soil		Well-graded-soil	
	Range	Typical value	Range	Typical value
Soil Type				
Loose sand	1.70-1.90	1.75	1.75-2.00	1.85
Dense Sand	1.90-2.10	2.07	2.00-2.20	2.10
Soft Clay	1.60-1.90	1.75	1.60-1.90	1.75
Stiff clay	1.90-2.25	2.00	1.90-2.25	2.07
Silty soils	1.60-2.00	1.75	1.60-2.00	1.75
Gravelly soils	1.90-2.25	2.07	2.00-2.30	2.15

References

Abbiss C.P. 1981. *Shear wave measurements of the elasticity of the ground*: Geotechnique, **31**, 91-104.

Aki, P. K. & Richards, P. G. , 1980. *Quantitative seismology: Theory and methods*: W. H. Freeman & Co.

Bergamo, P. & Socco, L. 2013. *Estimation of P- and S-wave velocity models of unconsolidated granular materials through surface wave multimodal inversion*: SEG Technical Program Expanded Abstracts 2013: pp. 1776-1781., accessed October 1, 2013; http://dx.doi:10.1190/segam2013-1061.1.

Boiero, D., Wiarda, E., & Vermeer, P. 2013. *Surface- and guided-wave inversion for near-surface modeling in land and shallow marine seismic data*: The Leading Edge, **32**, 6 , 638-646.

Buchen, P.W. & Ben-Hador, R., 1996. *Free-mode surface-wave computations*: Geophys. J. Int., **124**, 3, 869-887.

Curtis, A. & Lomax, A., 2001. *Prior information, sampling distributions, and the curse of dimensionality*: Geophysics, **66**, 2, 372-378.

Caylak C. , Gokturkler G, and Coskun Sari , 2012. Inversion of multi-channel surface wave data using a sequential hybrid approach: Journal of Geophysics and Engineering, **9**, 19-28.

Drijkoningen ,G. October 2011. *Introduction to Reflection Seismology*, TA 3520. TU Delft. Version 1.2.

Dunkin, J., 1965. *Computation of modal solutions in layered, elastic media at high frequencies*: Bull. seism. Soc. Am. , **55**, 2, 335-358.

Ernst, F., 2007. *Long-wavelength statics estimation from guided waves*: Proceedings of the 69th EAGE Conference and Exhibition, Extended Abstracts, E033, London, UK.

Ernst F. 2008. *Multi-mode inversion for P-wave velocity and thick near-surface layers*. Near Surface 2008.

Everett, M. E., 2013. *Near-surface applied geophysics* : Cambridge University Press.

Foti, S. *Multistation methods for geotechnical characterization using surface waves*. PhD thesis, Politecnico di Torino, 2000.

Foti, S., 2002. *Numerical and experimental comparison between 2-station and multistation methods for spectral analysis of surface waves*: RIG Italian Geotech. J., **36**,1, 11-22.

Forbriger, T., 2003. Inversion of shallow-seismic wavefields. Part I. Wave- field transformation: Geophys. J. Int., **153**, 3, 719-734.

Ganji V., Gucunski,N.& Nazarian, S., 1998. *Automated inversion procedure for spectral analysis of surface waves*,:J. Geotech. Geoenviron. Eng., **124**, 8, 757-770.

Haskell, N., 1953. *The dispersion of surface waves on multilayered media*: Bulletin of the Seismological Society of America,**43**, 17-34.

Maraschini, M. *: A new approach for the inversion of Rayleigh and Scholte waves in site characterization*, PhD thesis, Politecnico di Torino, 2007.

Maraschini, M., Ernst, F., Foti, S.& Socco, L.V., 2010. *A new misfit function for multimodal inversion of surface waves*: Geophysics, **75**, 4, 31-42.

Marashini M. and Foti S. 2010. *A Monte Carlo multimodal inversion of surface waves*: Geophysical Journal International, **18** , 3, 1557-1566.

Menke, W., 1989. (Revised). *Geophysical data analysis: discrete inverse theory*: International Geophysics Series.

Park, C. B., R. D.Miller, & J. Xia, 1999. Multichannel analysis of surface waves: Geophysics, **64**, 800-808.

Richard, F. E., Hall, J. R., and Woods, R. D. 1970, *Vibrations of Soils and Foundations*: Prentice Hall, Englewood Cliffs, 414p.

Sheriff, R. E., 1989. *Geophysical methods*: Prentice-Hall, Inc.

Sheriff, R. E., 1991. *Encyclopedic Dictionary of Exploration Geophysics*: Soc. Expl. Geophys.

Stokoe, K.H., II and Santamarina, J.C., 2000. *Seismic-Wave-Based Testing in Geotechnical Engineering*: International Conference on Geotechnical and Geological Engineering, 1490-1536.

Strobbia, C. L. *Surface wave methods: acquisition, processing and inversion*. PhD thesis, Politecnico di Torino, 2003.

Strobbia, C. L , Laake, A. Vermeer, P.L. & Glushchenko, A. 2009. *Surface Waves - Use them , then Lose them* , 71 st EAGE Conference & Exhibition.

Strobbia, C. L , Laake, A. , Glushchenko, A. & Re, S., 2010. *Surface waves : Processing, inversion and attenuation* : First Break, **28**, 8, 85-91.

Strobbia, C., El Emam, A., Al-Genai, J. and Roth, J., 2010. *Rayleigh wave inversion for the near- surface characterization of shallow target in a heavy oild field in Kuwait* : First Break, **28** ,103-109.

Socco L.V. & Strobbia C. 2004. *Surface wave method for near surface characterization: a tutorial*: Near Surface Geophysics , **2**, 4, 165-185.

Socco, L.V. & Boiero, D., 2008. *Improved Monte Carlo inversion of surface wave data* , Geophys. Prospect. , **56**, 3, 357-371.

Socco, L.V., D. Boiero, S. Foti, & R.Wisen, 2009. *Laterally constrained inversion of ground roll from seismic reflection records* : Geophysics , **74**, 6, G35-G45.

Socco L.V, Foti S. & Boiero D. 2010. *Surface wave analysis for building near surface velocity models. Established approaches and new perspectives*: Geophysics, **75**, 5, 83-102.

A. Tarantola. 2005. *Inverse problem theory. Society for Industrial and Applied Mathematics*: SIAM.

Thomson,W. T., 1950. *Transmission of elastic waves through a stratified solid medium* : Journal of Applied Physics, **21**, 89-94.

Tokimatsu, K., 1997. *Geotechnical site characterization using surface waves*: in Proceedings of the First International Conference on Earth- quake Geotechnical Engineering, 1333-1368, IS-Tokyo 95, Tokyo, Balkema, Rotterdam.

S. Wright, J. Roesset, & K. Stokoe II. 1991. *Analitical and experimental studies of surface wave measurements to detect gas hydrates offshore*. In 23th OTC.

Woods, R.D. 1968. *Screening of Surface Waves in Soils, J. Soil Mechanics and Foundation Division* : Geophysics, **94**, 4, 951-979.

Xia, J., R. D. Miller, & C. B. Park, 1999. *Estimation of near-surface shear wave velocity by inversion of Rayleigh wave* : Geophysics , **64** , 691-700

Zhang, S.X. & Chan, L.S., 2003. *Possible effects of misidentified mode number on Rayleigh wave inversion*: J. appl. Geophys., **53**, 1, 17-29.

Oilfield Glossary Schlumberger, 2013, http://www.glossary.oilfield.slb.com , accessed 31 September ,2013.

Schlumberger, WesternGeco . 2013, Surface Wave Analysis, Modeling, and Inversion (SWAMI) –Velocity Modeling. http://www.slb.com/services/westerngeco/services/dp/technologies/signal/nearsurface/swami_velocitymod.aspx, accessed 21 August, 2013.

Weisstein, E. W. Log Normal Distribution. From MathWorld–A Wolfram Web Resource. http://mathworld.wolfram.com/LogNormalDistribution.html, accessed 22 August, 2013.